Numerical and Experimental Studies on Organic Rankine Cycle for Low-Medium Waste Heat Sources

Thesis submitted in partial fulfillment for the

Award of Degree

Doctor of Philosophy

By

Mayank Srivastava

DEPARTMENT OF MECHANICAL ENGINEERING
INDIAN INSTITUTE OF TECHNOLOGY
(BANARAS HINDU UNIVERSITY)
VARANASI-221005
INDIA

20131510 **2024**

CERTIFICATE

It is certified that the work contained in the thesis titled "**Numerical and Experimental Studies on Organic Rankine Cycle for Low-medium Waste Heat Sources**" by **Mr. Mayank Srivastava** has been carried out under our supervision and that this work is not submitted elsewhere for any degree.

It is further certified that the student has satisfactorily fulfilled all the requirements of the Comprehensive examination, Candidacy and SOTA for the award of the Ph.D. degree.

Prof. Jahar Sarkar
(Supervisor)
Department of Mechanical Engineering
IIT (BHU) Varanasi

प्राध्यापक / Professor
विभाग/Deptt. of Mechanical Engg
संस्थान/Indian Institute of Technology
(का०हि०वि०/B.H.U.)
वाराणसी-२२१००५/Varanasi-221005

Prof. Arnab Sarkar
(Co-supervisor)
Department of Mechanical Engineering
IIT (BHU) Varanasi

प्राध्यापक / Professor
विभाग/Deptt. of Mechanical Eng
संस्थान/Indian Institute of Technology
(का०हि०वि०/B.H.U.)
वाराणसी-२२१००५/Varanasi-221005

DECLARATION BY THE CANDIDATE

I, **Mayank Srivastava**, certify that the work embodied in this thesis is my own bonafide work carried out by me under the supervision of **Prof. Jahar Sarkar** and **Prof. Arnab Sarkar** for a period of 4 years from January 2021 to December 2024 at IIT (BHU), Varanasi. The material contained in this thesis has not been submitted for the award of any other degree. I declare that I have faithfully acknowledged and given credits to the research workers wherever their works have been cited in my work in this thesis. I further declare that I have not wilfully copied any others work, paragraphs, text, data, results, etc. reported in journals, books, magazines, reports, dissertations, thesis, etc. or available at website and have not included them in this thesis and have not cited as my own work.

Date: 16/12/2024

Place: IIT (BHU), Varanasi

(Mayank Srivastava)

DECLARATION BY THE SUPERVISORS

This is to certify that the above statement made by the candidate is correct to the best of my knowledge.

Prof. Jahar Sarkar

(Supervisor)

प्राध्यापक / Professor
विभाग/Deptt. of Mechanical Eng
संस्थान/Indian Institute of Technology
(का०हि०वि०/B.H.U.)
वाराणसी-२२१००५/Varanasi-221005

Prof. Arnab Sarkar

(Co-supervisor)

प्राध्यापक / Professor
विभाग/Deptt. of Mechanical Eng
संस्थान/Indian Institute of Technology
(का०हि०वि०/B.H.U.)
वाराणसी-२२१००५/Varanasi-221005

Head of the Department

Mechanical Engineering Department, IIT (BHU), Varanasi

COPYRIGHT TRANSFER CERTIFICATE

Title of the Thesis: Numerical and Experimental Studies on Organic Rankine Cycle for Low-medium Waste Heat Sources.

Candidate's Name: Mayank Srivastava

COPYRIGHT TRANSFER

The undersigned hereby assigns to the Indian Institute of Technology (Banaras Hindu University) Varanasi all rights under copyright that may exist in and for the above thesis submitted for the award of the "***Doctor of Philosophy***" degree.

Date: 16/12/2024

Place: IIT (BHU), Varanasi

(Mayank Srivastava)

Note: However, the author may reproduce or authorize others to reproduce material extracted verbatim from the thesis or derivative of the thesis for author's personal use provided that the source and University's copyright notice are indicated.

ACKNOWLEDGEMENTS

I take this opportunity to express my deep sense of gratitude 🙏 to my supervisor **Prof. Jahar Sarkar** for their continuous guidance and whole-hearted cooperation in carrying out this work. His meticulous and valuable review and constructive criticism of the manuscript have greatly improved the quality of work. Sir, for your faith in me and the desire to live up to your expectations, has constantly pushed me to work harder. I would extend my gratitude to my co-supervisor **Prof. Arnab Sarkar** for his support at all stage of research activity.

My grateful appreciation also goes to **Dr. S. S. Mondal** and **Dr. J. P. Chakraborty** for serving on my research progress evaluation committee (RPEC). Thank you all for sparing your valuable time and assisting me throughout my research and completion of this thesis. I wish to extend my sincere thanks **to Prof. Sandeep Kumar**, Head, Department of Mechanical Engineering for providing me the necessary resources to enable me to complete this research work. During my stay at IIT (BHU) Varanasi, I have met many people who have made this period of my life memorable and very pleasant. Among them, I would like to sincerely acknowledge the assistance and motivation provided by **Prof. Rashmi Rekha Sahoo, Prof. J. V. Tirkey, and Prof. Amitesh Kumar.** I want to thank my seniors at IIT (BHU) Varanasi, especially to **Dr. Mayaram Sahu, Dr. Prashant Srivastava, Dr. Satish Upadhyay, and Dr. Archana Kumari** and my colleagues **Mr. Harendra Kumar Yadav, Mr. Aishwary Pratap** and **Mr. Ujjawal Kumar Singh** for encouraging me to finish this work. My precious moral support, other than IIT (BHU) Varanasi, were **Mr. Rakesh Singh, Mr. Ashish Kumar Yadav, Mr. Piyush Srivastava, Mr. Shailesh Vishwakarma**, **Mr. Vishal Srivastava,** and all my other beloved ones whose continuous motivation made me stronger. The experimental part of this thesis has been carried out at the Department of Mechanical Engineering IIT (BHU) Varanasi. A number of persons have assisted and supported me in designing and development of the test rig. I would like to extend my sincere thanks to **Mr. Moolchand** and **Mr. Barmeshwar Prashad** for giving the valuable ideas while performing experiments and providing the measurement tools and instruments whenever needed for the research work without any hesitation.

I wish to express my profound and heartfelt gratitude to my dearest parents 🙏 - my father, **Mr. Mahendra Pratap Srivastava**; my mother, **Mrs. Uma Srivastava**; and my cherished sister, **Mrs. Shalu Srivastava**. Their unconditional love, selfless sacrifices, constant emotional encouragement, belief in my potential and unwavering financial support have been the foundation and gave me strength, upon which my academic and personal growth has flourished. This work is a testament to your profound sacrifices, and my heart overflows with eternal gratitude. I would like to extend my gratitude to my paternal and maternal family members, as well as my friends, for their constant support, faith, and love.

I also wish to extend my heartfelt gratitude to the Almighty **Lord Vishwanath/Mahadev** 🙏 for bestowing upon me the strength and divine guidance to stay steadfast on my path to success.

Date: 16/12/2024

Place: IIT (BHU), Varanasi **(Mayank Srivastava)**

Table of Contents

Chapter 1: Introduction 1

1.1. Background and Motivation 1

1.2. Literature Reviews 3

1.2.1. Power Cycles for Low-Medium Grade Heat Recovery 3

1.2.2. ORC modification 5

1.2.3. Experimental Studies of ORC 6

1.2.4. Case study of NPP 11

1.3. Research Gaps 12

1.4. Objectives and Novelty 13

1.5. Thesis structure 14

Chapter 2: Power Cycles for Low-Medium Grade Heat Recovery 17

2.1. Cycle Description 17

2.1.1. ORC using dry fluid 17

2.1.2. ORC using wet fluid 18

2.1.3. CO_2 Rankine cycle 19

2.1.4. Kalina cycle 20

2.1.5. Organic flash cycle 21

2.1.6. Trilateral flash cycle 22

2.2. Methodology 23

2.2.1. Mathematical Modelling 23

2.2.2. Simulation and Validation 29

2.3. Results and Discussion 33

2.3.1. Performance comparison 34

2.3.2. Parametric study 37

2.3.3. Effect of condenser temperature 42

2.3.4. Techno-economic analysis 43

2.4. Important Findings 46
Chapter 3: Organic Rankine Cycle Modifications 49
3.1. Cycle Description 49
3.2. Modelling and Simulation 52
3.1.1. Mathematical Modelling 52
3.1.2. Proposed economic models 53
3.1.3. Simulation procedure 54
3.1.4. Model validation: 56
3.3. Results and Discussion 56
3.4. Important Findings 73
Chapter 4: Experimental Investigation 75
4.1. Experimentation 75
4.1.1. Setup Description 75
4.1.2. Experimental Procedure 86
4.1.3. Data Reduction 89
4.1.4. Uncertainty Analyses 91
4.1.5. Optimization and Prediction 91
4.2. Results and Discussion 95
4.2.1. Effect on operating and performance parameters 95
4.2.2. ANOVA model for optimization and prediction 103
4.3. Important Findings 108
Chapter 5: Case Study for Nuclear Power Plant 111
5.1. Selection of Location – Feasibility Study 111
5.2. Modelling and Simulation 117
5.2.1. Mathematical Modelling 117
5.2.2. Simulation and Validation 119
5.3. Result and Discussion 121

5.3.1. Comparison of two feasible cases 121

5.3.2. Working fluid behaviour on the output parameter 124

5.3.3. Parametric study 126

5.3.4. Simulation vs Experimental 133

5.3.5. Nanofluid-enhanced WHR for ORC 135

5.4. Important Findings 142

Chapter 6: Conclusions and Future Study 145

6.1. Conclusions 145

6.2. Future Study 146

References 149

List of Publications 163

List of Figures

Figure 1.1. Layout and temperature-entropy diagram of waste heat recovery ORC 2
Figure 2.1. Layout and T-s diagram of ORC with dry working fluid..................................... 18
Figure 2.2. Layout and T-s diagram of ORC with wet working fluid 19
Figure 2.3. Layout and T-s diagram of CO_2 Rankine cycle 20
Figure 2.4. Layout and T-s diagram of Kalina cycle 21
Figure 2.5. Layout and T-s diagram of OFC 22
Figure 2.6. Layout and T-s diagram of TFC 23
Figure 2.7. Flow chart of the simulation procedure 31
Figure 2.8. Component irreversibility of different cycles at 90°C 36
Figure 2.9. Exergy analysis of different cycles at 90°C source temperature 37
Figure 2.10. Variation of net work output with heat source temperature 38
Figure 2.11. Variation of thermal efficiency with heat source temperature 39
Figure 2.12. Variation of exergy efficiency with heat source temperature 39
Figure 2.13. Variation of annual total cost required with heat source temperature 40
Figure 2.14. Variation of total annual profit with heat source temperature 41
Figure 2.15. Variation of annual CO_2 saving with heat source temperature 42
Figure 3.1. Schematic layout of proposed EEORC-1 50
Figure 3.2. Temperature-entropy diagram of proposed EEORC-1 50
Figure 3.3. Schematic layout of proposed EEORC-2 51
Figure 3.4. Temperature-entropy diagram of proposed EEORC-2 52
Figure 3.5. Flow chart of the simulation procedure for EEORC 55
Figure 3.6. Effect of waste heat inlet temperature variation on net work output 61
Figure 3.7. Effect on ejector pressure with the variation of waste heat inlet temperature....... 62
Figure 3.8. Improvement of net work output with waste heat inlet temperature 63
Figure 3.9. Effect on thermal efficiency with waste heat inlet temperature 64
Figure 3.10. (a) Effect on entrainment ratio by variation of WHT, (b) Effect of PLR by the variation of WHT for different cycles 65
Figure 3.11. Irreversibility value of different cycle components at 70 °C 66
Figure 3.12. Effect on exergy efficiency with WHT for different cycles 67
Figure 3.13. Effect on size parameter of turbine with WHT for different cycles 68
Figure 3.14. Effect on total evaporator and condenser areas with WHT for different cycles . 69

Figure 3.15. Value comparison on components cost rate of different cycles at 70 °C............ 70
Figure 3.16. (a) Variation on total profit and selling price of EEORC-1 (R123) with WHT, (b) Variation on net annual profit with WHT for different cycles and working fluids. 72
Figure 3.17. Variation of CO_2 saved with WHT for different cycles and working fluids....... 73
Figure 4.1. Layout of the experimental setup for the Organic Rankine Cycle 76
Figure 4.2. (a) Fabrication of the vertical separator and (b) modification of the scroll compressor to expander.. 77
Figure 4.3. (a) Fabrication of the heating load and control unit with oil tank, (b) Pressurized storage tank for working fluid 79
Figure 4.4. Installation of instruments and sensors to ORC setup... 81
Figure 4.5. Lab-scale ORC experimental setup 84
Figure 4.6. Isometric view and running condition of ORC experimental setup 86
Figure 4.7. Normal plot of variation between predicted and actual value of net power and cycle efficiency.. 94
Figure 4.8. Effect on (a) Evaporator temperature and (b) Mass flow rate of working fluid.... 95
Figure 4.9. Effect on (a) expander inlet temperature and (b) expander outlet temperature..... 96
Figure 4.10. Effect on pressure ratio of (a) pump and (b) expander....................................... 98
Figure 4.11. Effect on isentropic efficiency of (a) pump and (b) expander............................. 99
Figure 4.12. Effect on (a) net power output and (b) cycle efficiency................................... 100
Figure 4.13. Effect on (a) exergy and (b) exergy efficiency... 102
Figure 4.14. Desirability for net power and cycle efficiency for prediction analysis............ 104
Figure 5.1. Alternator’s capital cost correlation by trendline analysis between capacity (kW) and market price (USD) 119
Figure 5.2. Flowchart of simulation process for feasible location in NPP to install ORC 120
Figure 5.3. Schematic diagram of suggested ORC to be installed at NPP waste heat recovery site 121
Figure 5.4. (a) ORC T-s diagram of case-1, (b) ORC T-s diagram of case-2........................ 124
Figure 5.5. Effect of condenser and cold fluid inlet temperatures on net work output 126
Figure 5.6. Effect of condenser and cold fluid inlet temperatures on thermal efficiency...... 127
Figure 5.7. Effect of condenser and cold fluid inlet temperatures on NPV of total investment 128
Figure 5.8. Effect of condenser and cold fluid inlet temperatures on yearly profit............... 129
Figure 5.9. Effect of condenser and cold fluid inlet temperatures on LCOE 130
Figure 5.10. Effect of condenser and cold fluid inlet temperatures on DPP 131

Figure 5.11. Effect of condenser and cold fluid inlet temperature on IRR for different case cycles 132
Figure 5.12. Effect of the condenser and cold fluid inlet temperature on annual CO_2 emission saving........ 133
Figure 5.13. T-s Diagram and layout of nanofluid based ORC 136
Figure 5.14. Net work comparison with different hot fluids and working fluids 138
Figure 5.15. Thermal efficiency comparison with different hot fluids and working fluids... 139
Figure 5.16. Working fluid mass flow rate comparison with different hot fluids and working fluids 140
Figure 5.17. Capital investment comparison with different hot fluids and working fluids ... 141
Figure 5.18. Earned profit comparison with different hot fluids and working fluids 142

List of Tables

Table 1.1. Literature review of experimental ORC's…………………………………………....9

Table 2.1. Component irreversibility calculation 24

Table 2.2. Heat exchanger area design 25

Table 2.3. Capital investment of system components [103,104]. 26

Table 2.4. Validation of different low/medium grade thermodynamic cycles 32

Table 2.5. Input parameters used for different thermodynamic cycle analyses....................... 33

Table 2.6. Fluid properties for different thermodynamic cycles 33

Table 2.7. Comparison of optimized result outputs of various thermodynamic cycles at a source temperature of 90°C 34

Table 2.8. Effect of increasing and decreasing the T_{con} by 3°C on output parameters at a source temperature of 90°C 42

Table 2.9. Various challenges associated with thermodynamic cycles 44

Table 2.10. Comparison of solar ORC and solar P-V system [117]....................................... 46

Table 3.1. Comparison of result obtained from reference with simulated values 56

Table 3.2. Selection of working fluids [119]……………………………………………….. 56

Table 3.3. Input parameters for Basic and EEORCs ………………………………………….. 57

Table 3.4. Comparison of different cycles and working fluids at WHT = 70 ˚C…………….58

Table 4.1. ORC component description and technical details 80

Table 4.2. ORC sensors description, along with technical details.. 82

Table 4.3. ORC experimental data at various heat loads and mean input condition 89

Table 4.4. Uncertainty analyses of major input and output parameter 91

Table 4.5. Design of Experiment Table by Central Composite Method 92

Table 4.6. ANOVA coefficients and fit statistics of the model 93

Table 4.7. ANOVA optimization constraints 103

Table 4.8. Validation of optimized condition output result with the experimental run at same optimized condition 105

Table 4.9. Predicted data for net power and cycle efficiency in an ORC system, highlighting both experimental and theoretical predictions.. 106

Table 4.10. Advantages of current developed system with previously developed systems ... 106

Table 5.1. Waste heat disposal components and its temperature of Indian NPP data provided by BRNS.. 113

Table 5.2. Input condition data to check the feasibility of running ORC............................. 114

Table 5.3. The market price of the alternator of different capacities and different manufacturer 117
Table 5.4. Recommended component design and specification for ORC installation 121
Table 5.5. Various input and output parameters for case 1 and case 2 122
Table 5.6. Effect on output parameter with working fluid for both feasible cases 125
Table 5.7. Simulation and experimental variation of Case-1 NPP 133
Table 5.8. Simulation and experimental variation of Case-2 NPP 134
Table 5.9. Input parameters used 136
Table 5.10. Thermophysical properties relevant to nanofluids [99,128] 137
Table 5.11. Organic working fluid properties 137

List of Symbols

Abbreviation

EEORC	Ejector Enhanced Organic Rankine Cycle
OFC	Organic Flash cycle
ORC	Organic Rankine cycle
PLR	Pressure Lift Ratio
PPTD	Pinch point temperature difference
TFC	Trilateral flash cycle
WHT	Waste Heat source Temperature

Nomenclature

A	Area [m^2]
Bo	Boiling number
C	Cost [USD]
c	Velocity [m/s]
c_p	Specific heat [kJ/kg]
CRF	Capital recovery factor
D	Diameter [m]
Ex	Exergy [kW]
F	Fuel cost [USD]
G	Mass velocity (kg/s-m^2)
h	Specific enthalpy [kJ/kg]
i	Interest rate
I	Irreversibility [kW]
k	Thermal conductivity [W/m-K]
l	Length/height [m]
LMTD	Log mean temperature difference [K]
$\dot{m}$	Mass flow rate [kg/s]
n	Number of years
OM	Operation and maintenance cost [USD]
P	Pressure [kPa]
Pr	Prandtl number
Q	Heat interaction [kW]

Re	Reynolds number
s	Specific entropy [kJ/kg-K]
SP	Size parameter
t	Thickness [m]
T	Temperature [°C]
$T\dot{C}$	Total cost rate [USD/h]
U	Overall convective heat transfer coefficient [W/m^2-K]
v	Specific volume [m^3/kg]
W	Work transfer [kW]
x	Dryness fraction
z	Annual working hour [h]
Z^{CI}	Capital investment cost [USD]

Greek letters

$\sum$	Sigma (sum notation)
α	Convective heat transfer coefficient [W/m^2-K]
β	Chevron angle
η	Efficiency
μ	Dynamic viscosity [N-s/m^2]
ρ	Density [kg/m^3]
ω	Entrainment ratio

Subscripts

1,2…12	State points
alt	Alternator
amb	Ambient
blr	Boiler
cf	Cold fluid
con	Condenser
d	Diffuser section of ejector
dp	Two-phase fluid
eje	Ejector
ele	Electricity
eq	Equivalent
evp	Evaporator

ex	Exergy
hf	Hot fluid
in	Inlet
ise	Isentropic
j	Any selected component
l	Saturated liquid state
liq	Liquid state
m	Mixing chamber of ejector
mix	Mixture
nz	Nozzle section of ejector
o	Outlet
pre	Preheater
pri	Primary
rec	Recuperator
req	Required
sec	Secondary
sep	Separator
sl	Saturated liquid state
sp	Single phase fluid
sub	Subcooled region
sup	Superheated region
sv	Saturated vapor state
t/tur	Turbine
th	Thermodynamic
thrt	Throttling
v	Saturated vapor state
vap	Vapor state
wet	Wet region (phase change)
wf	Working fluid

Abstract

The rapid growth in population and increasing demand for comfort and luxury in daily life have resulted in a substantial rise in electricity consumption. Global electricity usage has surged from 7,320 TWh in 1980 to nearly 27,000 TWh in 2023, driven by industrialization and improved access to power worldwide. However, this demand remains heavily reliant on fossil-based energy sources, contributing significantly to environmental issues such as global warming, ozone layer depletion, and deforestation. Despite advancements in renewable energy technologies, fossil fuels still dominate electricity generation. To sustainably meet the growing energy needs, it is imperative to explore alternative, efficient, and environmentally friendly power generation technologies. The Organic Rankine Cycle (ORC) has emerged as a promising solution to harness low- and medium-temperature heat sources, including geothermal, solar, and industrial waste heat. Compared to the traditional steam Rankine cycle, ORC is better suited for low-grade heat applications, offering higher feasibility and efficiency. Studies indicate that waste heat constitutes 20–50% of industrial energy consumption, with 18–30% of this recoverable. However, challenges such as low thermal efficiency, high cost-to-power ratios, and limited technology maturity hinder widespread ORC adoption. This study focuses on improving ORC performance through numerical analysis and experimental investigation. Developing indigenous ORC systems tailored to local needs can significantly reduce reliance on fossil fuels, promote renewable energy utilization, and provide economic and environmental benefits. The outcomes aim to support ORC technology deployment in India, advance sustainable energy goals, and address the energy demand gap.

Various thermodynamic power cycles can be utilized to convert low-to-medium temperature heat (available from many sources and has huge potential) to electricity. A detailed comparison between them is essential to identify the suitable one. Hence, to fulfill this research gap, six thermodynamic power cycles (Organic Rankine cycle with dry fluid, Organic Rankine cycle with wet fluid, Transcritical CO_2 Rankine cycle, Kalina cycle, Organic flash cycle and Trilateral flash cycle) have been compared for various heat source and sink temperatures. Objective functions are power generation, efficiency, irreversibility, cost, profit, environmental benefit, techno-economic parameters, etc. The study shows that the trilateral flash cycle is best for medium heat source temperature and the CO_2 Rankine cycle for low heat source temperature. The trilateral flash cycle shows an 11.5% higher exergy efficiency and 16.16% increment in annual profit at 160°C heat source temperature compared to the organic Rankine cycle with dry fluid. A decrease in condenser temperature is more advantageous than an

increase. The study reveals that the CO_2 Rankine cycle would be advantageous for low-grade heat sources while the trilateral flash cycle for medium-grade heat sources in terms of performance, cost, design, operation and environmental benefits.

The need for organic Rankine modification by various means can be realized for low-medium grade heat recovery. Hence, two new ejector-enhanced organic Rankine cycles (EEORC-1 and EEORC-2) are presented in this study. Three new economic models (M1, M2, and M3) have been chosen to study the feasibility in the real world and ensure market entry of the technology for commercialization, leading to mutual benefit to both industries and consumers. Energy, exergy, economic and environmental performances are evaluated for various working fluids and waste heat inlet temperatures by optimizing cycle parameters to maximize net work output. Economic simulation is performed to judge the best model suitable for the minimum possible selling price along with the maximum possible profit to the industry. Results show that EEORC-1 with R123 performs best and renders a maximum 18% increment in net work output at 70 °C heat source temperature. The basic cycle has maximum thermal and exergy efficiencies of 3.8% and 40.0%, respectively at 70°C heat source temperature. M2 model is suitable for consumers as well as government and private-owned power plants. The proposed M2 economic model gives a maximum of 7.32% increment in profit by EEORC-1. Extra profit can be generated by earning more carbon credit.

A laboratory-scale ORC system is designed and developed for electricity generation from low-medium-grade heat sources. The experimentation involves component selection, fluid selection, design, fabrication and testing. A custom-designed separator has been fabricated and used to ensure saturated vapor at the turbine inlet. R601a has been used as a working fluid due to its zero ODP and negligible GWP. Parametric analyses examined the effects of heat loads (5–11.5 kW), hot fluid flow rates (40–60 L/min), and cold air inlet temperatures (29–37°C) on system performance. At 11.5 kW, the net power peaked at 0.939 kW, and cycle efficiency increased from 2.34% to 8.08%, demonstrating the benefits of optimized heat input. Exergy efficiency is found to be highest at moderate flow rates (40 L/min), with evaporator effectiveness ranging from 0.78 to 0.84. RSM-ANOVA tool has been used for simultaneous optimization of net power and cycle thermal efficiency and validated performance predictions with minimal errors (1.55% for net power, 2.01% for efficiency). Findings have been extended to analyze waste heat recovery from an Indian nuclear power plant (NPP), demonstrating the ORC system's versatility. This research offers practical insights and guidelines to enhance ORC systems for industrial waste heat recovery applications.

A feasibility study is essential before installing a power generation system to recover waste heat from nuclear power plants. Hence, nine possible waste heat locations of Indian nuclear power plants are identified and two feasible cases (case-1 and case-2) are deduced to use the organic Rankine cycle as a bottoming cycle. ORC is used for waste heat recovery from a nuclear power plant (NPP) without alteration of any existing system and components to avoid any safety issues. Energy, exergy, economic and environmental performances are evaluated for selected working fluids and given waste heat conditions for selected feasible cases. Capital investment in alternators has been correlated with the help of the available market price of alternators and applied in economic analysis. The economic study is based on Net present value, Discounted payback period, Levelized cost of energy, Internal rate of return, Profit and per unit build-up cost of ORC to suggest whether the installation is worth the venture or not. The result is compared in tabulated form for both feasible cases and different working fluids. Different working fluid behaviors are also compared to get the best working fluid. The result shows that below 41°C condenser temperature, case-2 based bottoming ORC should be the priority to install and at the availability of sufficient funds, both cases can be installed, which will cumulatively produce 499.3 kW of electricity from waste energy with a total of 204.62 thousand USD annual profit from the total capital investment of 764.96 thousand USD. For 40 years of the system's lifetime, a total of 1.392 million USD will be used if both cases are employed and the invested cost will be returned in 8.73 years.

Chapter 1: Introduction

The rapid growth in the global population and increasing demand for comfort and luxury have led to a surge in electricity-dependent household and commercial appliances, driving energy consumption to unprecedented levels. This trend risks exacerbating environmental hazards such as global warming - a crisis further amplified by industrial practices like dumping low-grade waste heat, deforestation, mining, and ozone layer depletion. To address these challenges, sustainable power generation technologies that utilize low-grade waste heat without additional environmental harm have emerged as critical solutions. Among these, thermodynamic cycles like the ORC stand out due to their efficiency in converting low and medium-temperature heat sources, including renewable energy and industrial waste heat, into electricity. Unlike traditional steam Rankine cycles, ORC systems excel at low-temperature applications, making them ideal for waste heat recovery. However, widespread adoption of ORC technology faces barriers such as low thermal efficiency, high cost-to-power ratios, and technological immaturity compared to established cooling/heating systems. A key limitation is the inherently low temperature lift of low-grade heat sources, which restricts heat recovery performance. Consequently, advancing ORC systems through modifications to enhance efficiency and validating these improvements through targeted experimentation is urgently needed to unlock their full potential for sustainable energy generation.

1.1. Background and Motivation

The rapid expansion of electricity-powered residential and commercial systems, driven by population growth and the pursuit of comfort, has led to surging global energy demands. According to a Statista report by Bruna Alves, worldwide electricity consumption rose from 7,320 TWh in 1980 to approximately 27,000 TWh in 2023, fuelled by industrialization and expanded electricity access. By 2050, global electricity generation capacity is projected to exceed 14.7 terawatts [1]. In 2020, renewable energy contributed 2.8 terawatts of capacity, still lagging behind fossil fuels (4.4 terawatts), with coal and peat remaining the dominant sources [1]. China leads the adoption of renewable energy1 terawatt capacity), followed by the USA (325 GW) [1]. India ranks as the third-largest electricity producer, with an installed capacity of 404.13 GW as of July 2022, of which 39.91% (161.29 GW) comes from renewables, including solar (57.97 GW), wind (40.89 GW), biomass (10.68 GW), and hydropower (46.85 GW). Despite generating 1,598 TWh in 2019–20, India faced a 212.56 GW peak demand in January 2023, underscoring the need for expanded capacity [2]. By 2035, energy use in non-OECD countries is expected to rise by 84%, with China and India leading this surge [3]. The design and operational efficiency of thermal power plants have been optimized through innovative technologies, making them a viable solution for energy generation from high-grade temperature sources but at the cost of emission of carbon footprint [4]. The UN Agenda 2030's Sustainable Development Goals (SDGs) outline this transition to a low-carbon economy, incorporating social, economic, and environmental sustainability [5]. Harnessing low-medium grade heat sources—such as geothermal energy, solar heat, and industrial waste heat—offers significant potential. Industrial processes discard 20–50% of energy as waste heat, with 18–30% recoverable for power generation. Thermodynamic cycles, particularly the organic Rankine cycle (ORC), are preferred for large-scale applications due to their efficiency and adaptability. While traditional steam Rankine cycles excel above 340–370°C, ORC systems (Figure 1.1) use organic fluids to efficiently convert lower-temperature waste heat into electricity. ORC technology is already operational globally, with installations in the USA, Canada, Italy, Austria, Germany, and others, demonstrating its feasibility for diverse energy recovery applications. ORC technology is commercially utilized in sectors worldwide, with prominent manufacturers like Turboden (Italy) and Ormat (USA). However, no significant research or commercial development has occurred in India.

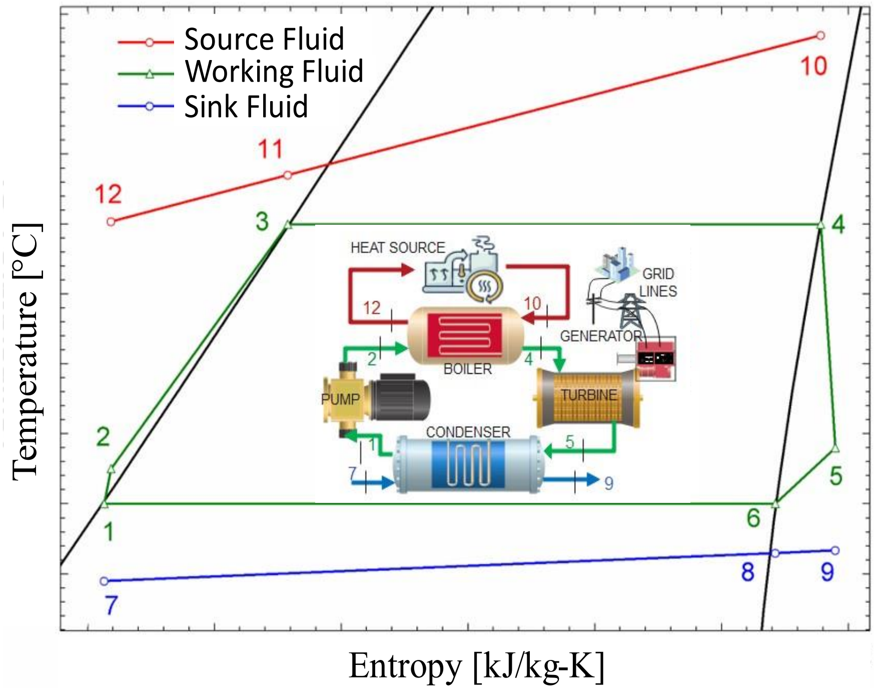

Figure 1.1. Layout and temperature-entropy diagram of waste heat recovery ORC

While attempts to use imported ORC technology have faced challenges, developing indigenous ORC systems, particularly for Nuclear Power Plants, offers a cost-effective solution for converting waste heat into electricity. This initiative can significantly boost the Indian economy, reduce coal dependency, and improve air quality, delivering health benefits to the public. The present study aims to accelerate ORC technology deployment, with recommendations to the Government of India through BRNS (Board of Research in Nuclear Sciences) for nationwide adoption and public benefit.

1.2. Literature Reviews

1.2.1. Power Cycles for Low-Medium Grade Heat Recovery

Waste heat recovery (WHR) improves energy efficiency across industries, reduces environmental impact, and cuts fuel costs, especially in fossil fuel systems. WHR approaches include heat-to-heat, heat-to-work, and heat-to-power conversions, though efficiency decreases with each conversion due to thermodynamic losses. Low-grade waste heat, often rejected by conventional power plants, can be utilized through advanced energy conversion technologies and optimized heat exchangers or fluids to enhance performance. There are a variety of methods for producing electricity from renewable heat sources, but heat engine-based power production systems are typically favoured for large-scale applications due to their adaptability and higher efficiency [6–8]. If solar photovoltaic panels with battery storage and organic Rankine cycle coupled with thermal energy storage are compared technically and economically, it was found that ORC offers improved reliability in power supply and can be scaled up to achieve higher efficiency. Comparison has been carried out on the basis of levelized cost of electricity (LCOE) at the same capital utilization factor to suggest the appropriate one between solar photovoltaic and thermodynamic cycles [9]. Various thermodynamic power cycles have been designed for their specific purpose and condition to produce electricity from low-medium heat sources, such as the organic Rankine cycle, supercritical CO_2 Rankine cycle, Kalina cycle, organic flash cycle (OFC), and trilateral flash cycle (TFC) [10–13]. ORC was developed in the early 19th century with unique qualities to utilize low and variable-temperature heat sources and it reached a sizable niche market in the power sector of the twenty-first century as it is simple, inexpensive, and compact [10]. Kalina cycle was developed in the early 1980s, and it has been cited as one of the options that better fit the heat transfer curves of the heat source and the heat recovery system [11]. However, the Kalina cycle's layout is somewhat more complicated due to the additional separators and heat exchangers, which also come at an added expense. In order to recover heat from low-temperature sources, it was observed that the Kalina cycle is a very inefficient one and suggested OFC for power generation instead of ORC and Kalina cycle [12]. Ho et al. [13] investigated 10 different siloxanes and aromatic hydrocarbons as suitable working fluids for the comparison of OFC and ORC's and results revealed that aromatic hydrocarbons were more suitable due to their higher power output and simpler turbine designs, and both cycles possess comparable utilization efficiencies. Some studies were performed to suggest better cycle and system performance among the OFC and ORC, such as net power production, thermal and exergy efficiencies, and exergy destruction ratios at each component of the systems [14]. TFC is a modified ORC in which the organic working fluid is heated to saturation liquid condition under high pressure rather than boiled [15]. Under the same operating conditions, the TFC system may recover more waste heat than the ORC [16]. It was discovered that the TFC Power production is greater than the ORC's by 14% to 29% for the same low to medium heat and heat sink conditions if the heat source temperature is just below 100°C [17,18]. Transcritical CO_2 Rankine cycle is also used for low-temperature heat sources and it provides better temperature glide in the evaporator section [19,20]. CO_2 transcritical power cycle and Kalina cycle were compared, and it was found that the Kalina cycle shows a lower cost per net power and better economic performance [21]. The advantage of OFC is a close match between the heat transfer curves [22]. CO_2 transcritical cycle and OFC were compared using R245fa and R600 and observed that CO_2 cycle produces slightly higher per unit work and better exergy efficiency; besides, OFCs can provide an economically better solution. However, R245fa may lead to some environmental impact due to its higher GWP and there is the chance of explosion with R600 OFC [23]. Another study showed the comparison of transcritical reheat CO_2 cycles to the ORC and the Kalina cycle and deduced that the transcritical CO_2 cycle has the largest net power production and the economic performance is between the Kalina cycle and the ORC [24]. When OFC, ORC and TFC were compared to recognize the potential solutions for low-grade heat recovery, then it was investigated that TFC obtains the largest net power output (13.6 kW) at the evaporation temperature of 152°C, which is 37% higher than that of ORC (9.9 kW) and 58% higher than that of OFC (8.6 kW) [25]. When selecting a working fluid for power cycles, factors like thermodynamic properties, stability, compatibility, safety, environmental impact, cost, availability, and regulations must be carefully considered. Environmentally friendly fluids, including hydrofluoro-olefins (HFOs), are increasingly used in ORC and OFC systems. HFOs offer advantages over conventional refrigerants like HCFCs and HFCs, including lower global warming potential, higher energy efficiency, and improved safety.

While research on their properties, flammability, and oil compatibility is ongoing, their favourable thermodynamic and environmental characteristics have garnered significant attention [26]. Many refrigerants were simulated as working fluids in ORC, including toluene, R123 [27–32], R134a [33], R245fa [34–37]. HFE-7000, HFE-7100, n-pentane and isopentane [38], R245fa/isopentane and R123/R245fa. Zeotropic refrigerant mixtures, composed of two or more refrigerants with different boiling points, are used to tailor working fluid properties for specific system designs. Properly mixed zeotropic fluids improve critical temperature, pressure, boiling point, flammability, ozone depletion, and global warming potential. Unlike pure refrigerants, zeotropic mixtures evaporate and condense over a temperature range, offering advantages like better temperature glide, enhanced capacity, and increased energy efficiency [39–41].

Despite extensive research on waste heat recovery cycles such as the ORC, OFC, TFC, Kalina, and transcritical CO_2 cycles, a clear consensus on the optimal system for low-grade heat recovery remains elusive. While each cycle offers unique benefits, trade-offs exist in terms of net power output, thermal and exergy efficiency, and economic performance. Moreover, existing studies often focus on individual aspects like working fluid selection or component design, with limited comprehensive comparisons under uniform conditions. There is also a need to further assess environmentally friendly fluids and zeotropic mixtures, highlighting an important research gap for integrated, multi-criteria optimization studies.

1.2.2. ORC modification

Within the last few years, many ORC modifications have been investigated. Safarian and Aramoun [42] presented three modified organic Rankine cycles (incorporating turbine bleeding, regeneration and both of them) and showed that the ORC integrated with turbine bleeding and regeneration has the highest thermal and exergy efficiencies. Research has been done to determine the best-performing combination of regenerative ORC with both an open-feed liquid heater and an internal heat exchanger [43]. According to some research, the ORC combined with turbine bleeding and regeneration has the maximum thermal and exergy efficiency. Internal heat exchangers, bleed turbines and turbine bleeding/regeneration are also incorporated into ORC to study the effect of thermal and environmental [44]. Various working fluids are also being studied with modified ORC to see the effect [45]. Kheiri et al. [46] analysed four modifications of ORC integrated with an ejector and reported a thermal efficiency improvement in the range of 13-19%. Chen et al. [47] studied vapor-liquid ejector-modified ORC using various working fluids. Haghparast et al. [48] introduced the ejector in

ORC to lower the turbine exit pressure driven by a second-stage evaporator and got improved power generation. Oyekale et al. [49] studied the modified hybrid ORC plant and concluded that 60% of irreversibility cost rates could be minimized by proper optimization of each system component. Tashtoush and Algharbawi [50] did a parametric study and optimization of the organic Rankine cycle with two turbines and an ejector. Zhang et al. [51] found that the use of an ejector in ORC power plant at different equipment locations will increase the net power production. Jafary et al. [52] proposed two novel ORCs with a solar-powered system (one with an internal heat exchanger and the other with a mixture heater) and analysed the overall energy and exergy efficiencies. Saini et al. [53] studied the thermodynamic and economic performances of an ejector-enhanced ORC and reported cost reduction, efficiency enhancement and CO_2 emission saving. Yu et al. [54] proposed recuperative transcritical ORC and found better thermodynamic performance. Surendran et al. [55] analysed the effect of using the ejector on increasing the work output. Li et al. [56] reported the enhancement of energy performances by coupling the ejector in an organic Rankine flash cycle driven by geothermal energy. They have also found that the ejector-enhanced system is better in terms of exergy efficiency and levelized energy cost [57].

Recent research on ORC modifications has explored turbine bleeding, regeneration, and internal heat exchangers, with some studies reporting that ejector integration can improve thermal efficiency by 13–19% and boost net power output. However, there remains a significant gap in fully optimizing ejector-driven ORC systems. In particular, comprehensive evaluations of ejector positioning, operating conditions, and their effects on exergy efficiency and cost performance are limited, underscoring the need for further investigation into these configurations for enhanced low-to-medium grade heat recovery.

1.2.3. Experimental Studies of ORC

Comparative studies suggest that ORC with dry fluids is optimal for low-to-medium temperature applications when techno-economic factors are considered [58]. The basic differences in the experimental analyses on ORC are in terms of component (pump, expander, evaporator, condenser and working fluids) types [27–38,59,60]. Pump used is mainly a multi-stage centrifugal pump, magnetic gear pump, plunger pump, piston pump and diaphragm pump. Heat exchangers (condenser and evaporator) used are mainly plate, fin-tube and shell-tube types (plate heat exchanger is generally preferred for liquid secondary fluid and others are preferred for gaseous secondary fluid). Expander may be of two-types: turbine (radial turbine) and positive displacement machines. As the experimental ORC setups reported in the open literature are of small capacity (power output was limited to 10kW), the positive displacement machines were used in most of the experimental studies. Hence, the expanders used are mainly scroll expanders [28,30,35,36], screw expanders [29,33,60], rolling piston expanders [34] and vane expanders [38]. Redial turbines, axial turbines, and impulse turbines are also used as expanders in some experimental studies of ORC [27,31,37]. The optimized parameters used inlet temperatures, inlet pressure, heat load and outcome parameters behaviour are considered to maximize the output [61,62]. It has been concluded from the study that 6 system parameters, including temperature and pressure at the evaporator outlet, temperature and pressure at the condenser inlet, expander shaft efficiency and working fluid pump efficiency, play important roles in the ORC net power output and thermal efficiency [63]. Some literature suggested that hermetic scroll expanders are widely adopted for small-scale ORC systems to produce electricity [64]. An ORC experimental setup using R123 as the working fluid and heat source temperature 130°C to 160°C affects in increased net work from 0.44 kW to 0.55 kW and efficiency from 6.71% to 8.72% [65]. Similar performance improvements were noted with higher cooling water flow rates [65]. Similarly, small-scale ORC experiment is performed with R123 under various cooling conditions and cooling water mass flow rate and obtained a maximum thermal efficiency of 5.30%, turbine isentropic efficiency of 75.2% at a water flow rate of 0.591 kg/s [66]. Research has emphasized the importance of selecting suitable working fluids and configurations to enhance ORC performance. It has also been validated experimentally that for low-temperature heat sources, simple ORC produces greater expander work output than complex ORC with R123 working fluid [67]. Experimental studies of a 0.3 kW micro-ORC system using R1233zd-E as the working fluid, featuring a likely world's smallest scroll expander, revealed optimum power generation and thermal efficiency of 0.266 kW and 7%, respectively when compared with other small-scale ORC systems [68]. The study reveals that pentane is effective working fluids, achieving net electric efficiencies ranging from 3.1% to 7.1%, across 2.7–6.0 pressure ratios in air-cooled waste heat systems [69]. Liu et al. [70] explored the effects of different working fluid charge levels on key system parameters under off-design conditions, concluding that overcharging the working fluid slightly enhances expander output power. The volumetric expanders are a good option for small to medium-sized ORC systems because of their inexpensive cost, slow rotation speed, and two-phase operation capability. The most common types of volumetric expanders are scroll expanders [71], vane expanders [72], screw expanders [73], and piston expanders [74] are used in ORC for power generation. Experimental studies have been performed on many types of volumetric expanders and a study shows that up to 77% isentropic expander efficiency can be obtained with a scroll expander of R245fa working fluid [75]. Many experimental studies showed that a scroll expander is the best choice for small-scale power generation and the evaporator's inlet and outlet condition are critical parameters and its fluctuations are hard to maintain at steady-state conditions and give direct fluctuation results on expander inlet mass flow rate [71,76]. It has been proven that the maximum net power output condition will be achieved at the saturated vapor state of the expander inlet [77]. So, to find the optimum condition of maximum net power output, a separator is required before the expander inlet to get the pure vapor at saturated vapor condition to generate maximum power. Liang and Yu [77] conducted a lab-scale investigation of an ORC system and revealed that maintaining a superheat degree of zero at the expander inlet yielded optimal performance, with a maximum electric power output of 0.61 kW and a thermal efficiency of 4.09% at a heat source temperature of 96.8°C. Some studies investigated the experimental parametric study of pressures, temperatures, and mass flows and projected them as performance indicators on net power output and cycle efficiency [78,79]. Zhou et al. [80] found that cycle efficiency, expander output power and exergetic efficiency increase with the evaporating pressure and heat source temperature, while the superheat degree of the working fluid has negative effects on system performance. At the optimized condition the maximum cycle efficiency and net output power of the expander are 8.5% and 645 W, respectively, with R123 working fluid [80]. Wang et al. [40] established a small-scale ORC experimental apparatus utilizing a scroll expander to investigate the thermodynamic performance under varying turbine inlet pressures, rotational speeds, and cooling water flow rates. Their findings indicated that both thermal and exergy efficiencies increased with higher turbine inlet pressures and cooling water flow rates at R245fa, R141b working fluid. Feng et al. [81] experimentally examined the effect of pump outlet pressure, expander inlet temperature and mass flow rate on net power output and thermal efficiency and found that the net power production shows an increasing trend as the mass flow rate rises, whereas the thermal efficiency produces a smooth tendency. Wronski et. al. [82] have done the experiment at evaporation temperatures ranging from 125 °C to 150 °C and condensation temperatures ranging from 20 °C to 40 °C and found maximum net power 2.5 kW of electricity with an isentropic efficiency of approximately 70%. Bademlioglu et al. [83] numerically analyzed the factors influencing system performance using the Taguchi and ANOVA methods, concluding that the evaporator and condenser temperatures, as well as turbine efficiency, significantly affected system thermal efficiency, however, $PPTD_{evap}$, $PPTD_{con}$ and pump efficiency were least effective. Tauveron et al. [84] validate optimization models for both the ORC's condenser and evaporator application when hot and cold source temperature variation occurs, along with experimentally validating that 50% reduction in the power output associated with a 20°C increase in the cold source temperature. There is less work done on life cycle assessment (LCA) on ORC scroll expander-based experimental setup. Some researchers have done LCA on ORC using R134a and R1234ze [85]. Some experiments have been performed on R245fa working fluid at the superheated state of distributed power plants of 1-2 kW and managed to get the thermal efficiency of range 5-7% [79,86]. Hijriawan et.al [87] produce power from ORC experimental setup at 10 °C condenser temperature by employing R134a working fluid but at higher pressure. For the easy comparison of experimental ORC cycles following Table 1.1 is drawn which has main focus on components, fluids, power output, thermal efficiency along with type of ORC (saturated/superheated).

Table 1.1. Literature review of experimental ORC's

Year & Authors	Working Fluid	Expander	Condenser, Cooling Fluid	Pump	Evaporator, Heating Fluid	Capacity	Cycle Efficiency	Configuration
2013 Zheng et. al [74]	R245fa	Rolling-piston expander	Plate heat exchanger, water	Diaphragm metering pump	Plate heat exchanger, water	0.35 kW	5%	NA
2014 Zhang et. al [29]	R123	Single-screw expander	Multi-channel parallel type, Forced air	Multistage centrifugal pump	Spiral-tube	10.38 kW	6.48%	NA
2015 Miao et.al [30]	R123	Scroll	Plate heat exchanger, water	Piston pump	Tube-in-tube, oil	4 kW	6.39%	Superheated ORC

2016 Lei et.al [60]	R123	Single screw expander	Finned air condenser, air	Multistage centrifugal pump	Shell and tube, NA	8.35 kW	7.98%	Superheated ORC
2017 Li et.al [37]	R245fa	Turbo expander	Finned-tube condenser, forced air	Variable speed pump	Plate heat exchanger, thermal oil	NA	3.44%	Superheated ORC
2017 Pang et.al [32]	R245fa, R123 and their mixtures	Scroll	Plate heat exchanger, Water	Plunger	Plate heat exchanger, Oil	1.56 kW (1:0) , 1.66 kW (2:1)	4.4%	Superheated ORC
2017 Shao et.al [66]	R123	Radial inflow expander	Brazed plate heat exchanger, Water	Diaphragm pump	Brazed plate heat exchanger, Thermal oil	1.24 kW	5.2%	Superheated ORC
2018 Zhao et.al [88]	R123	Single screw expander	Shell and tube, Water	Rotary pump	Shell and tube, Oil	3.27 kW	3.04%	NA
2019 Wronski et.al [89]	n-pentane	Reciprocating piston	Brazed plate heat exchan	Air-driven piston pump	Brazed plate heat exchanger, Oil	2.5 kW	~14%	NA

			ger, Water					
2020 Usmaan et.al [86]	R245fa	Scroll	Brazed plate heat exchanger, Water	Screw type pump	Brazed plate heat exchanger, Water	0.967 kW	7.36%	Superheated ORC
2021 Li et.al [90]	R245fa	Scroll	Plate heat exchanger, Oil	Piston pump	Plate heat exchanger, Water	1-2 kW	4.9% - 5.7%	Superheated ORC
2022 Hijriawan et.al [87]	R134a	Scroll	Spiral tube-type, Water	Scroll compressor	Spiral tube-type, Refrigeration system	584.5 W	3.17%	Superheated ORC

Based on the above literature review, experimental studies were performed mostly at the expander inlet superheated state (although it produces less expander power output when compared with saturated vapor state at the same expander inlet pressure). To the best of the author's knowledge and literature review, no experimental study was performed on R601a (isopentane) working fluid despite having numerically proven great potential in waste heat recovery. No previous ORC experimental study optimizes the condition for maximum power output and experimentally validated it with data driven numerical analysis along with prediction of ORC performance. The previous experimental studies also lack in comprehensive parametric analyses involving simultaneous variations in heat load, source fluid flow rate, and sink fluid inlet temperature.

1.2.4. Case study of NPP

Nuclear power plants generally have 33-35% efficiency and dispose 60% of waste heat into nearby waterbeds and air. In some cases where disposed waste heat can be used for fish farming, farm cultivation and desalination purposes but in most cases, these are disposed of in the environment due to the remote location of NPP's (Nuclear power plants) site [91]. Heat is released from the condensation of steam into a heat sink (i.e., seas, lakes, and air) [92]. There are several techniques for waste heat utilization from NPP [93]. Indian NPP having 300-MWe AHWR releases its waste heat from the main condenser, MHT (main heat transport) purification system and heat exchangers of moderator cooling system and feed water system make ideal NPP site to study the waste heat utilization for power generation [93,94]. However, several experimental and numerical studies showed the potential of ORC technology to harness power from a range of low-medium grade waste heat sources [89]. ORC system's performance is highly dependent on the working fluid used, heat source, and heat exchanger technology [95]. ORC is well-suitable with solar thermal-based collector technologies and has been demonstrated to be a dependable technology capable of efficiently trans forming low-to-medium-level heat sources into useable uses [96]. Despite having some limitations with ORC technology, environmental benefits and payback period also play a crucial role in decision-making [97]. On the other hand, NPP produces no direct CO_2 emission and if ORC is combined with NPP, then no significant effect in CO_2 emission will obtain. Nanofluid has recently emerged as an improved heat transfer fluid for WHR [98]. Nanoparticles enhance thermal conductivity in base fluids by creating nanofluid, resulting in a higher heat transfer rate. Hence, the overall performance of WHR system will be enhanced by using nanofluids. Plate heat exchangers with improved thermal conductivity of nanofluids experience faster heat transfer rates [99].

Despite extensive research on ORC systems for low and medium-grade waste heat recovery, significant gaps remain in harnessing nuclear power plant waste heat, particularly moderator and MHT purification system heat. Nuclear plants typically operate at 33–35% efficiency and discharge about 60% of their heat into the environment. While some waste heat is used for secondary applications, much is wasted due to remote locations. There is a clear need to design and optimize ORC systems operating at source temperatures of 60–70°C and sink temperatures around 30°C, potentially incorporating nanofluids, plate heat exchangers, and scroll expanders to efficiently generate electricity and reduce cooling losses.

1.3. Research Gaps

Based on the above literature reviews, the author found below research gaps.

- No study compares all the low-medium grade heat recovery power cycles on the basis of thermodynamic, economic, environmental and technical perspectives.

- No technical and economic comparison was made between the heat recovery power cycle and solar P-V photovoltaic panels with battery storage for better selection.
- A comparative study based on energy, exergy, economics, and environmental factors of ejector-enhanced novel ORC modifications is missing in a single platform.
- The optimum ratio of an azeotropic mixture of working fluid and novel working fluids analyses is missing in numerical studies as well as experimental studies.
- No such economic model for the power cycle was used in literature, which can fulfill the interest of the consumer as well as the industry simultaneously.
- Experimental parametric performances of ORC were missing for simultaneous variation of heat load, source fluid flow rate and sink fluid inlet temperature.
- The lack of separators to ensure saturated vapour at the expander inlet hinders accurate net power output calculations in an experimental study.
- Comparative experimental analyses of volumetric expanders under diverse conditions are insufficient, and sensitivity studies on system performance parameters are limited.
- ORC's experimental study contains various research gaps, like life cycle assessment (LCA), working fluid development, system stability, and design optimization. Conventional and Machine learning-based optimization and prediction of performance parameters of ORC experimental data is missing.
- No real application-based feasibility analyses of case studies have been done using numerical and experimental validation along with estimated capability for power generation from waste heat sites.
- A complete 4E study and the effect of hot oil-based nanoparticle performance on ORC working fluid is missing at a case study of a real waste heat recovery site.

1.4. Objectives and Novelty

The author identified the objectives below based on the research gaps mentioned above.

- Six thermodynamic power cycles (ORC with dry fluid, ORC with wet fluid, CO_2 Rankine cycle, Kalina cycle, OFC and TFC) have been compared on energy, exergy, economic and environmental basis to select the best power cycle for waste heat recovery. Parametric and techno-economic analyses have been performed for all cycles to generate the maximum power from low-medium grade heat sources.
- Comparative studies of two novel ejector-coupled advanced ORCs have been proposed to further enhance the performances of output parameters and complete 4E analyses at

optimized conditions have been done. A new economic model has also been introduced for consumer and manufacturer benefits.

- ❖ A lab-scale experimental ORC setup using isopentane (R601a) has been developed and various parametric performances have been analysed. A tailor-made separator has been fabricated and installed to get a saturated vapor condition at the turbine inlet. RSM-ANOVA has been used to optimize and predict performance parameters.
- ❖ A feasibility analysis, along with a complete thermodynamic and economic analysis has been done on the Indian nuclear power plant site for potential power generation and waste heat recovery. ORC parametric study (variations of condenser temperature and cold fluid inlet temperature) was taken in the case study. The performance of a dry ORC power cycle using nanofluid as hot fluid with various organic working fluids has been analysed for a real waste heat recovery site.

The novelties of the present study are as follows: (i) 4E analysis and techno-economic comparison of all possible thermodynamic power cycles have been conducted for the low-medium grade waste heat recovery, (ii) Two novel ejector-enhanced ORCs have been presented, followed by 4E analysis, to generate maximum power, (iii) A novel combination of scroll expander with isopentane working fluid is tested with ORC experimental setup under various operating conditions, (iv) Tailored made separator has been used in the ORC experimental setup, which plays an essential role for more power generation and (v) A feasibility study, along with parametric analyses, has been done to implement ORC technology for waste heat recovery from Indian nuclear power plant.

1.5. Thesis structure

The present thesis has been organized into seven chapters.

Chapter 1 includes the background and motivation, literature reviews, research gaps, thesis objective and novelty.

Chapter 2 contains the identification and comparison of low-medium waste heat source-based thermal power cycle. In this chapter, six possible waste heat recovery cycles (Dry ORC, Wet ORC, CO_2 Rankine cycle, Kalina cycle, Organic flash cycle and Trilateral flash cycle) were studied to find the best possible cycle.

Chapter 3 provides the numerical analysis of two novel ejector-enhanced ORC. The influence of different working organic fluids on the cycle is also analysed in each modification to draw maximum work output.

Chapter 4, includes a detailed design and development of the lab-scale ORC setup by including component details, fabrication process, and sensors used. The effect of heat load, the volume flow rate of hot fluid and cold fluid inlet temperature were simultaneously studied. Optimization and prediction are also done to find out the best condition at which both net power and thermal efficiency are maximized.

Chapter 5 consists of a detailed case study of an Indian nuclear power plant. A feasibility analysis has been done to find out the location of the waste heat source for maximum power generation at maximum profit. The effect of using nano-oils as heat source fluid for the ORC is also investigated.

Chapter 6 concludes the significant findings of the present investigation and possibilities for future work.

Chapter 2: Power Cycles for Low-Medium Grade Heat Recovery

The present analysis considers power generation from low- and medium-grade heat sources, including renewable and waste energies. Low/medium grade heat sources are solar collector heat, geothermal heat, industrial waste heat, heat absorbed by moderators and cooling rods in nuclear power plants, etc. Solar collectors (flat plate, evacuated tube, compound parabolic concentrator, parabolic trough collector, linear Fresnel reflector and parabolic dish) have a wide range of indicative temperatures (50-250°C). Typically, geothermal heat sources have a temperature range of 70-90°C but can be increased to 150°C in some places. Depending on the industrial process, the temperature of the waste heat varies widely, spanning a range of around 50°C to 1000°C [100]. The low/medium-grade waste heat can be used to drive the various thermodynamic power cycles and analysis is required to find the best option.

2.1. Cycle Description

In this study, 6 thermodynamic power-producing cycles are compared for low-medium-grade heat recovery. The essential components of the system are the evaporator/heater, turbine, condenser and pump. These cycles are differentiated by method and desired state of heating of the working fluid in the evaporator/heater.

2.1.1. ORC using dry fluid

ORC is the most popular thermodynamic cycle used for low-medium-grade heat recovery. Layout and temperature-entropy diagram of ORC using dry working fluid (isopentane) are shown in Figure 2.1. The pressurized isopentane is heated in an evaporator till saturated vapor state 3 and then is allowed to expand in a turbine to a superheated state 4. Working fluid gets exited from the turbine at state 4 and condenses to saturated liquid state 1. A counter-flow evaporator is used to heat the working fluid from the pump exit (state 2) to the saturated vapor state 3, passing by saturated liquid state 3l. From the turbine expansion state 3 to 4, the net work is generated.

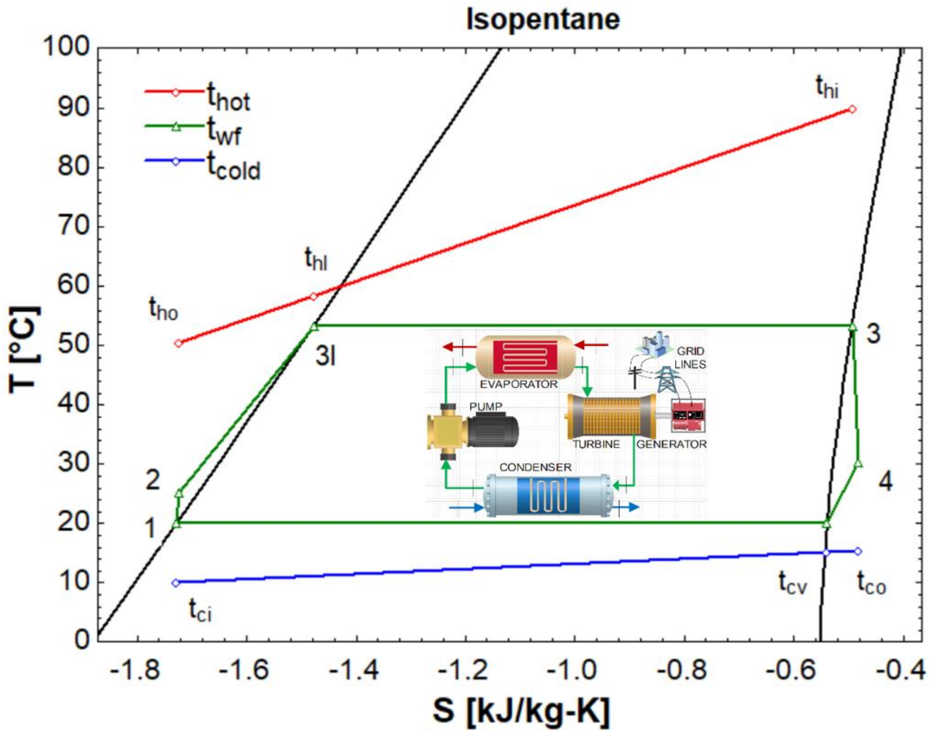

Figure 2.1. Layout and T-s diagram of ORC with dry working fluid

2.1.2. ORC using wet fluid

Likewise, ORC using dry working fluid the ORC using wet working fluid also performs in the same way; only the difference is that ammonia is heated in the evaporator up to superheated state 3, passing by saturated liquid (state 3l) and saturated vapor state (state 3v). Work output is produced due to working fluid expansion in the turbine from superheated state 3 to saturated vapor state 4. For practical uses, turbine exit state 4 is kept slightly superheated to avoid turbine blade damage due to moisture/liquid droplets. The rest of the working states are the same as ORC with dry fluid (Figure 2.2).

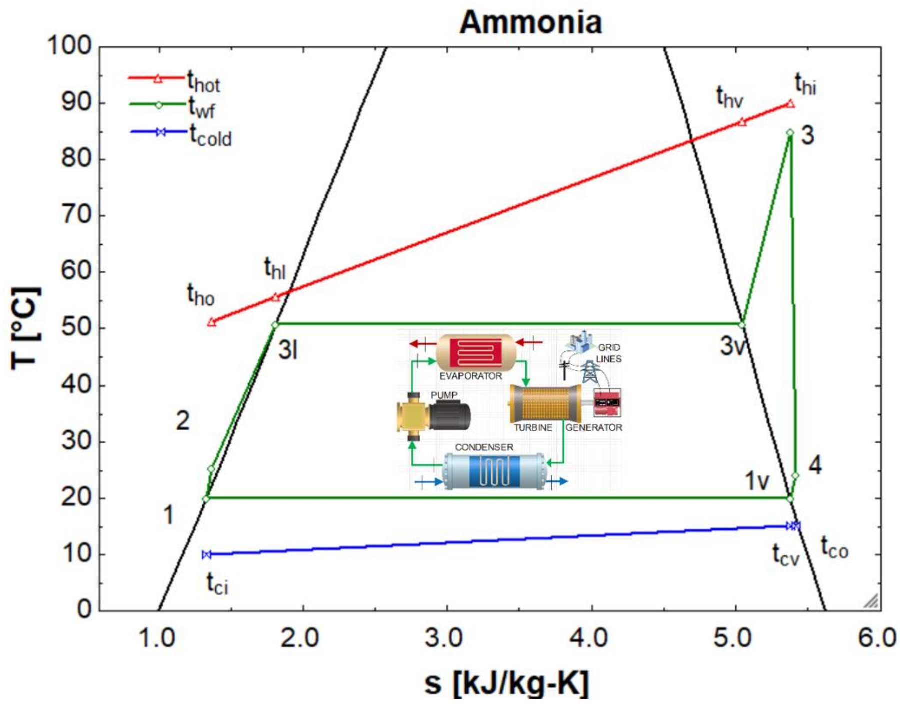

Figure 2.2. Layout and T-s diagram of ORC with wet working fluid

2.1.3. CO_2 Rankine cycle

Figure 2.3 presents the transcritical CO_2 Rankine cycle. In the evaporator, the carbon dioxide working fluid with supercritical pressure (state 2) is heated to the supercritical vapor (state 3) by the energy dis- charged from the heat source. The vapor of high pressure and temperature is subsequently expanded through the turbine from state 3 to superheated state 4 to generate electricity. Due to the available low temperature of low-grade heat sources, CO_2 transcritical power cycle will be more promising to be adopted than CO_2 Brayton cycle due to its relatively lower system pressure and high expansion ratio.

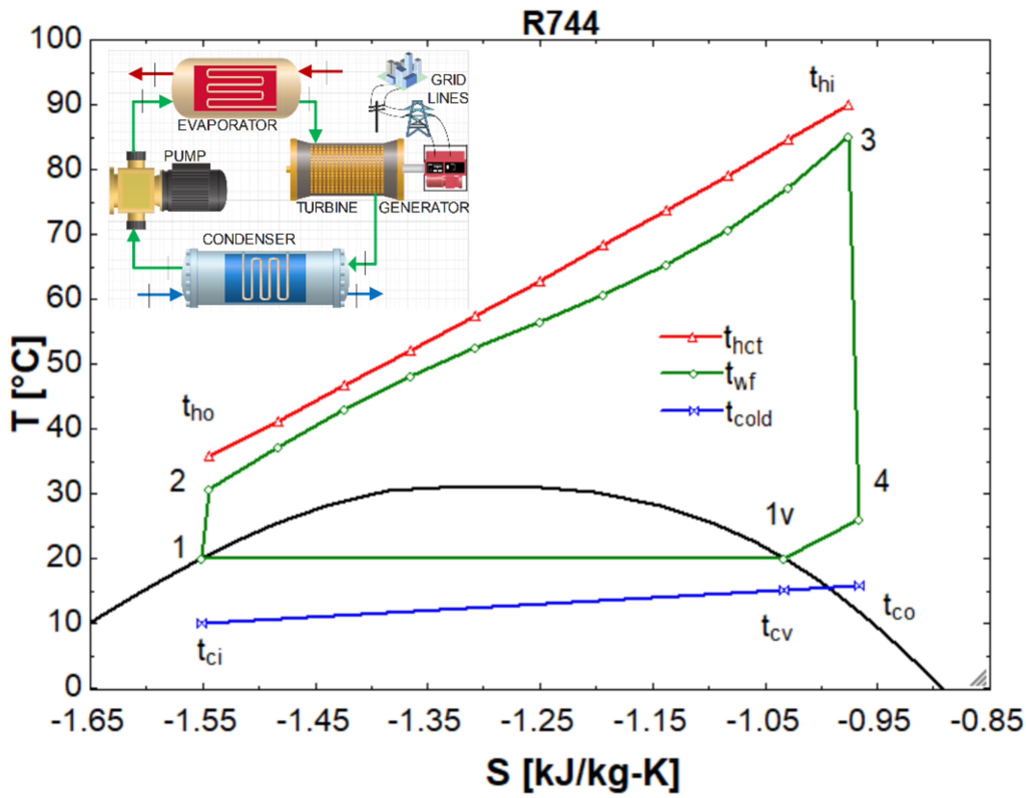

Figure 2.3. Layout and T-s diagram of CO_2 Rankine cycle

2.1.4. Kalina cycle

The working fluid for the Kalina cycle is a mixture of two fluids (ammonia and water mixture) with various boiling points. More heat can be removed from the source than with a pure working fluid because the solution boils over a wider temperature range during distillation. The exhaust (condensing) end is the same. It can be clearly seen from Figure 2.4 schematic layout diagram embedded in T-s diagram that the separator, throttling valve, recuperator and mixture have extra components besides ORC basic components. The boiling point of the working solution can be modified to meet the heat input temperature by selecting the proper ratio between the solution's components. The most popular combination is water and ammonia, while additional combinations are possible. In Figure 2.4, the working fluid is pumped from states 1 to 2, then released heat from the lean mixture (from states 6 to 8) is absorbed by pumped fluid from state 2 to state 3 in the recuperator. Recovery heat is added to the system from the evaporator (states 3 to 4). From state 4, a separator is used to separate rich (state 5) and lean mixture (state 6). The rich mixture from state 5 is then expanded in the turbine to state 7 and then mixed up with the lean mixture at state 10. Fluid is now condensed from state 10 to 1 in the condenser by cold fluid.

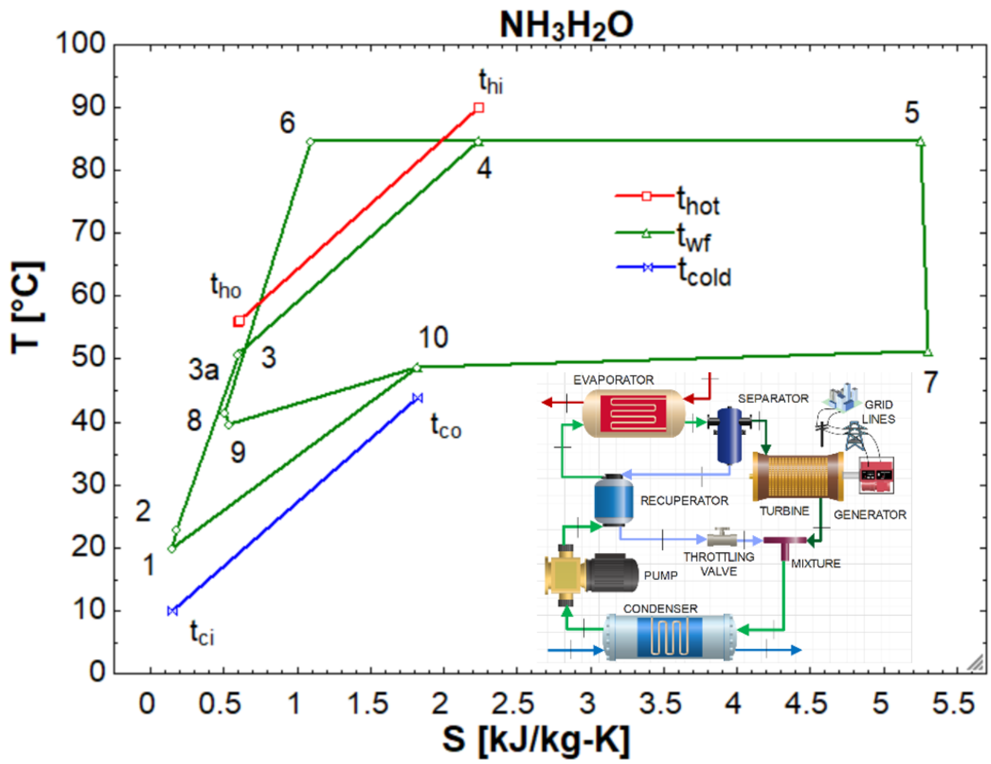

Figure 2.4. Layout and T-s diagram of Kalina cycle

2.1.5. Organic flash cycle

A schematic layout and temperature-entropy diagram of OFC are given in Figure 2.5. The main difference between OFC and ORC is to heat the working fluid as isopentane in the evaporator up to a saturated liquid state. Before entering the turbine, the heated working fluid gets throttled from saturated liquid state 3 to state 4 for depressurizing and then the wet working fluid gets separated at state 4 into liquid (state 5) and vapor (state 6) phases. The vapor phase is allowed to expand in turbine superheated state 7 and power is produced. Throttled fluid from state 6 and expanded fluid from state 7 is then mixed in the mixing chamber at state 9 and then condensed by cold fluid to state 1.

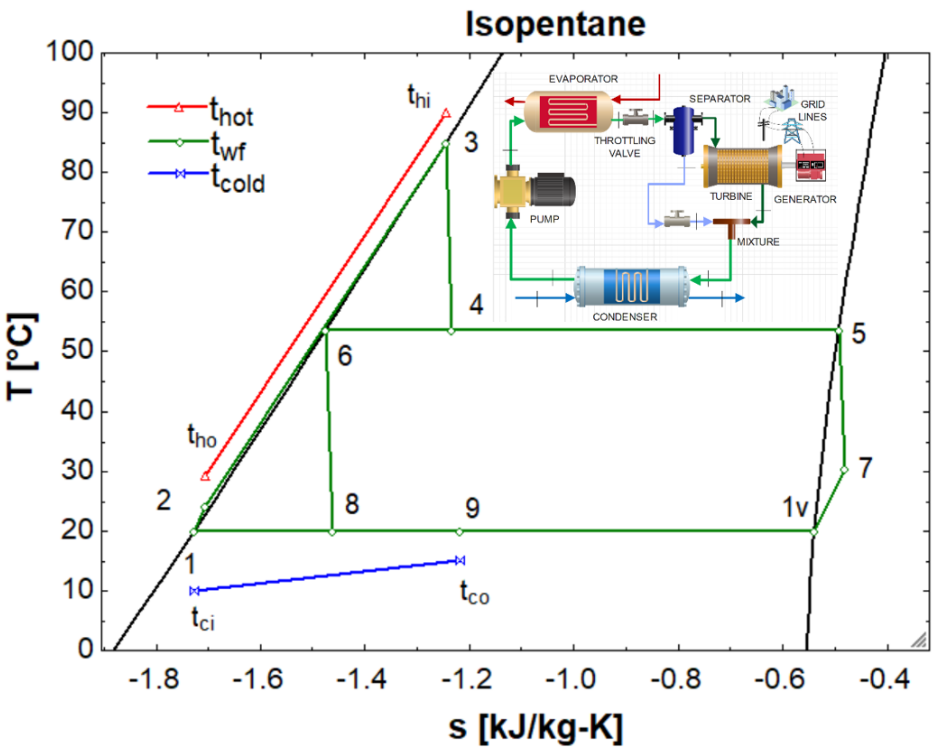

Figure 2.5. Layout and T-s diagram of OFC

2.1.6. Trilateral flash cycle

The T-s diagram of a typical TFC system, which is nothing more than a modified ORC system where the working fluid's (Isopentane) phase transition in the heat exchanger has been skipped (states 2 to 3), as shown in Figure 2.6. Additionally, the expansion in TFC is a two-phase flash expansion (state 3 to 4), contrary to an ORC's single-phase expansion. The processes in the condenser and pump are the same as ORC.

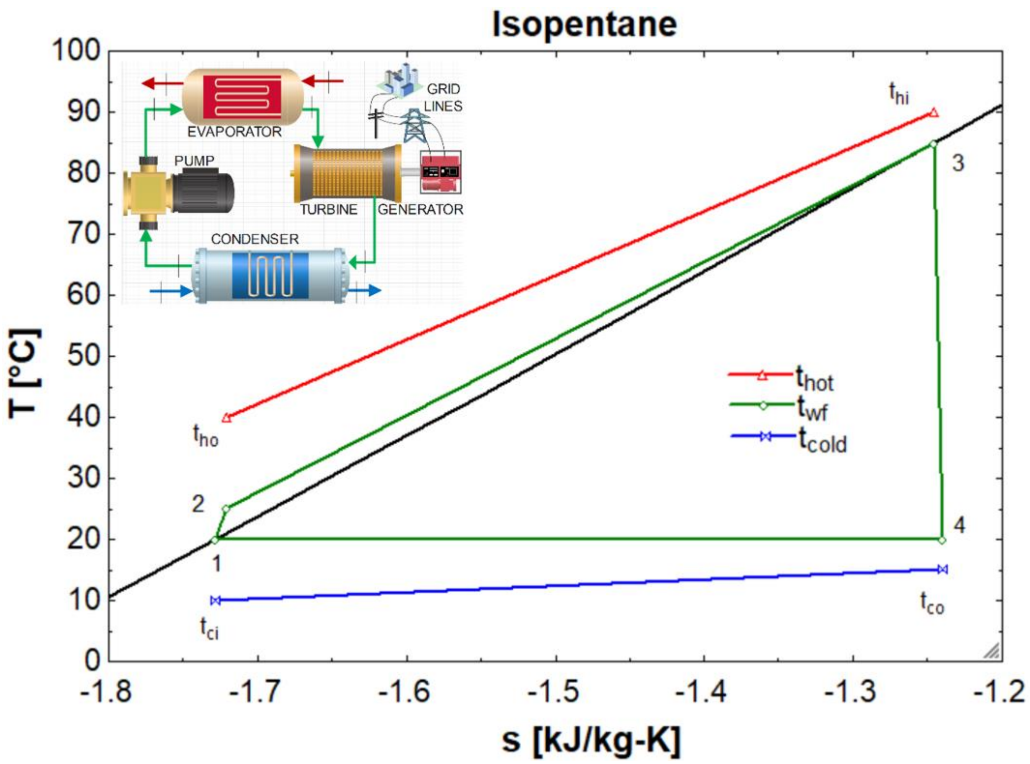

Figure 2.6. Layout and T-s diagram of TFC

2.2. Methodology

2.2.1. Mathematical Modelling

The best-performing cycle among possible heat recovery cycles based on thermodynamics (mass, momentum and energy equations), economics and environmental point of view. The following assumptions were taken into consideration while evaluating the cycles in the simplified form [55–57]:

(i) Pressure drop is neglected in all heat exchangers and connecting tubes.

(ii) No heat loss from components to the environment is taken into consideration.

(iii) Atmospheric pressure and temperature are taken as 101.325 kPa and 30 °C.

(iv) The condenser outlet and evaporator inlet are in a saturated liquid state and the evaporator outlet is in a saturated vapor state.

(v) The turbine, pump and nozzle have given isentropic efficiencies.

(vi) PPTD of the heat exchanger is taken into consideration while designing the evaporator, preheater and condenser.

(vii) The selling price and carbon credit price are taken as constant for the studied range of heat source temperature.

Based on the above assumptions, the following equations are framed to analyze the cycle performance. PPTD is considered to calculate the intermediate minimum temperature difference in the evaporator and condenser:

$$T_{hf,l} = T_{wf,sl} + PPTD_{evp} \tag{2.1}$$

$$T_{cf,v} = T_{wf,sv} - PPTD_{con} \tag{2.2}$$

Energy balance in the two-phase and preheating section of the evaporator, respectively:

$$Q_{in,wet} = \dot{m}_{hf} c_{p_{hf,wet}} \left(T_{hf,in} - T_{hf,l}\right) = \dot{m}_{wf}\left(h_{evp,wet,out} - h_{evp,wet,in}\right) \tag{2.3}$$

$$Q_{in,sub} = \dot{m}_{hf} c_{p_{hf,sub}} \left(T_{hf,l} - T_{hf,out}\right) = \dot{m}_{wf}\left(h_{evp,sub,out} - h_{evp,sub,in}\right) \tag{2.4}$$

Hence total heat input to the cycle is given by,

$$Q_{in} = Q_{in,wet} + Q_{in,sub} \tag{2.5}$$

The energy balance of the condenser is given by:

$$Q_{con} = \dot{m}_{cf} c_{p_{cf}} \left(T_{cf,out} - T_{cf,in}\right) = \dot{m}_{wf}\left(h_{con,in} - h_{con,out}\right) \tag{2.6}$$

Turbine work is calculated as:

$$W_{tur} = \dot{m}_{wf,tur}\left(h_{tur,in} - h_{tur,out}\right) = \dot{m}_{wf,tur}\left(h_{tur,in} - h_{tur,out,ise}\right)\eta_{tur} \tag{2.7}$$

Pump work is calculated as:

$$W_{pump} = \dot{m}_{wf}\left(h_{pump,out} - h_{pump,in}\right) = \dot{m}_{wf} \frac{\left(h_{pump,out,ise} - h_{pump,in}\right)}{\eta_{pump}} \tag{2.8}$$

Hence, the net work output is calculated as:

$$W_{net} = W_{tur} - W_{pump} \tag{2.9}$$

Cycle thermodynamic efficiency is calculated as:

$$\eta_{th} = \frac{W_{net}}{Q_{in}} \tag{2.10}$$

Exergy in and out of the ORC system can be calculated as:

$$Ex_{in} = \dot{m}_{hf} c_{p_{hf}} \left[\left(T_{hf,in} - T_{hf,out}\right) - T_{amb} \ln\left(\frac{T_{hf,in}}{T_{hf,out}}\right)\right] \tag{2.11}$$

Equations of the irreversibility of various components are listed in Table 2.1.

Table 2.1. Component irreversibility calculation

Components	Irreversibility
Pump	$I_{pump} = \dot{m}_{wf} T_{amb}\left(s_{pump,out} - s_{pump,in}\right)$
Turbine	$I_{tur} = \dot{m}_{wf,tur} T_{amb}\left(s_{tur,out} - s_{tur,in}\right)$
Condenser	$I_{con} = \dot{m}_{wf}\left[\left(h_{con,in} - h_{con,out}\right) - T_{amb}\left(s_{con,in} - s_{con,out}\right)\right]$

Evaporator	$I_{evp} = Ex_{in} - \dot{m}_{wf}\left[\left(h_{evp,out} - h_{evp,in}\right) - T_{amb}\left(s_{evp,out} - s_{evp,in}\right)\right]$
Ejector	$I_{eje} = T_{amb}\left(\dot{m}_{wf}s_{con,in} - \dot{m}_{wf,tur}s_{tur,out} - \dot{m}_{wf,eje}s_{eje,in}\right)$

Now, the overall exergy balance is given by:

$$Ex_{in} = W_{net} + I_{pump} + I_{tur} + I_{evp} + I_{con} + I_{sep} + I_{mix} + I_{thrt} \tag{2.12}$$

Then, the exergy efficiency is calculated as:

$$\eta_{ex} = \frac{W_{net}}{Ex_{in}} \tag{2.13}$$

The turbine size parameter can be calculated as [18]:

$$SP = \frac{\left(\dot{m}_{wf,tur}v_{tur,out,ise}\right)^{0.5}}{\left[\left(h_{tur,in} - h_{tur,out,ise}\right) \times 1000\right]^{0.25}} \tag{2.14}$$

Table 2.2. Heat exchanger area design

Heat exchanger	Area	Overall convective heat transfer coefficient
Preheater	$A_{evp,sub} = \frac{1000Q_{in,sub}}{U_{evp,sub}lmtd_{evp,sub}}$	$\frac{1}{U_{evp,sub}} = \frac{1}{\alpha_{evp,sub,hf}} + \frac{t_{plate}}{k_{plate,evp,sub}} + \frac{1}{\alpha_{evp,sub,wf}}$
Evaporator	$A_{evp,wet} = \frac{1000Q_{in,wet}}{U_{evp,wet}lmtd_{evp,wet}}$	$\frac{1}{U_{evp,wet}} = \frac{1}{\alpha_{evp,wet,hf}} + \frac{t_{plate}}{k_{plate,evp,wet}} + \frac{1}{\alpha_{evp,wet,wf}}$
Condenser	$A_{con} = \frac{1000Q_{con}}{U_{con}lmtd_{con}}$	$\frac{1}{U_{con}} = \frac{1}{\alpha_{con,wf}} + \frac{t_{plate}}{k_{plate,con}} + \frac{1}{\alpha_{con,cf}}$

The preheater, evaporator and condenser are assumed as the plate heat exchanger. The enlargement factor and plate spacing are taken as 1.17 and 5 mm, respectively. The calculation of the overall convective heat transfer coefficient and area of different heat exchangers is given in Table 2.2. The total area of the evaporator (A_{evp}) is the combination of the evaporator and preheater areas.

The convective heat transfer coefficient of single-phase fluid can be calculated using Muley's correlation [101,102] at $\beta = \pi/4$:

$$\alpha_{sp} = \frac{k_{plate}}{D_{eq}}\left[0.44\left(\frac{6\beta}{\pi}\right)^{0.38} Re_{eq}{}^{0.5} Pr^{\frac{1}{3}}\left(\frac{\mu}{\mu_{wall}}\right)^{0.14}\right] \tag{2.15}$$

The convective heat transfer coefficient of two-phase fluid can be calculated using Yan-Lin's correlation [102]. Where x, ρ and D_{eq} are dryness fraction, density and equivalent diameter correspondingly:

$$\alpha_{dp} = \frac{k_{plate}}{D_{eq}}\left[1.926 Re_{eq}{}^{0.5} Pr^{\frac{1}{3}} Bo_{eq}{}^{0.3}\left\{1 - x + \left(\frac{\rho_{sl}}{\rho_{sv}}\right)^{0.5}\right\}\right] \tag{2.16}$$

Table 2.3. Capital investment of system components [103,104].

Component	Capital investment ($)
Evaporator	$Z_{evp}^{CI} = 130\left(\frac{A_{evp}}{0.093}\right)^{0.78}$
Condenser	$Z_{con}^{CI} = 130\left(\frac{A_{con}}{0.093}\right)^{0.78}$
Pump	$Z_{pump}^{CI} = 3540\left(W_{pump}\right)^{0.71}$
Turbine	$Z_{tur}^{CI} = 6000(W_{tur})^{0.7}$

Correlations for capital costs of the evaporator (including preheater), condenser, pump and turbine are given in Table 2.3. The overall hourly cost rate (sum of capital investment and operation and maintenance costs) of the k^{th} component can be associated as follows:

$$\text{Total cost rate, } T\dot{C}_k = \frac{Z_k^{CI} CRF \phi}{z} \tag{2.17}$$

$$\text{Capital recovery factor, } CRF = \frac{i(1+i)^N}{(1+i)^N - 1} \tag{2.18}$$

Where maintenance factor ø = 1.06, and annual working hour z = 7000 h.

The total cost consumed rate of running ORC is the sum of the overall hourly cost rate of all ORC components and the total cost earned rate is the product of the net amount of electricity generated and cost per unit of electricity. For this study, the average electricity cost per unit in India is 0.132 $/kWh (10 Rupees/kWh) [105–107]. Electricity cost may be varied rapidly by country, rural/urban, state, government/private owned, industries/domestic, etc.

$$T\dot{C}_{consumed} = \sum T\dot{C}_k \tag{2.19}$$

$$T\dot{C}_{earned} = W_{net} C_{ele} \tag{2.20}$$

Total hourly profit, ($/h) when the ORC system is running at the optimum condition:

$$\text{Profit}_{\text{total}} = \text{T}\dot{\text{C}}_{\text{earned}} - \text{T}\dot{\text{C}}_{\text{consumed}} \tag{2.21}$$

Per unit hourly profit ($/kWh) when the ORC system is running at the optimum condition:

$$\text{Profit}_{\text{unit}} = \left(\frac{\text{T}\dot{\text{C}}_{\text{earned}} - \text{T}\dot{\text{C}}_{\text{consumed}}}{\text{W}_{\text{net}}}\right) \tag{2.22}$$

Environmental analysis of the ORC system is based on the amount of CO_2 saved. CO_2 saving means the amount of CO_2 generated when the same amount of power is generated from the coal-fired power plant. The input energy required to produce the same amount of power:

$$\text{E}_{\text{annual,in}} = \frac{3600\text{W}_{\text{net}}\text{z}}{\eta_{\text{th}}} \tag{2.23}$$

The NCV (net calorific value) is 4500 kcal/kg for Indian coal (carbon weight percentage as 50%). Amount of annual CO_2 production if required energy is obtained from burning of coal:

$$\text{CO}_{2\text{AP}} = \left(\frac{44}{12}\right)(0.5)\frac{\text{E}_{\text{annual,in}}}{\text{NCV}} \tag{2.24}$$

This technology requires no cost-intensive heat input because all the required heats are collected from the waste heat source, which are to be wasted otherwise. The cost associated with CO_2 saving in terms of carbon credit can benefit power plant industries through international and governmental environmental agencies. CO_2 saving cost per ton varies rapidly with demand. In this paper, the average CO_2 saving cost is taken as 10 $/ton [108].

$$\text{CO}_2 \text{ saving cost} = \frac{\text{CO}_{2\text{AP}}\text{C}_{\text{CO}_2}}{1000\text{z}} \tag{2.25}$$

The payback period helps to determine how long it takes to recover the initial costs associated with an investment. The shorter payback an investment has, the more attractive it becomes, which means it would take less time to break even. It tends to be more useful in industries where investments become obsolete very quickly and where a full return on the initial investment is, therefore, a serious concern. As the payback period does not consider the time value of money, it becomes a less predictable tool to assess an investment. The time value of money has been considered in the discounted payback period (DPP), which is the amount of time that it takes for the initial cost of a project to equal the discounted value of expected cash flows or the time it takes to break even from an investment. It is the period in which the cumulative net present value of a project equals zero.

$$DPP = years\ before\ break\ even + \frac{unrecovered\ amount}{Discounted\ cash\ flow\ in\ recovery\ year} \tag{2.26}$$

$$Discounted\ cash\ flow = \frac{C_n}{(1+i)^n} \tag{2.27}$$

The Levelized Cost of Energy (LCOE) can be calculated by first taking the net present value of the total cost of building and operating the power-generating asset divided by the total electricity generation over its lifetime. LCOE is the per-unit cost of generating energy (usually electricity) for a particular system. It is an economic assessment of the cost of the energy-generating system, including all the costs over its lifetime: initial investment, operations and maintenance, cost of fuel, and cost of capital. The LCOE can be used to determine whether a project will be a worthwhile venture. The basic economics metric for any generating plant is the levelized cost of electricity (LCOE). If LCOE is less than the price at which production may be sold, the project is at least marginally profitable and should be further examined to see whether it is a sensible investment. On the other hand, the project is not a good long-term investment if the LCOE exceeds the price at which power may be supplied. In addition, the LCOE assesses if a project will be profitable or reach a break-even point.

A spreadsheet-based model for calculating LCOE was developed and can be calculated as follows:

$$\mathrm{LCOE} = \frac{\sum_{n=1}^{n} \frac{\left(Z_n^{CI} + OM_n + F_n\right)}{(1+i)^n}}{\sum_{n=1}^{n} \frac{W_{net,n}}{(1+i)^n}} \tag{2.28}$$

$$F = \frac{FC * W_{net}}{\eta_{th}} \tag{2.29}$$

Where: F = Fuel cost and FC is the fuel cost per unit of energy input. In this case, FC is taken as zero due to boiler heat up from NPP waste heat energy.

OM = Operation and maintenance cost, which is 6% of capital investment.

The internal rate of return (IRR) is a metric used in financial analysis to estimate the profitability of potential investments. IRR is a discount rate that makes the net present value (NPV) of all cash flows equal to zero in a discounted cash flow analysis. IRR calculations rely on the same formula as NPV does. The internal rate of return (IRR) is the annual rate of growth that an investment is expected to generate. The ultimate goal of IRR is to identify the rate of discount, which makes the present value of the sum of annual nominal cash inflows equal to the initial net cash outlay for the investment. IRR is ideal for analyzing capital budgeting projects to understand and compare potential rates of annual return over time. In addition to being used by companies to determine which capital projects to use, IRR can help investors determine the investment return of various assets. If the IRR is greater than the required rate of return (discount rate), the investment is considered attractive because it generates returns higher than the cost of capital.

$$\sum_{n=1}^{n} \frac{C_n}{(1+IRR)^n} - C_o = 0 \tag{2.30}$$

Where: C_n = net cash inflow during period y

C_o = NPV of total investment cost

IRR= Internal rate of return

Worldwide emissions of carbon dioxide (CO_2) from burning fossil fuels total about 34 billion tons per year. About 45% of this is from coal, about 35% from oil and about 20% from gas. Nuclear power reactors do not produce direct carbon dioxide emissions. Unlike fossil fuel-fired power plants, nuclear reactors do not produce air pollution or carbon dioxide while operating. For both nuclear and renewable generation, emissions are produced indirectly, for example, during the construction of the plant. Over its life cycle, nuclear produces about the same number of CO_2-equivalent emissions per unit of electricity as wind and about one-third that of solar [109,110]. 1kg of CO_2 can be expressed as 0.27 kg of carbon, as this is the amount of carbon in the CO2. Nuclear power plants do not produce carbon dioxide directly during operation. However, there are some emissions associated with the mining, processing, and transportation of uranium, as well as the construction and decommissioning of nuclear power plants. According to the IPCC 2015 report, 18 grams of CO_2 are produced from 1 kWh of power generation [109].

Standard amount of CO_2 emission from NPP's = 18 g/kWh (2.31)

2.2.2. Simulation and Validation

Based on the above mathematical models, the simulation code has been developed in Engineering Equation Solver (EES) for each thermodynamic power cycle. The code can predict the cycles' performance for the given heat source, heat sink, ambient temperature, and component efficiencies. PPTD is defined effectively when designing the evaporator and condenser. All physical and thermodynamic properties of considered fluids are calculated using an in-built subroutine in software. All cycles have been optimized for maximum net work output using the in-built Nelder–Mead method. Nelder–Mead technique is a heuristic search method that has been chosen due to its working range in multidimensional space and application to nonlinear optimization problems for which derivatives may not be known. For dry ORC, wet ORC and TFC thermodynamic cycles, evaporator pressure is optimized for each heat source temperature. CO_2, Kalina and OFC thermodynamic cycles are optimized considering two parameters simultaneously at each heat source temperature. The CO_2 cycle is optimized on the degree of superheat and evaporator pressure parameters to such a limit that the corresponding evaporator temperature would be lower than the critical temperature of the CO_2 cycle to avoid the use of a compressor after the pump. Kalina cycle is optimized on ammonia-water mixture ratio and evaporator pressure parameters. OFC is optimized by considering separator pressure and evaporator pressure parameters. Further, sink temperature is also varied to know the effect on net work output for each cycle. The heat exchanger area is calculated to determine the capital investment cost. Economic analysis is performed on the software to analyze the best thermodynamic cycle suited to give more power and profit. Figure 2.7 represents the flow chart of the whole simulation process.

Codes of thermodynamic cycles have been validated by experimental/simulation values taken from various references presented in Table 2.4. Net work, thermal efficiency, exergy efficiency, evaporator pressure, heat exchanger area and total cost have been validated for all 6 low-medium grade heat source thermodynamic cycles by possible data available from individual experimental/simulation reference values. The variation in evaporator pressure across all six thermodynamic cycles is attributed to the calibration and range limitations of the pressure measurement instruments. However, the observed error remains within an acceptable range. Similarly, other key parameters influencing net work, thermal efficiency, and exergy efficiency, such as mass flow rate and temperature, are measured using a mass flow meter and RTD sensor, respectively. These measurements inherently exhibit some degree of deviation between simulation and experimental results. Despite these variations, all six thermodynamic cycles demonstrate reliability for further analysis.

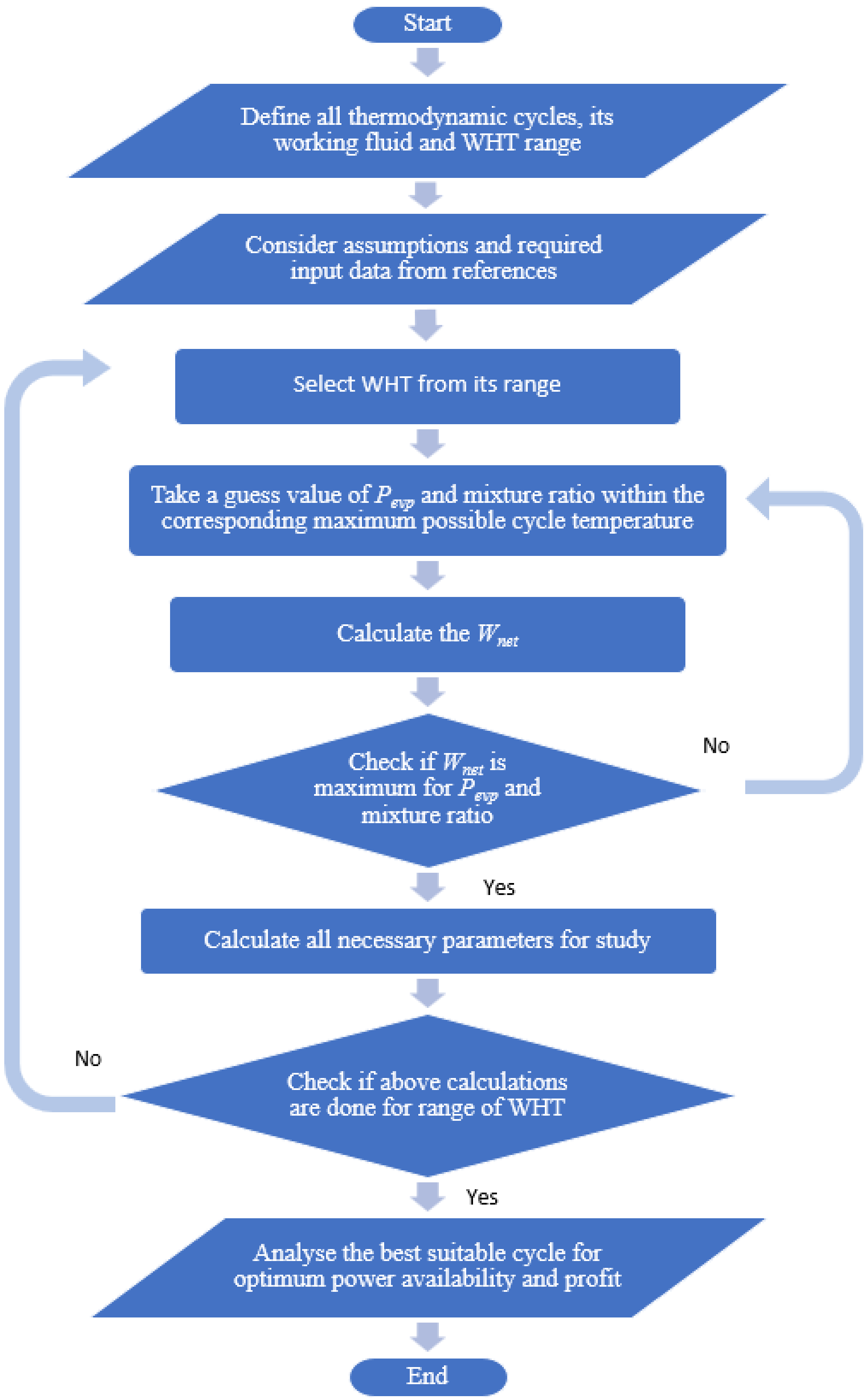

Figure 2.7. Flow chart of the simulation procedure

Table 2.4. Validation of different low/medium grade thermodynamic cycles

Parameter	ORC (dry fluid)		ORC (wet fluid)		CO_2 cycle		Kalina cycle		OFC		TFC	
	Reference Values	Simulated values	Reference Values	Simulated values	Reference Values	Simulated values	Reference Values	Simulated values	Reference Values	Simulated values	Reference Values	Simulated values
Net work [kW]	66.98 [38]	68.70	1800 [111]	1870	199.1 [21]	201.7	3401 [112]	3367	-	-	0.212 [43]	0.213
Thermal efficiency (%)	2.59 [38]	2.59	8.47 [111]	8.44	6.5 [21]	6.45	-	-	5.90 [113]	5.87	1.661 [43]	1.663
Exergy efficiency (%)	-	-	47.6 [111]	46.8	56.8 [21]	57.6	44.21 [112]	43.85	31.43 [113]	31.88	24.64 [43]	24.60
Evaporator pressure [kPa]	225 [38]	217	2797 [111]	2705	13723 [21]	13978	4170 [112]	4125	2352 [113]	2406	124.8 [43]	124.8

2.3. Results and Discussion

Table 2.5 lists the input parameters for the comparison of thermodynamic cycles for low-medium-grade heat sources. The hot fluid mass flow rate is chosen in a way that work output can be analysed numerically and can be scaled further by scaling the mass flow rate. The reference is given for all additional input parameters. The thermodynamic properties of the working fluid, viz. critical temperature, pressure, and environmental factors, are provided in Table 2.6. Selected working fluids should adhere to the ASHRAE safety groups and have a lesser tendency to deplete the ozone layer and contribute to global warming.

Table 2.5. Input parameters used for different thermodynamic cycle analyses

Input parameter	Value	Input parameter	Value
Source inlet temperature	90°C	Annual working hour	7000 h
Cold source inlet temperature	10°C	Number of annuities received	20 year
Condenser temperature	20°C	Annual Interest rate	10%
Ambient temperature	15°C	Spacing between heat exchanger's plates	5 mm
Hot fluid mass flow rate	10 kg/s	Thickness of heat exchanger's plates	0.5 mm
$PPTD_{evp}$	5°C [114]	Length of heat exchanger's plates	150 mm
$PPTD_{con}$	5°C [114]	Diameter and height of storage tank	30 cm, 70 cm
Pump efficiency	0.8 [115]	1 ton carbon credit value	10 $ [1]
Turbine efficiency	0.9 [116]	1 unit (kWh) of electricity cost	0.132 $ [2]

Table 2.6. Fluid properties for different thermodynamic cycles

Working fluid	2-Methylbutane	CO_2	NH_3
Alternative name	R601a (Isopentane)	R744 (Carbon dioxide)	R717 (Ammonia)

Cycle used	ORC (dry fluid), TFC, OFC	Transcritical CO_2 cycle	ORC (wet fluid), Kalina cycle
Critical temperature [°C]	187.2	31.1	132.5
Critical pressure [MPa]	3.37	7.37	11.3
Normal boiling point [°C]	27.85	-78.5	-33.3
Triple point temperature [K]	112.65	216.5	195.4
ODP	0	0	0
GWP (100 years)	5	1	0

2.3.1. Performance comparison

Table 2.7 compares performance for the investigated mean input values (Table 2.5) for various low/medium grade thermodynamic power cycles. The heat source temperature of 90°C is selected for the comparative analysis of different thermodynamic cycles. Power-producing cycles have different values at different parameters. The maximum and minimum values of each parameter are highlighted in orange and green color, respectively, for easy comparison.

At 90°C heat source temperature, the maximum net work output is maximum for CO_2 cycle, but it also has the highest pump work required because of the thermodynamic property of the CO_2 working fluid. Due to CO_2 thermodynamic property, the cycle operates at comparatively higher evaporator and condenser pressures, which increases the cost of each component and, thus, total capital investment increases. Although CO_2 cycle produces maximum work output but due to the highest total capital investment cost among other power-producing cycles, the profit earned is not maximum. Similarly, payback period and discounted payback period is maximum for CO_2 cycle, which is not favourable from investor point of view. On the other hand, TFC has lesser work output but gives maximum profit because of the working fluid and operating pressure range. TFC also saves the maximum carbon emission when the heat source is replaced from fossil fuel to waste heat or renewable energy source and thus earns maximum carbon credit.

Table 2.7. Comparison of optimized result outputs of various thermodynamic cycles at a source temperature of 90°C

Parameter	**Dry ORC**	**Wet ORC**	**CO_2**	**Kalina**	**OFC**	**TFC**

W_{net} [kW]	55.35	54.83	75.07	40.36	50.48	62.94
W_p [kW]	0.51	1.25	51.18	0.6	6.03	6.03
W_{tr}[kW]	55.86	56.08	126.2	40.96	56.51	68.97
P_{co} [kPa]	76.6	857.8	5729	223.8	76.6	76.6
P_{evp} [kPa]	225.9	2071	12474	616.1	514.7	514.7
η_{th} (%)	8.27	8.36	8.29	6.99	4.72	5.88
η_{ex} (%)	51.7	51.9	59	41.9	37.4	46.7
Ex_{in} [kW]	107.1	105.7	127.2	96.36	134.8	134.8
I_{total} [kW]	51.77	50.87	52.16	56	84.37	71.91
$\dot{m}_{cold}$ [kg/s]	27.93	28.44	35.12	3.76	48.71	48.11
*$\dot{m}_f$ [kg/s]	1.68	0.5	4.84	1.02	6.82	6.82
Q_{in} [kW]	669	656.2	905.1	577.5	1070	1070
T_{max} [°C]	53.3	85	85	85	85	85
Total C.I. [$]	114532	115402	264723	100658	143970	159061
A_{con} [m^2]	8.76	7.14	13.6	10.49	9.04	8.94
A_{evp} [m^2]	14.6	12.68	67.7	28.96	77.7	77.71
Profity [$/year]	36885	36294	36402	24762	28721	38356
$Profit_{y,co2}$ [$/year]	53299	52396	58611	38933	54975	64609
Total cost consumed [$/h]	2.04	2.05	4.71	1.79	2.56	2.83
Total cost earned [$/h]	7.31	7.24	9.91	5.33	6.66	8.31
Payback period [year]	3.1	3.2	7.3	4.1	5	4.1
Discounted payback period [year]	3.7	3.8	11.3	5.1	6.7	5.2
CO_2 annual saving [ton]	1641	1610	2221	1417	2625	2625
Coal saving [ton]	895	878	1211	773	1432	1432
Earned Carbon credit [$/h] ($CO_2$ saving cost)	2.35	2.3	3.17	2.02	3.75	3.75

* $\dot{m}_f$ is the part of working fluid which is going in the turbine to produce work. For Kalina and OFC cycle whole working fluid mass flow rate does not contribute to work production.

Figure 2.8 represents the component irreversibility of different power-producing cycles at 90°C heat source temperature. It can be seen that cycle irreversibility depends upon the different components dominating its irreversible value. OFC has maximum irreversibility value due to dominating component of the throttling valve and highest exergy and lowest exergy efficiency value. Similarly, TFC and Kalina cycle has turbine and condenser dominating irreversible component, respectively. The evaporator influences the irreversibility of ORC with both working fluids. It can be seen that among all power cycles, the CO2 cycle has a very balanced component's irreversibility.

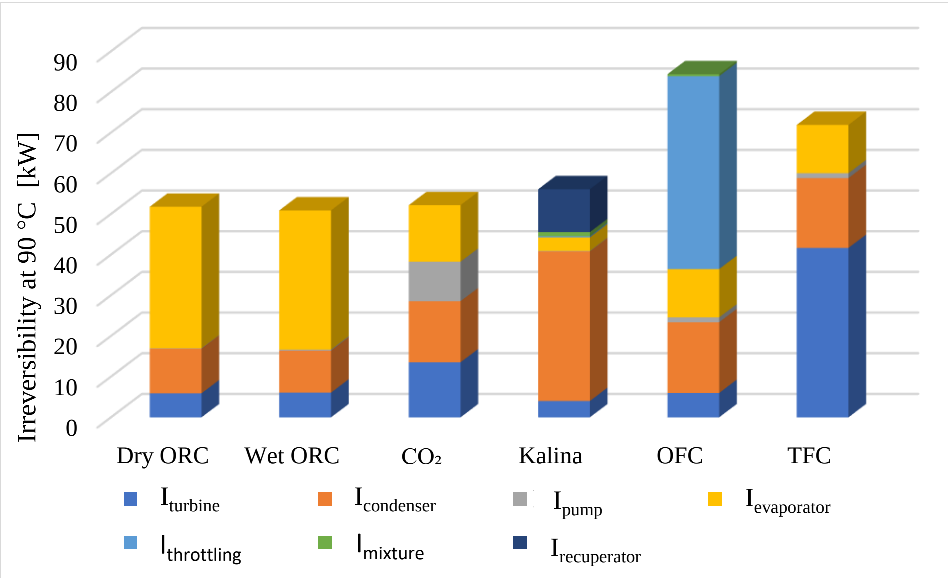

Figure 2.8. Component irreversibility of different cycles at 90°C

Complete exergy analysis can be understood by a donut chart, which represents the fraction of work obtained and individual component irreversibility (Figure 2.9) at 90°C heat source temperature. OFC has minimum work share and maximum irreversibility, as depicted in Figure 2.8 and Table 2.7. However, the net work output of OFC is greater than that of the Kalina cycle due to the highest working fluid mass flow rate and exergy. CO_2 cycle has maximum work share in exergy and can be seen in Table 2.7 as well. Due to the maximum work produced, CO_2 cycle has a maximum exergy efficiency value. TFC has the highest exergy and working fluid mass flow rate. Although having a lesser percentage share of work, its numerical value is more than both ORC's and comes after CO_2 cycle. The net work share of the Kalina cycle is greater than that of OFC.

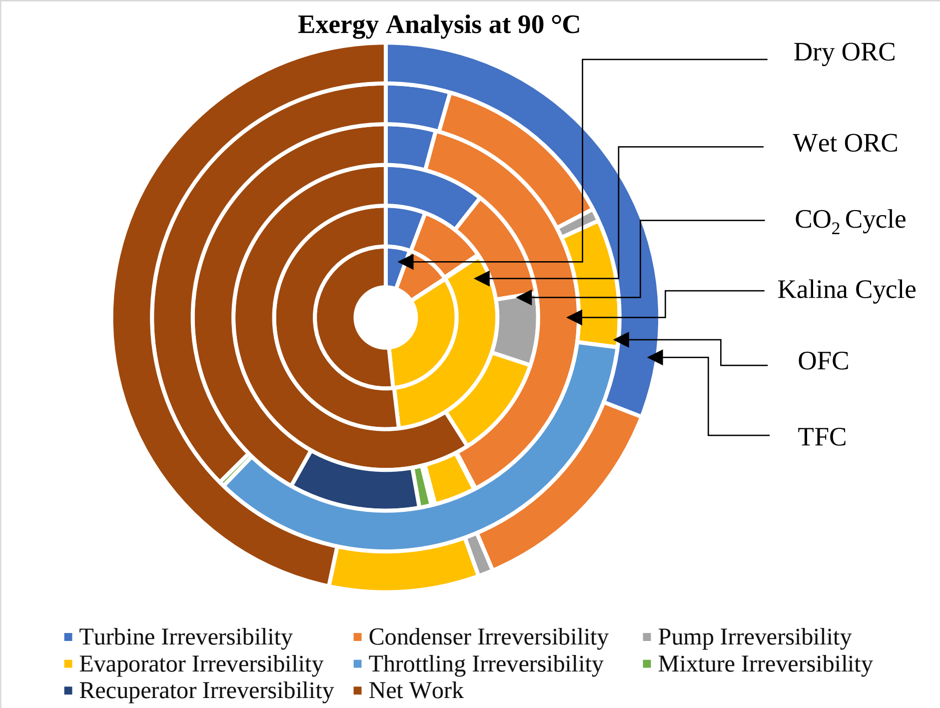

Figure 2.9. Exergy analysis of different cycles at 90°C source temperature

2.3.2. Parametric study

Figure 2.10 shows the net work output of different power cycles with heat source temperature. Net work output depends upon the difference of specific enthalpy difference of turbine and pump work and the corresponding cycle mass flow rate. Net work output increases with increasing the heat source temperature because the amount of heat added to the evaporator is high and so higher the working fluid enthalpy at the turbine inlet (evaporator exit). Higher turbine inlet enthalpy is the main dominating factor in to increase in net work output. It can be observed that up to 100°C CO_2 cycle has maximum net work output and after that TFC remains highest because of the high operating turbine higher and lower pressure. ORC with dry fluid, ORC with wet fluid and OFC have the same trend and almost have the same value of work output through the range of heat source temperature but lower than TFC. Kalina cycle is the least-performing cycle for work production.

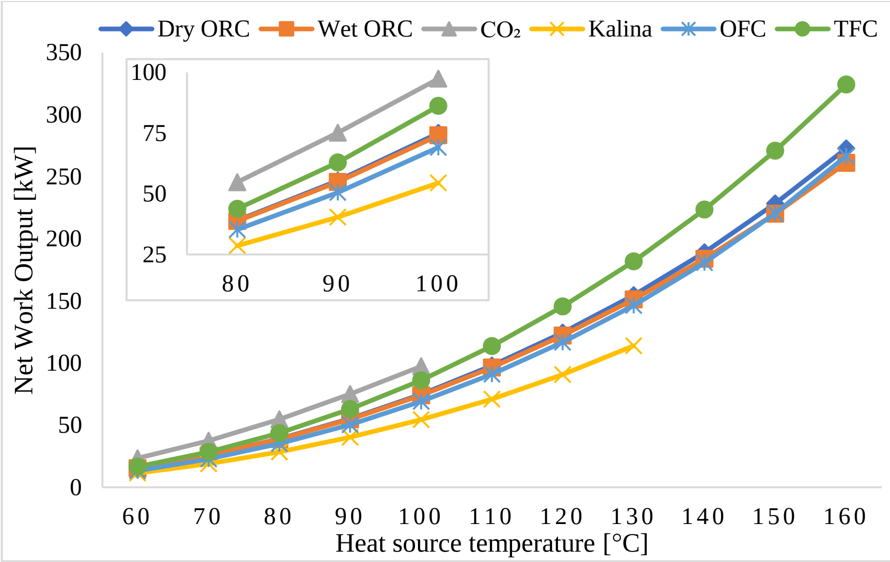

Figure 2.10. Variation of net work output with heat source temperature

Figure 2.11 represents the thermal efficiency of the power cycle with heat source temperature. It can be concluded that, at maximized work output conditions, ORC with dry fluid, ORC with wet fluid and CO_2 cycle have almost same efficiency at lower heat source temperature range and ORC with wet fluid shows maximum efficiency at higher heat source temperature range. ORC with wet fluid has maximum efficiency for all ranges of heat source temperature because of the minimum irreversibility and two PPTD locations in the evaporator section. TFC has the lowest efficiency because of the highest heat input required at the same condition.

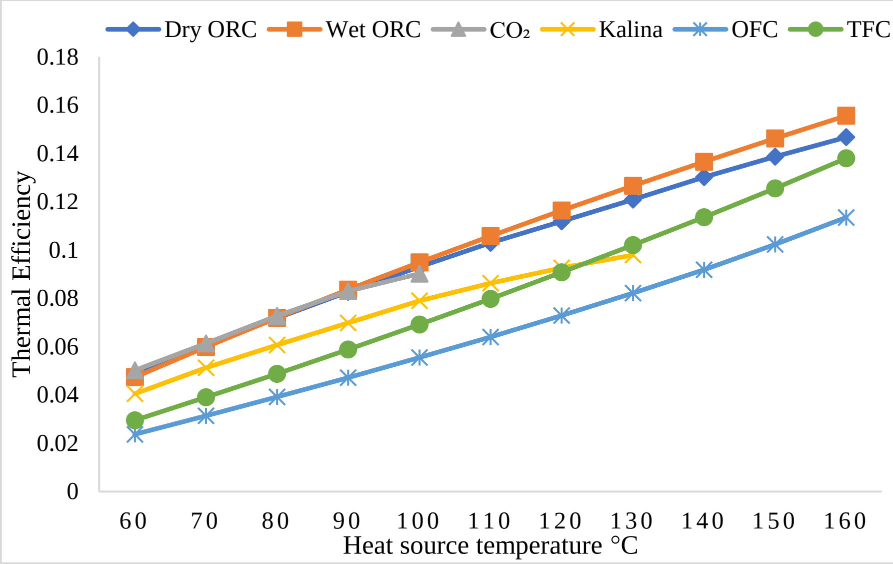

Figure 2.11. Variation of thermal efficiency with heat source temperature

Figure 2.12 shows the variation of exergy efficiency along with heat source temperature. The exergy efficiency of all cycles increases with heat source temperature. CO_2 has maximum exergy efficiency for low-grade temperature due to a good match of evaporator temperature profile and operating at higher pressure. Apart from the highest exergy efficiency rate of TFC, dry and wet ORC comes before TFC for low-grade temperature range and after 120°C TFC exergy efficiency becomes superior. TFC has saturated liquid conditions at turbine entry and higher exergy, making it a less effective system for a low heat source temperature range.

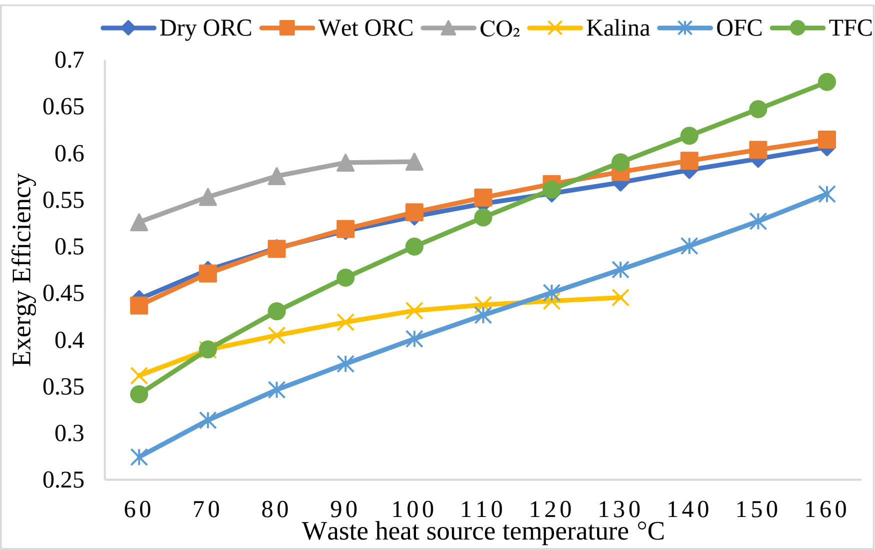

Figure 2.12. Variation of exergy efficiency with heat source temperature

Figure 2.13 shows the variation of the total annual cost required for different cycles with heat source temperature. Total annual cost increases with heat source temperature for all cycles. CO_2 cycle has a higher jump for all temperature ranges because of its operation at higher pressure, which requires more material for the component to withstand pressure. TFC and OFC follow the same trend, but TFC has a higher value due to the production of more power. Both ORC's have almost the same value at all temperature points. Kalina cycle requires the lowest total cost to run the plant at the same condition because of the lowest value of heat transfer, work output, exergy, and cold fluid mass flow rate among all cycles.

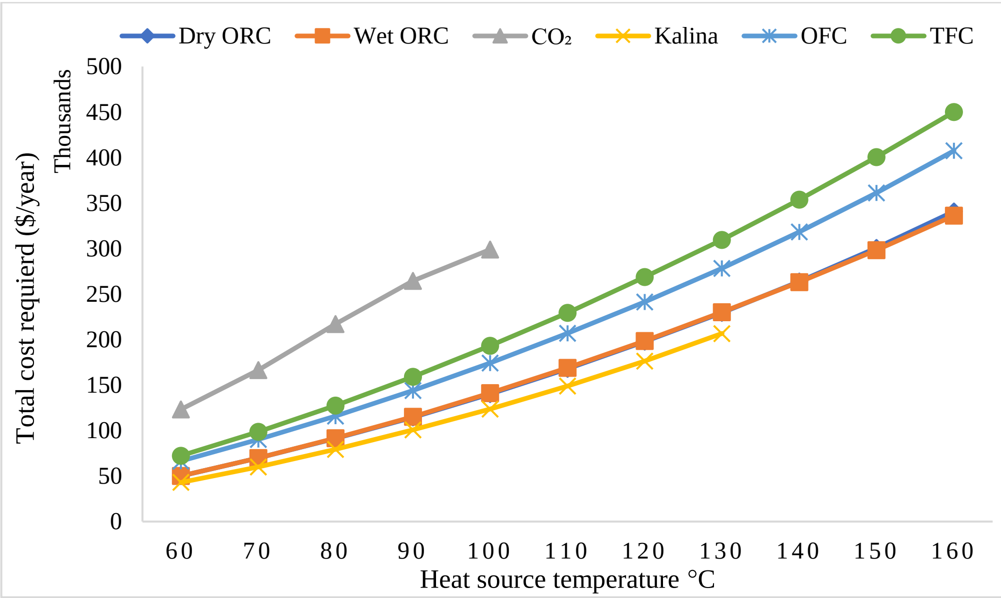

Figure 2.13. Variation of annual total cost required with heat source temperature

Figure 2.14 shows the variation of total annual profit for different cycles with heat source temperature. It can be clearly concluded that TFC gives the best result among all cycles for all range of temperature ranges, even when CO_2 cycle produces more work output than TFC at low-grade temperature ranges. TFC gives maximum profit because of its simple design and medium average cycle operation pressure. Apart from Kalina cycle, CO_2 cycle and OFC and both ORC's gives comparable profit.

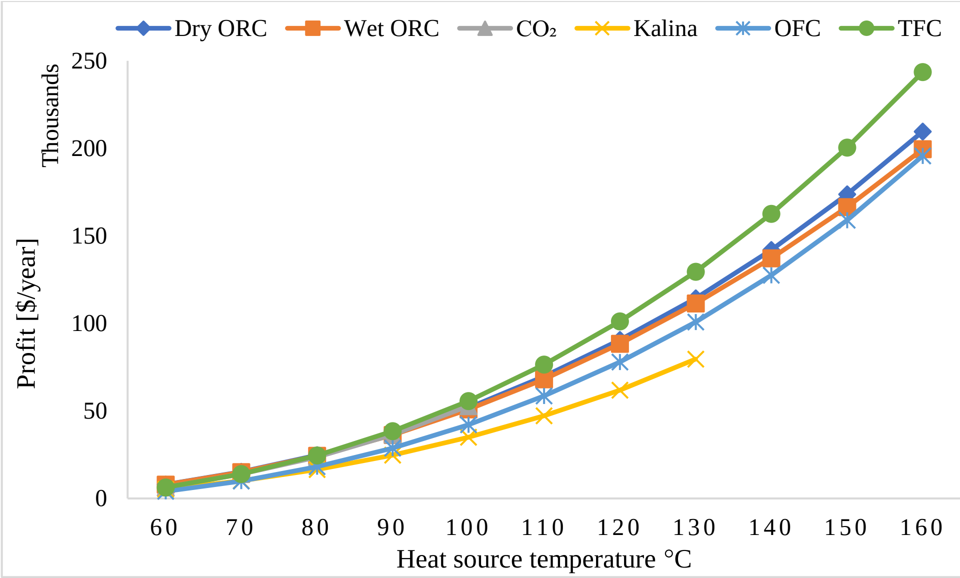

Figure 2.14. Variation of total annual profit with heat source temperature

Figure 2.15 shows the variation of annual CO_2 gas saving from different cycles with heat source temperature. This paper considers the heat source temperature, which can be obtained from industrial exhaust/waste release gas to ambient, solar collector, nuclear power plant cooling, geothermal energy, etc. If this energy source is utilized in the evaporator to heat the fluid instead of a conventional source of energy, then the following cycle can save CO_2 gas, which has to be released ultimately if a conventional heat source is used. It is very clear from Figure 2.15 that TFC saves the maximum amount of CO_2 gas if the same power is to be produced from TFC using the conventional source of energy, i.e., coal, petroleum, etc.

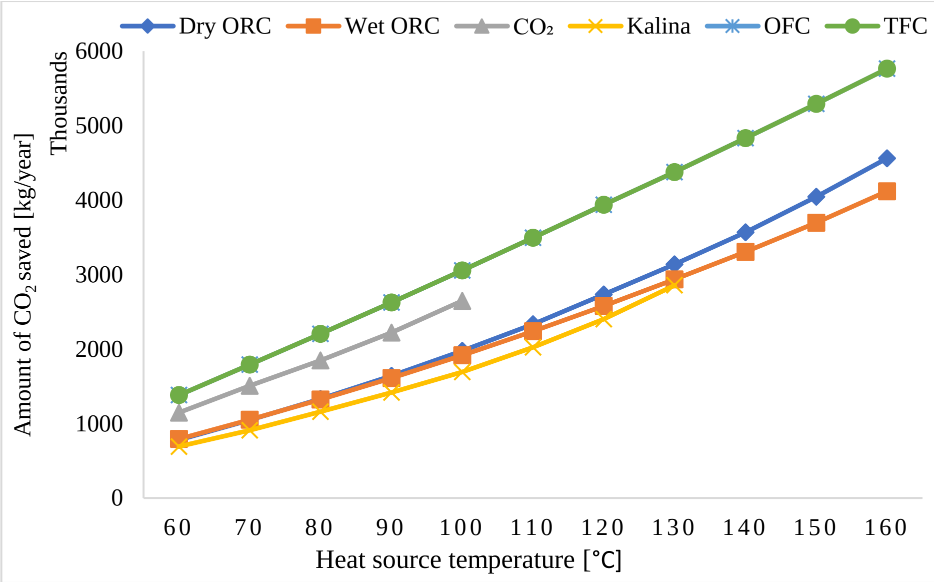

Figure 2.15. Variation of annual CO_2 saving with heat source temperature

2.3.3. Effect of condenser temperature

All cycles are analyzed at 90°C heat source temperature by increasing and decreasing the condenser temperature by 3°C from the original condenser temperature of 20°C. 90°C heat source temperature is chosen because of easy comparison with respect to data acquired in Table 2.8 for 20°C condenser temperature, considering CO_2 Rankine cycle behaviour at critical temperature. It can be seen from Table 2.8 that by increasing or decreasing the condenser temperature by the same amount (3°C) from base condenser temperature (20°C), the % change in each output parameter of their respective cycle will be almost the same other than the CO_2 cycle. By decreasing the CO_2 cycle condenser temperature, its effect will be favourable and maximum amongst all cycles, but due to closeness from the critical temperature, if the condenser temperature increased a little, then its performance would adversely change that is because of the getting closer to the critical temperature. The TFC also has a significantly favourable change when the condenser temperature is lowered.

Table 2.8. Effect of increasing and decreasing the T_{con} by 3°C on output parameters at a source temperature of 90°C

Thermodynamic cycle	T_{con} (°C)	Evaporator pressure (kPa)	W_{net} (kW)	Thermal Efficiency (%)	Total Irreversibility (kW)	Turbine inlet mass flow	Total cost ($)	Profit earned ($)

						rate (kg/s)		
Dry ORC	23	235.4	49.96	7.87	53.34	1.61	107140	32824
	20	225.9	55.35	8.27	51.77	1.68	114532	36885
	17	216.7	61.06	8.68	49.71	1.74	122097	41217
Wet ORC	23	2179.0	49.57	8.02	51.83	0.48	108183	32331
	20	2071.0	54.83	8.36	50.87	0.50	115402	36294
	17	1966.0	60.37	8.69	49.48	0.52	122739	40500
CO_2	23	10242.0	55.32	6.12	71.81	4.89	202297	25896
	20	12474.0	75.07	8.29	52.16	4.84	264723	36402
	17	12069.0	85.08	8.77	45.88	4.81	272269	44673
Kalina	23	616.1	36.92	6.76	61.96	1.05	93723	21833
	20	616.1	40.36	6.99	56.00	1.02	100658	24762
	17	616.1	43.93	7.24	48.78	0.99	108026	27810
OFC	23	514.7	45.16	4.51	90.12	7.04	135994	25036
	20	514.7	50.48	4.72	84.37	6.82	143970	28721
	17	514.7	55.96	4.94	78.24	6.57	152277	32621
TFC	23	514.7	56.59	5.53	76.69	6.82	149949	33618
	20	514.7	62.94	5.88	71.91	6.82	159061	38356
	17	514.7	69.66	6.24	66.27	6.83	168367	43406

2.3.4. Techno-economic analysis

Comprehensive information is required to recommend the best suitable power plant technology, a techno-economic analysis becomes necessary. Even the 4E (energy, exergy, economic, and environmental) analysis may not be sufficient in addressing all challenges nowadays. Even when a device is thermodynamically feasible, its manufacture, installation, and maintenance might be quite difficult.

Based on Table 2.9, dry fluid ORC technology is matured and used in several waste heat recovery power plants throughout the world. Commercialization is also made possible by the lowest discounted payback period (Table 2.7). While there are no installation issues with the dry ORC, there are less technical and maintenance issues. Because the CO_2 cycle is a less developed technology, special attention must be paid during its maintenance and operation.

TFC, which follows the CO_2 Rankine cycle and produces a good quantity of electricity, has to be developed further for widespread application in industry. The biggest challenge for TFC is the two-phase turbine's cleaning and operation because they operate at a lesser pressure than CO_2 Rankine cycles. However, TFC is a safer alternative to CO_2 Rankine cycle. OFC and Kalina are sophisticated systems that are less developed and provide the least power. Hence, they are typically not used in commercial settings. The development of appropriate separation technology enables the use of OFC in particular locations. The CO_2 Rankine cycle has the longest payback and discounted payback periods, while dry ORC has the shortest. For safer side in industry-level power generation, ORC technology will be the preferred choice in terms of its versatility, discounted payback period, low source temperature, low cost and sustainability.

Table 2.9. Various challenges associated with thermodynamic cycles

Issues	**ORC (dry fluid)**	**ORC (wet fluid)**	**CO_2 Rankine cycle**	**Kalina cycle**	**OFC**	**TFC**
Installation and fabrication issue	Difficult to fabricate low-pressure turbine.	Difficult to fabricate low-pressure turbine.	No issue is recognised	For complex system extra care is required.	No issue detected	No issue detected
Maturity (Developed) level	Fully developed technology, many systems are in operation	Fully developed technology	Not developed	Less developed	Separator needs some attention to become mature	Less developed
Maintenance issue	Less skilled maintenance Required	Less skilled maintenance Required	Maintenance is easy, but carefully handled	High maintenance is needed due to complexity	More inner cleaning is needed for its	Two-phase turbine needs timely

			due to high pressure	and more components	component s	proper cleaning
Technical issue	Turbine blade erosion is due to the droplet or wet evaporation	Carefully consideratio n of PPTD	Pump exit and compressor inlet is difficult to locate while fluid is flowing	It is hard to locate recuperator's entry and exit due to the mixture of working fluid	100% vapor separation is practically difficult in the separator	More time requires for the developme nt of two-phase turbine
On ground operation issue	No issue	Handling issue due to hazardous working fluid (ammonia)	Extra care is required due to high compressor discharge pressure	Extra care is needed to prevent the leakage of working fluid (ammonia)	Large amount of heat interaction	No issue

For distributed 50 kW power production unit, various parameters of a solar-ORC and solar P-V system were evaluated and the cycles are compared based on technical and financial performance and tabulated in Table 2.10. The suggested method of independently altering the solar field area and storage capacity was used to estimate key performance indicators such as yearly energy production, capital utilization factor (CUF), LCOE, capital investment, and energy wasted. With a CUF value of 0.56, the solar-ORC system produced a minimum value of LCOE, i.e., 0.19 USD/kWh. The solar P-V system generates an LCOE of almost 0.26 USD/kWh for a comparable CUF value. Although the solar P-V system's minimum LCOE value results in 0.12 USD/kWh, however, it does not account for energy storage, which results in a much lower capacity factor. These findings pinpoint the fact that when power supply stability is prioritized, s-ORC technology with thermal energy storage, which is typically viewed as costly when compared to PV (usually without storage), can also be cost-effective.

Table 2.10. Comparison of solar ORC and solar P-V system [117]

	Solar ORC with thermal energy storage	P-V solar system with battery
Case significance	Both cases have been compared on same amount of capital utilization factor	
Annual energy generated [MWh]	246	246.2
Capital investment [$/kW]	5884.6	6044
Capital utilization factor	0.56	0.56
Energy wasted [MWh]	21.8 (thermal)	155.4 (electrical)
LCOE [$/kWh]	0.19	0.26
Solar field [m^2]	1029	1742
Storage hours [h]	9	3.6

2.4. Important Findings

In this research, six thermodynamic power cycles (ORC with dry fluid, ORC with wet fluid, CO_2 Rankine cycle, Kalina cycle, OFC and TFC) have been compared at the optimum operating conditions for a given range of heat source and sink temperatures to identify the suitable cycle for low-medium grade heat recovery. Various energy, exergy, economic, environmental and technical parameters have been taken as objective functions for comparison. From the study, the following major outcomes can be derived:

(i) For high heat source temperature, TFC shows better performance with an 18.84% increase in net work at 160°C; however, at low heat source temperature, CO_2 cycle has better performance with 29.91% more net work at 100°C.

(ii) Thermal efficiency is maximum for ORC with wet fluid for the studied heat source temperature range, with a maximum increase of 6.06% at 160°C, whereas TFC has lower thermal efficiency.

(iii) For the high heat source temperature range, TFC shows higher exergy efficiency with 11.5% at 160°C; however, in the low heat source temperature range, CO_2 has maximum exergy efficiency with 18.59% at 60°C.

(iv) Maximum profit is obtained using TFC for the studied source temperature range and increases with increasing heat source temperature. TFC has a maximum profit increment of 16.16% at 160°C despite the total cost increased by 32.05% using ORC with dry fluid.

(v) TFC and OFC save an equal amount of CO_2 emission with a maximum of approximately 26% at higher heat source temperatures.

(vi) It has been confirmed that at a lower heat source temperature range, CO_2 cycle performance is best. In this regard, if the condenser temperature is changed, then the effect is more favourable if the condenser temperature is decreased by the same value instead of increased. However, for higher heat source temperatures, TFC would give the best performance.

(vii) Lowest discounted payback period and the highest matured technology make dry ORC the first choice for large-scale commercialization purposes for power generation from waste heat sources.

(viii) When the solar P-V method is implemented for harnessing electricity from a given range of heat source and sink temperatures, due to less LCOE and efficiency, ORC will again be the first choice of consumers.

Overall, the CO_2 cycle would be beneficial for a low heat source temperature range, whereas TFC for medium grade heat source temperature range, by considering performance, design, cost, operation, and environmental benefits. However, if the matured technology with less technical issues is considered whose power output, efficiency, associated investment, profit and carbon emission are in the acceptable range (neither less nor high), then both ORCs (Dry ORC and wet ORC) will be preferred first to be used for the distributed method of power generation. Further performance improvement can be seen if a suitable working fluid mixture and cycle modification are used. If another method is considered for power generation apart from the conventional solar P-V method, then ORC will still be the first preference. However, in rural areas, the solar P-V method can be the better option for distributed power generation due to the engagement of minimally trained technicians and combining the empowerment of rural populations.

Chapter 3: Organic Rankine Cycle Modifications

This chapter contains energy, exergy and economic analyses of two novel ejector-enhanced organic Rankine cycles and a comparison with basic cycle.

3.1. Cycle Description

Components of reference (basic) organic Rankine cycle are the evaporator (vapour generator), power-producing expansion device (e.g., turbine), condenser, pump and working fluid. The type of working fluid may be dry, isentropic or wet fluid. Here, R123, R601a and R1233zd(E) are considered as working fluids, which are dry fluids. Two novel ejector-enhanced ORCs (EEORC), i.e., EEORC-1 and EEORC-2, along with basic ORC are analyzed and optimized for the given heat source temperature. The superheated isopentane is then allowed to expand in a turbine after being heated in an evaporator to a saturated vapour state 3 from the pressurized isopentane. At state 4, working fluid leaves the turbine and condenses into the saturated liquid condition 1. The working fluid is heated using a counter-flow evaporator from the pump outlet (state 2) to the saturated vapour state 3, passing via the saturated liquid state 3l. The net work is produced from states 3 to 4 of the turbine expansion. The presence of an ejector enhances the turbine work output by lowering the turbine exit pressure.

Figure 3.1 and Figure 3.2 show the schematic layout and T-s diagram of EEORC-1, respectively. In EEORC-1, the liquid working fluid is pumped (process 1-2) and enters into the preheater section, then divides into primary and secondary streams at the inlet of the evaporator section (saturated liquid state). Primary and secondary streams of the working fluid flow through the ejector and turbine, respectively. The primary working fluid stream is bleeding from the saturated liquid state of the evaporator (exit of preheater) and enters the nozzle section of the ejector. The motive stream flows through the nozzle and gets high velocity at the nozzle exit, which entrains the secondary stream. The secondary working fluid stream flows through the evaporator and gets heated to the saturated vapor state by the heat source fluid (Therminol-VP1 is used here). Then this fluid expands in the turbine and generates power. The secondary stream from the exit of the turbine enters the constant cross-section of the nozzle and gets mixed with the motive stream. This mixed stream then flows through the diffuser of the nozzle to increase the condenser pressure by slowing down the velocity. The diffuser exit stream enters the condenser, where heat is removed by cooling fluid (water). Then this stream is pumped to the evaporator pressure where it gets preheated and the cycle continues.

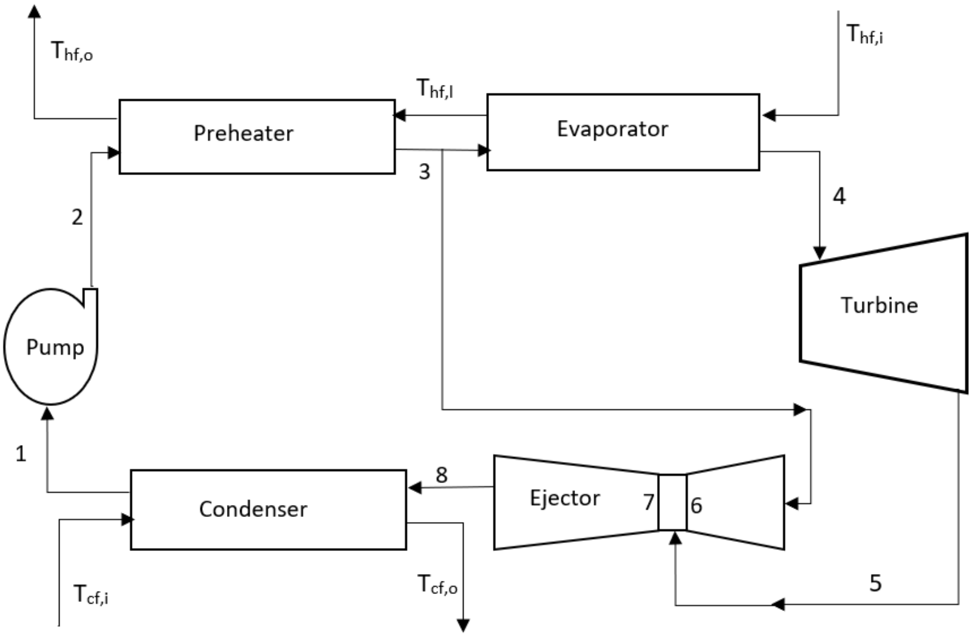

Figure 3.1. Schematic layout of proposed EEORC-1

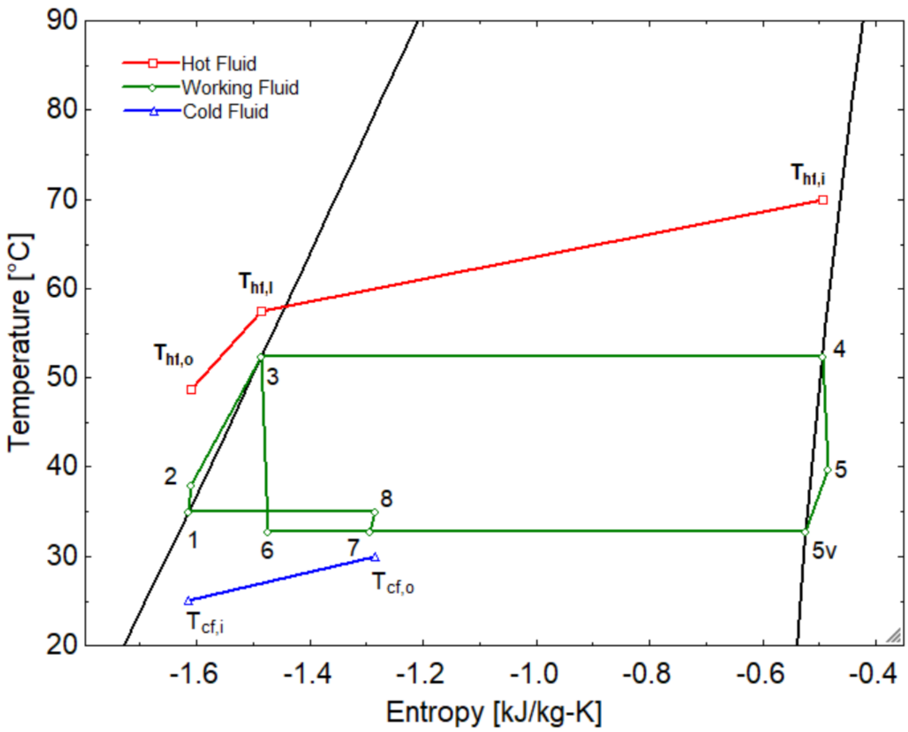

Figure 3.2. Temperature-entropy diagram of proposed EEORC-1

Figure 3.3 and Figure 3.4 show the schematic layout and T-s diagram of EEORC-2, respectively. The difference in EEORC-2 as compared to EEORC-1 is the presence of double pumps, double evaporators and the exit state of the motive stream. In EEORC-2, the working fluid at the condenser exit is divided into two streams. Pump-1 and pump-2 pump these two streams to comparatively high pressure and low pressure, respectively. The primary stream from pump-2 flows to the ejector through a low-pressure boiler (preheater + evaporator) and the secondary stream from pump-1 gets heated through a high-pressure boiler (preheater + evaporator) and expands in the turbine to generate power. Hot fluid (Therminol-VP1) enters the high-pressure boiler and divides into two streams. These streams are further used to heat the low-pressure boiler (preheater + evaporator) and high-pressure preheater and exit out to the surrounding. The low-pressure's primary stream is heated up to the saturated vapor state through the low-pressure boiler and then enters the ejector's nozzle section. The high-pressure's secondary stream is heated up to the saturated vapor state in the high-pressure boiler and then enters the turbine for power generation. The rest of the phenomena in the ejector are the same as those in the EEORC-1 ejector and then condense by cooling water, and the cycle repeats.

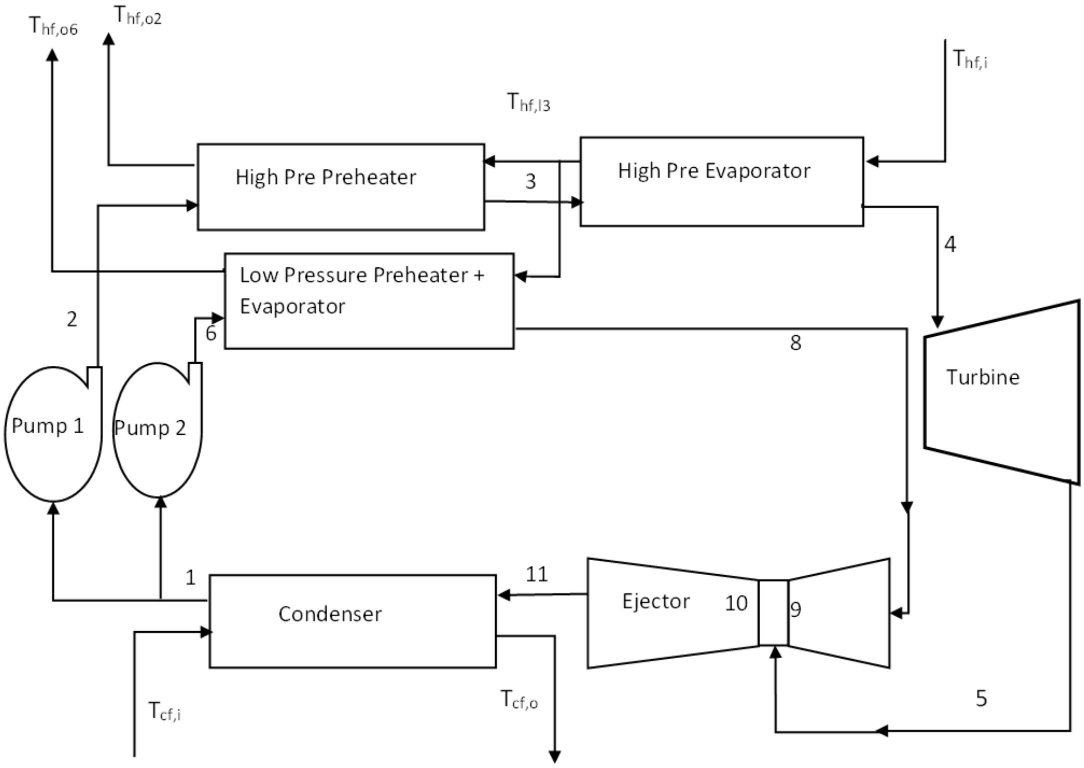

Figure 3.3. Schematic layout of proposed EEORC-2

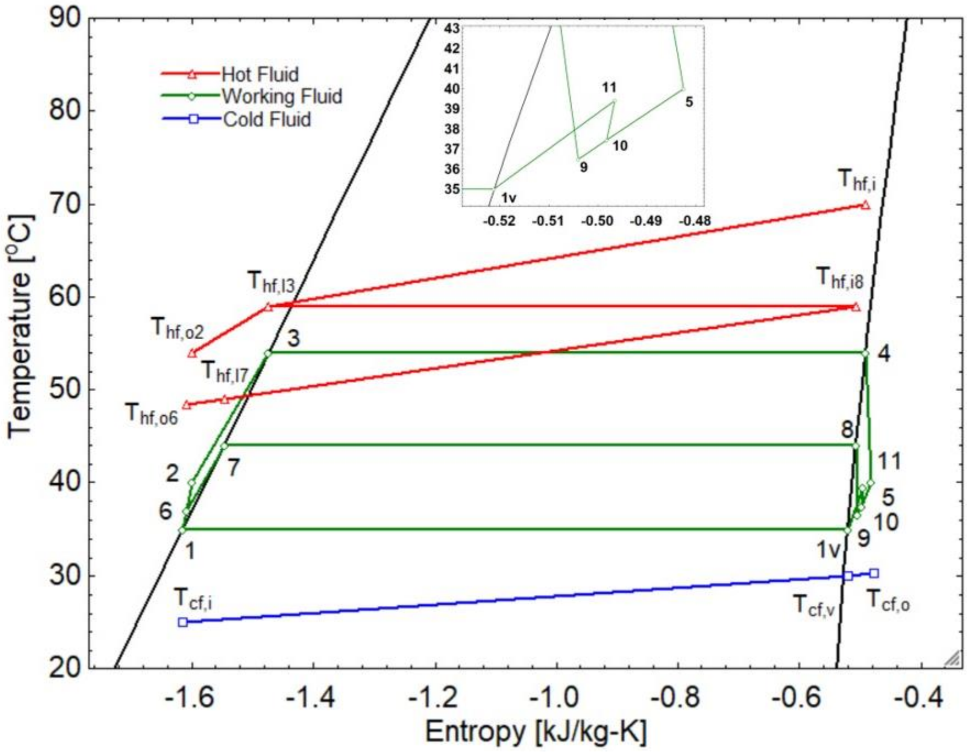

Figure 3.4. Temperature-entropy diagram of proposed EEORC-2

3.2. Modelling and Simulation

3.1.1. Mathematical Modelling

The required mathematical modelling for thermodynamic analysis and component design is taken from Chapter 2 (Eqs. 2.1 - 2.27). Other than the above, additional assumptions, equations and correlations are mentioned below.

(i) Nozzle and diffuser have given isentropic efficiencies.

(ii) Both the motive and the suction stream reach the same pressure at the inlet of the constant area mixing section of the ejector. There is no mixing between the two streams before the inlet of the constant area mixing section.

(iii) Similar to other components, ejector inlet and outlet velocities have been neglected.

(iv) The cost of the ejector has been ignored because the cost of the ejector is much lower than that of other equipment.

For the ejector, the nozzle exit velocity is given by:

$$c_{nz,out} = \sqrt{2000\left(h_{nz,in} - h_{nz,out}\right)} \tag{3.1}$$

Momentum and energy balances at constant area intermixing chamber of the ejector are given by, respectively:

$$\dot{m}_{wf,sec}c_{tur,out} + \dot{m}_{wf,pri}c_{nz,out} = \dot{m}_{wf}\frac{c_{d,in}}{\sqrt{\eta_m}} \tag{3.2}$$

$$\begin{aligned}\dot{m}_{wf,sec}\left[h_{tur,out} + \left(\frac{{c_{tur,out}}^2}{2000}\right)\right] + \dot{m}_{wf,pri}\left[h_{nz,out} + \left(\frac{{c_{nz,out}}^2}{2000}\right)\right] \\ = \dot{m}_{wf}\left[h_{d,in} + \left(\frac{{c_{d,in}}^2}{2000}\right)\right]\end{aligned} \tag{3.3}$$

The diffuser outlet of the ejector is calculated by the following equation:

$$h_{d,out} = h_{d,in} + \left(\frac{{c_{d,in}}^2}{2000}\right) \tag{3.4}$$

The pressure lift ratio of the ejector is calculated as:

$$\mathrm{PLR} = \frac{P_{con}}{P_{sec,nz,in}} \tag{3.5}$$

The ejector irreversibility of the ejector is calculated as:

$$I_{eje} = T_{amb}\left(\dot{m}_{wf}s_{con,in} - \dot{m}_{wf,tur}s_{tur,out} - \dot{m}_{wf,eje}s_{eje,in}\right) \tag{3.6}$$

Now, the overall exergy balance is given by:

$$Ex_{in} = W_{net} + I_{pump} + I_{tur} + I_{evp} + I_{con} + I_{eje} \tag{3.7}$$

3.1.2. Proposed economic models

To market and commercialize the new advanced technology (enhanced cycle) developed in the field of the energy production sector, increased power generation, total cost consumed and selling price are the main important parameters. The main aim of technological advancement is to generate more power at the same previous resources (source temperature, flow rate, etc.) used and to provide more hours of power availability at the same or cheaper rates so that more population can get benefitted from more hours of power availability but at a cheaper rate. To get the power (electricity) at a cheaper rate along with industry benefits using proposed novel cycles, three economic models have been chosen and compared with reference to basic ORC. Here, three different economic models (M1, M2 and M3) have been discussed for the two cases. 1st case is when only old technology is there and for 2nd case is when new technology completely replaces the old technology. In order to provide cheap electricity at a larger amount, the government may subsidize the total cost consumed on new technology and research & development work [118].

Let's consider the simple linear power production and selling price function.

$$C_{ele} = a_{ii} - b_{ii}W_{net} \tag{3.8}$$

Where, constant $a, b > 0$ and C_{ele} is the selling price of electricity and W_{net} is the power production of old and new technology, respectively.

The subscript "ii" refers to the economic model M1, M2 and M3. The condition of economic models is described below.

Economic model 1 (M1) is based on when the unit selling price of electricity is the same (real word functioning criteria):

$$C_{ele}^{case1} = C_{ele}^{case2} \tag{3.9}$$

Economic model 2 (M2) is based on when the total hourly profit is the same:

$$\mathrm{Profit}_{total}^{case1} = \mathrm{Profit}_{total}^{case2} \tag{3.10}$$

Economic model 3 (M3) is based on when the unit profit is the same:

$$\mathrm{Profit}_{unit}^{case1} = \mathrm{Profit}_{unit}^{case2} \tag{3.11}$$

3.1.3. Simulation procedure

Based on the above mathematical models, a simulation code has been developed in Engineering Equation Solver for the proposed EEORC systems. The code can predict the performances of proposed systems for the given heat source, heat sink, ambient temperature and component efficiencies. PPTD is defined effectively when designing the evaporator and condenser. All physical and thermodynamic properties of considered fluids are calculated using an in-built subroutine in software. Both proposed systems have been optimized for maximum net work output. The heat exchanger area is calculated to determine the capital investment cost. Proposed economic modelling is executed on the software to analyse the best thermodynamic cycle suited to give more power but at cheaper rates to the consumer. Figure 3.5 represents the flow chart of the whole simulation process.

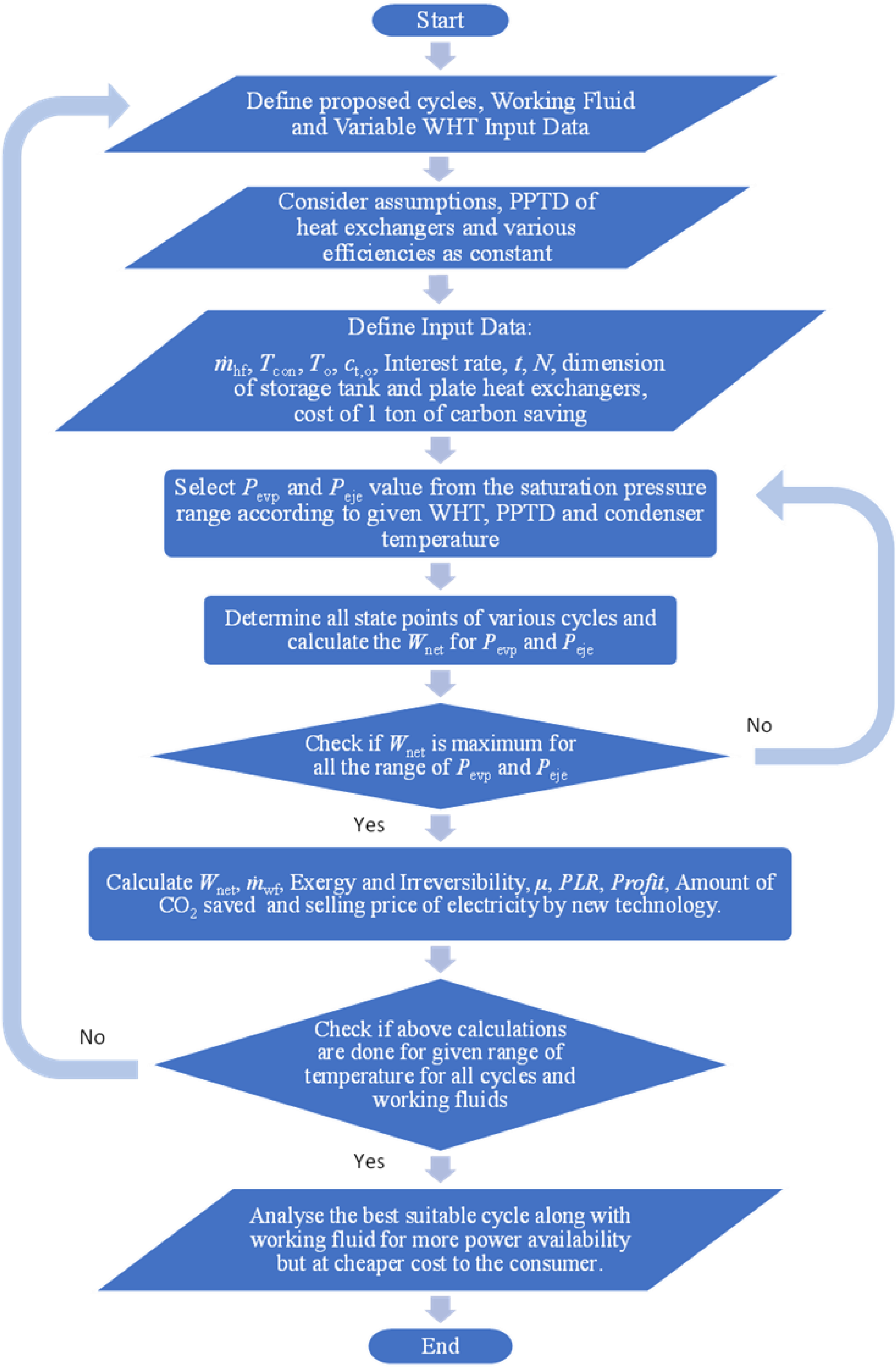

Figure 3.5. Flow chart of the simulation procedure for EEORC

3.1.4. Model validation:

Table 3.1. Comparison of result obtained from reference with simulated values

Parameter	Reference value	Calculated value	Error (%)
Pump work	2.50 W [38]	2.51 W	0.4
Turbine work	60.20 W [119]	63.58 W	5.61
Turbine work	64.48 W [38]	63.22 W	1.95
Thermal efficiency	2.59% [38]	2.59%	0
Ideal Rankine efficiency	7.93% [38]	7.87%	0.75
Evaporator area	0.60 m^2 [119]	0.62 m^2	3.3
Condenser area	0.80 m^2 [119]	0.85 m^2	6.3

As the proposed cycle is new, the basic ORC is validated only to check the accuracy. Under similar operating conditions to Farrokhi et al. [38] and Liu et al. [119], the simulation is performed and compared with the reference values, which are given in Table 3.1. Thermodynamic simulation achieves a good result with acceptable error for Farrokhi et al. [38]. The area of the evaporator and condenser also shows a good result with a maximum error of 6.4% despite the correlation used [119]. These results are obtained from current simulation analyses and reference experimental analyses with very small and accepted deviation caused by instrument calibration error and real-ideal phenomena differences.

3.3. Results and Discussion

Working fluid properties of novel modification of ORC are shown in Table 3.2.

Table 3.2. Selection of working fluids [120]

Working Fluid	Alternative name	Critical temperature [ºC]	Critical Pressure [MPa]	Normal boiling point [ºC]	Triple point temperature [K]	ASHRAE Safety group	ODP	GWP (100 years)
2-Methylbutane	R601a (Isopentane)	187.2	3.37	27.85	112.65	A3	0	5

2,2-Dichloro-1,1,1-Trifluoroethane	R123	183.7	3.66	27.78	166	B1	0.02	79
Trans-1-Chloro-3,3,3-trifluoropropene	R1233zd(E)	165.6	3.57	18.32	195.15	A1	0	4.5

Input parameters of novel studied EEORCs are given in Table 3.3. Cold source and condenser temperature is selected based on specific location ambient temperature. For this simulation, latitude 25.42° N and longitude 82.97° E Varanasi, India, are selected. The hot fluid mass flow rate is selected in such a way as to justify the work output. Other parameters are taken from the reference. The selection of working fluid is based on critical temperature, pressure and environmental effect. Desired critical temperature range is 150-200 °C for a wide temperature range of working. Working fluid should have lower ozone depletion potential and global warming potential and meet with the standard ASHARAE safety groups.

Table 3.3. Input parameters for Basic and EEORCs

Input Parameter	**Unit**	**Modified ORC**
Source inlet temperature	^oC	70
Cold source inlet temperature (Water)	^oC	25
Condenser Temperature	^oC	35
Ambient Temperature	^oC	30
Hot Fluid mass flow rate (Therminol VP1)	kg/s	100
$PPTD_{evp}$	^oC	5 [114]
$PPTD_{con}$	^oC	5 [114]
Pump Efficiency	-	0.7 [115]
Turbine Efficiency	-	0.85 [116]
Motive nozzle Efficiency	-	0.9 [121,122]
Mixing Efficiency	-	0.9 [121,122]
Diffuser Efficiency	-	0.85 [121,122]

Turbine exit velocity	m/s	0
Annual working hour	h	7000
Annual Interest rate	-	10%
Width and Length of PHE	mm, cm	5, 15
Diameter and height of tank	cm, cm	30, 70

Performance comparison is presented in Table 3.4 for studied mean input parameters (Table 3.3) for different power cycles and working fluids. For the comparative analysis of basic and advanced cycles for the different working fluids, the low-grade WHT of 70 °C is chosen. All cycles are optimized for maximum net work output. Ejector-enhanced cycles exact more heat from a given heat source and yield more net work but lower thermal efficiency due to lower optimum evaporator pressure. Basic cycle and EEORC-2 show almost equal maximum net work output for all working fluids, but EEORC-1 shows different value with different working fluid and a maximum for R123 working fluid. Thermal and exergy efficiencies are cycle-dependent and thus show very less variation on working fluid. The mass flow rates of the working fluid and cold fluid, entrainment ratio and pressure lift ratio are obtained in order to maximize net work output. The total cost invested in EEORC-1 is the maximum due to the highest irreversibility and evaporator area. At 70 °C source temperature, yearly profit is maximum for the basic cycle, but at a higher source temperature, either EEORC-1 or EEORC-2 may give a better result. The amount of CO_2 saving is maximum for EEORC-1 due to maximum irreversibility and heat input required and so converting of CO_2 saved amount in monetary value gives maximum total profit with CO_2.

Table 3.4. Comparison of different cycles and working fluids at WHT = 70 °C

Parameter	Basic ORC (R601a)	Basic ORC (R123)	Basic ORC (R1233zd(E))	EEORC 1 (R601a)	EEORC 1 (R123)	EEORC 1 (R1233zd(E))	EEORC 2 (R601a)	EEORC 2 (R123)	EEORC 2 (R1233zd(E))
Net work output [kW]	103.6	103.8	103.6	118.3	122.2	114.4	107.4	107.8	107.2

Thermal efficiency (%)	3.76	3.80	3.77	2.07	2.13	2.00	2.72	2.73	2.73
Exergy efficiency (%)	39.69	40.04	39.76	30.08	31.03	29.05	32.28	32.45	32.40
Working fluid mass flow rate [kg/s]	7.66	15.47	14.00	88.91	198.73	168.54	11.09	22.55	20.11
Coolant mass flow rate [kg/s]	123.3	123.9	124.7	267.3	268.1	268.5	178.6	180.5	179.1
Entrainment ratio	NA	NA	NA	0.086	0.077	0.086	1.880	1.850	1.690
Pressure lift ratio	NA	NA	NA	1.169	1.205	1.168	1.021	1.023	1.026
Total irreversibility [kW]	157.4	155.5	156.9	275.1	271.5	279.4	225.3	224.3	223.6
Evaporator area [m^2]	29.13	30.14	30.56	346	506.9	657.6	66.16	90.83	87.66
Condenser area [m^2]	25.31	24.72	24.78	36.32	36.73	36.98	78.98	79.66	79.93
Total cost invested [Thousand $]	183.12	183.08	184.68	308.26	340.21	366.67	213.14	219.34	220.17
Total cost consumed [$/h]	3.26	3.26	3.29	5.48	6.05	6.52	3.79	3.90	3.92

Total cost earned [$/h]	13.67	13.70	13.67	15.62	16.13	15.1	14.18	14.22	14.15
Profit [$/h]	10.42	10.45	10.39	10.14	10.08	8.59	10.38	10.32	10.23
Profit [Thousand $/year]	72.92	73.14	72.71	70.96	70.53	60.03	72.69	72.26	71.61
CO_2 Saving [ton/year]	6760	6710	6750	1400	1410	1410	9710	9700	9640
Profit with CO_2 [$/h]	20.08	20.03	20.02	30.15	30.16	28.66	24.25	24.18	24.00

Figure 3.6 represents the effect of waste heat inlet temperature variation on net work output. Net work output depends upon the difference of enthalpy difference of the turbine work and pump work for the same mass flow rate. Net work output is maximum for EEORC-1 due to the use of an ejector in a particular configuration system. In this configuration PLR and working fluid mass flow rate gives maximum value. In EEORC-1, the turbine's exit pressure will be lower and the secondary fluid mass flow rate will be higher. These parameters cumulatively maximize the net work output of EEORC-1. Net work output increases with increasing the waste heat inlet temperature because the amount of heat added to the evaporator is high and so higher the working fluid enthalpy at the turbine inlet (evaporator exit). Higher turbine inlet enthalpy is the main dominating factor to increase in net work output. EEORC-1 gives maximum net work output for the temperature range of 60-180 °C. At the lower temperature range of 60-150 °C, R123 and at the higher temperature range of 155-180 °C, R1233zd(E) has the highest net work output among the studied working fluids for EEORC-1. At 151-154 °C, all working fluids of EEORC-1 show almost equal net work output.

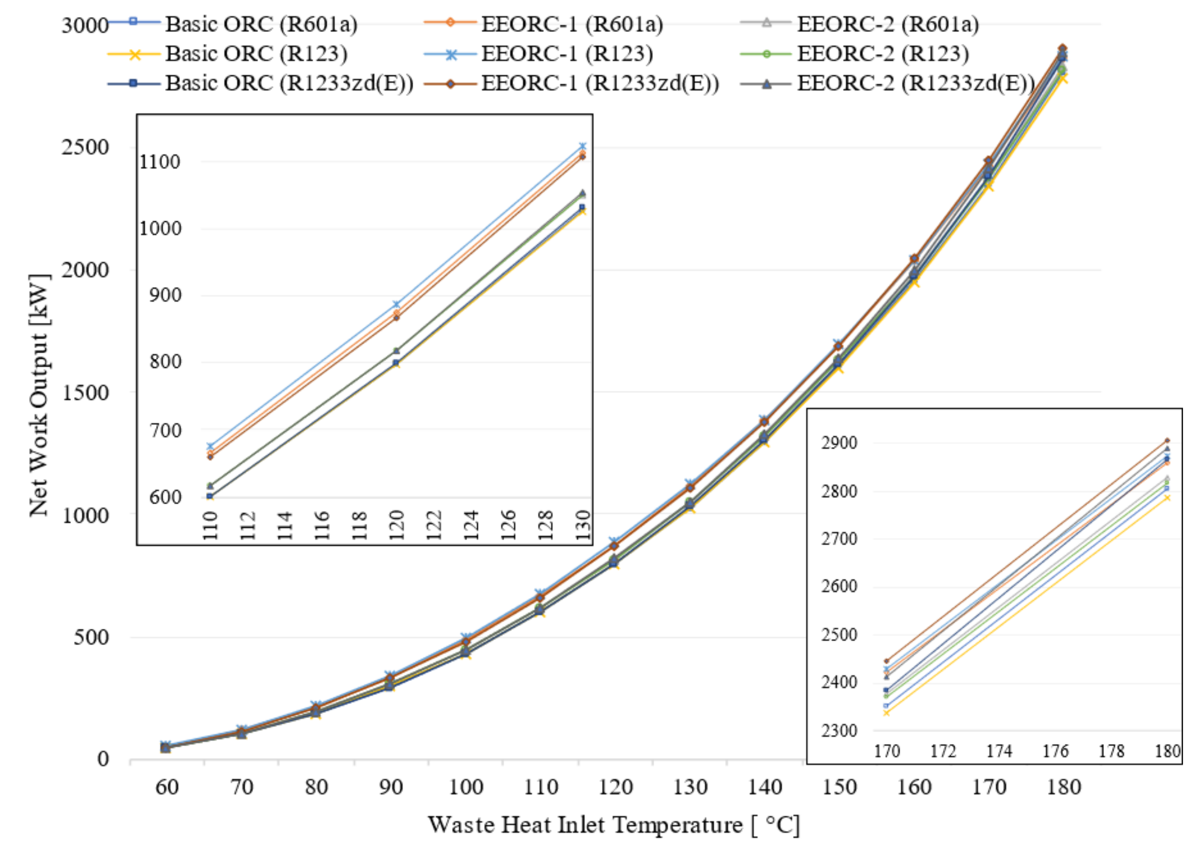

Figure 3.6. Effect of waste heat inlet temperature variation on net work output

Figure 3.7 represents the effect of the variation of waste heat inlet temperature on the ejector exit pressure. Figure 3.7 shows that ejector exit pressure first decreases to the minimum level and then increases. The value of ejector exit pressure depends on the optimized ejector exit pressure condition to maximize the net work of each ejector enhanced cycle at each temperature point to exist the cycles. The lower value of the ejector exit pressure helps to increase the net work output. In Figure 3.7, EEORC-1 has a lesser value of ejector exit pressure in comparison to EEORC-2 for the same working fluid in the temperature range of 60-180°C. Among all working fluids, R123-based EEORC-1 has a minimum ejector exit pressure value at each source temperature. The ejector pressure value cannot go below at higher temperatures because of thermodynamic constraints derived from the simulation method used to maximize the net work output. Thermodynamic constraints are primary and secondary mass flow rate values and temperature difference between hot source fluid exit and pump exit.

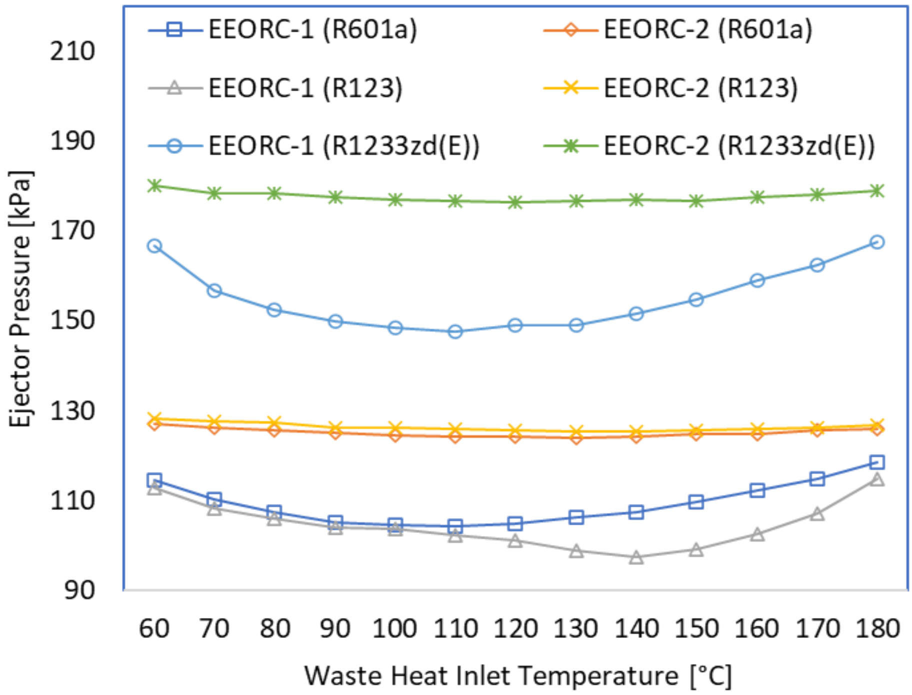

Figure 3.7. Effect on ejector pressure with the variation of waste heat inlet temperature

The Y-axis of Figure 3.8 represents the percentage increase of net work output on ejector-enhanced cycles (both EEORC-1 and EEORC-2) when compared with the basic ORC of the same working fluids. In Figure 3.8, the effect is shown for the percentage increase of net work output on the variation of waste heat inlet temperature. EEORC-1 has the greater and EEORC-2 has the lesser increase in net work output with downward concavity and linearly decreasing respectively with temperature increment. This is because the organic working fluid property is generally suitable for low-range temperature application and thus, irrespective of the cycles, at lower temperature range, organic working fluid shows promising results. On increasing heat source temperature, net work output value ratio of ejector-enhanced cycles (both EEORC-1 and EEORC-2) and the basic cycle will be decreasing because there is a limitation up to which turbine exit pressure can be lowered and so no significant increase in net work output of ejector-enhanced cycles.

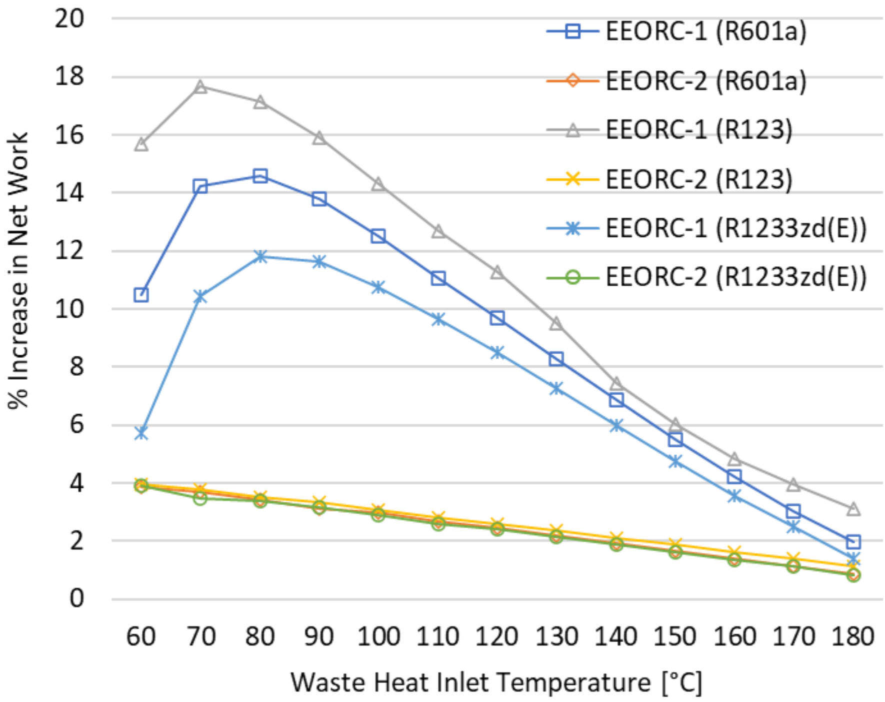

Figure 3.8. Improvement of net work output with waste heat inlet temperature

Figure 3.9 represents the effect on thermal efficiency with waste heat inlet temperature. For all temperature ranges, the thermal efficiency is maximum for basic ORC and least for EEORC-1. The basic cycle has maximum thermal efficiency than the studied ejector-enhanced cycles because less heat input is required at the same heat source temperature. Despite the lowest value of net work output of basic ORC, the cumulative effect of net work output and heat input maximizes the thermal efficiency of basic ORC. The amount of heat input plays a major role in the net work output. R123-based cycles have higher thermal efficiency because of increased net work output and so the basic ORC with R123 has the highest thermal efficiency for all temperature ranges. Due to the highest cycle temperature of EEORC-1, among others, it requires the highest heat input and so minimizes the cycle thermal efficiency.

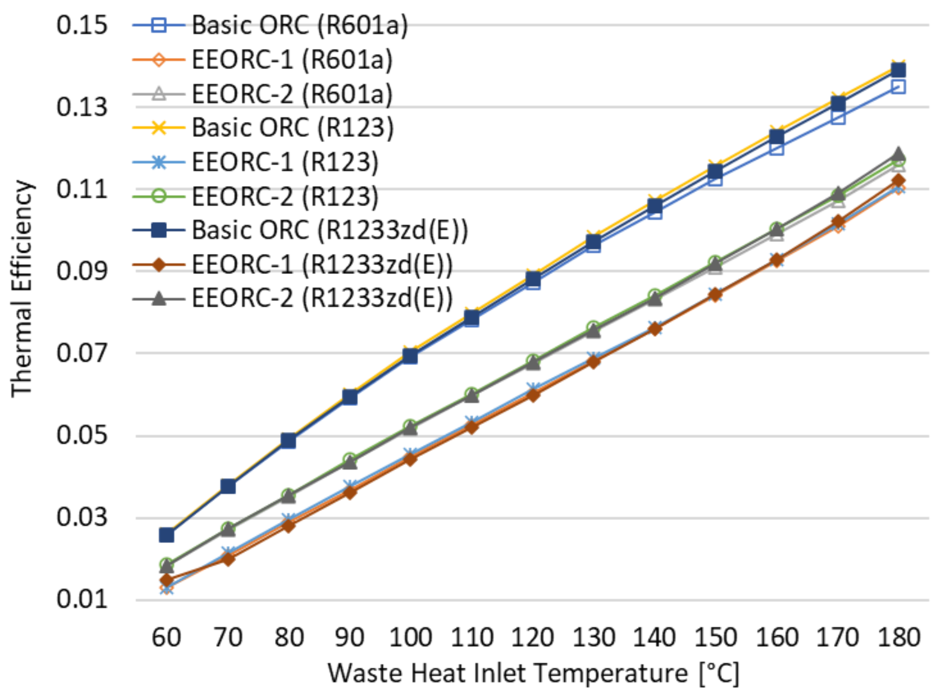

Figure 3.9. Effect on thermal efficiency with waste heat inlet temperature

Figure 3.10(a) and Figure 3.10(b) represent the effect on the entrainment ratio and pressure lift ratio with the variation of WHT, respectively. For all heat source temperature ranges, EEORC-1 has a lower entrainment ratio and higher-pressure lift ratio. The simulated value of the entrainment ratio and PLR is obtained from the maximum net work output condition. The R123-based cycle has the lowest entrainment ratio and highest PLR in its domain at a higher temperature range (greater than 140 °C) because of the fluid property. The lowest entrainment ratio and highest PLR are desirable for maximum net work output condition because of maximum enthalpy drop in the turbine due to more lowering of the turbine exit pressure.

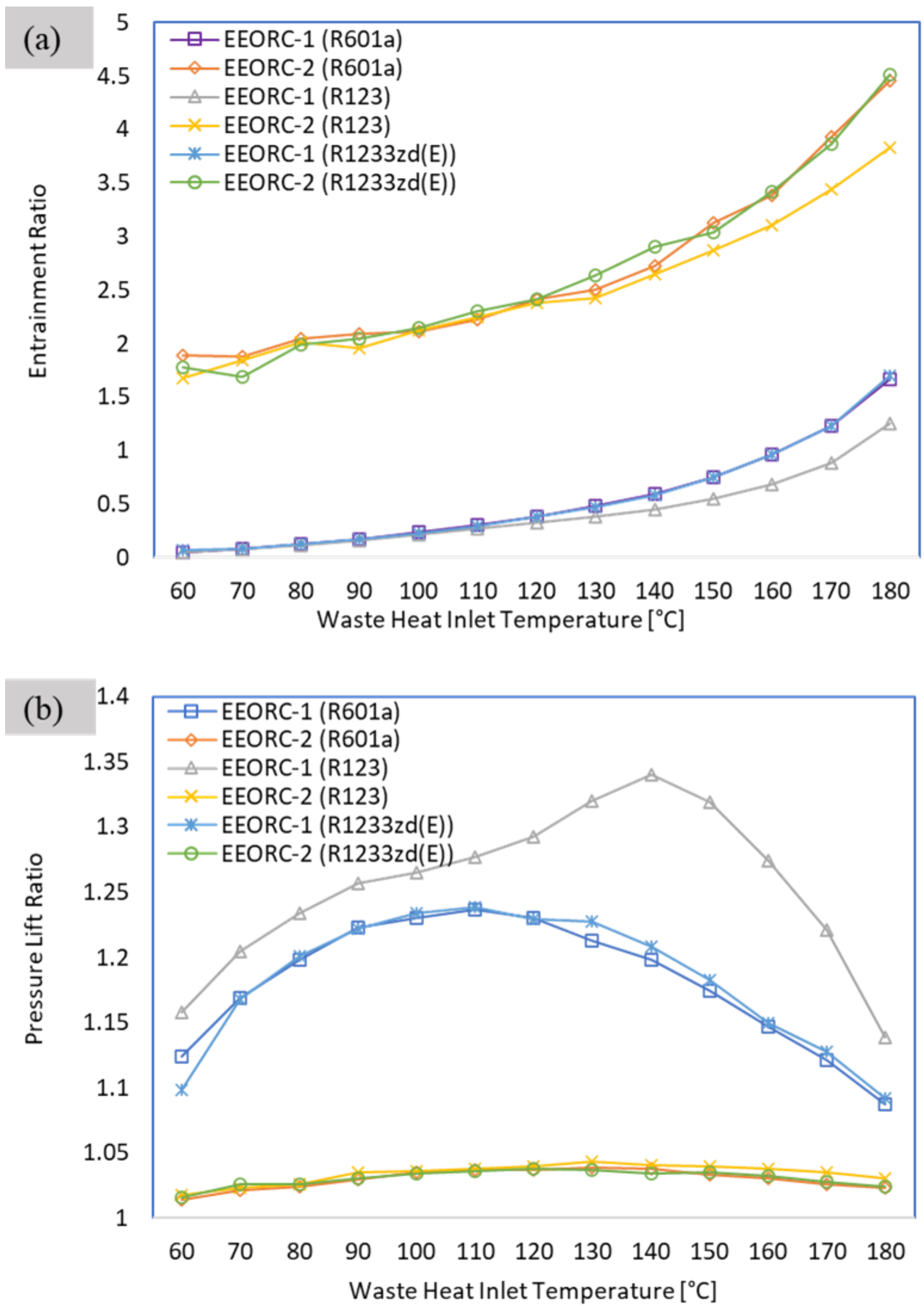

Figure 3.10. (a) Effect on entrainment ratio by variation of WHT, (b) Effect of PLR by the variation of WHT for different cycles

Figure 3.11 represents the effect on irreversibility at 70 °C for different components of various cycles and working fluids. This temperature is chosen for analysis purposes keeping in mind that the maximum % increase in net work output is at 70-85 °C temperature range and a comparative study is shown in Table 3.4 at 70 °C. Both ejector-enhanced cycles have higher irreversibility than basic due to higher evaporator pressure, ejector pressor and other components along with the ejector, which ultimately results in higher component irreversibility for maximum net work output. The presence of an extra component (ejector) will surely contribute to an increase in total irreversibility for EEORC. At a higher temperature range, each cycle's corresponding component irreversibility value will be lowered. Irreversibility of the evaporator and condenser becomes higher for another ejector-enhanced cycle due to handling more heat and thus the heat exchanger size increases. EEORC-1 with R1233zd(E) has the highest irreversibility and basic ORC with R123 has the lowest irreversibility at the heat source temperature of 70 °C.

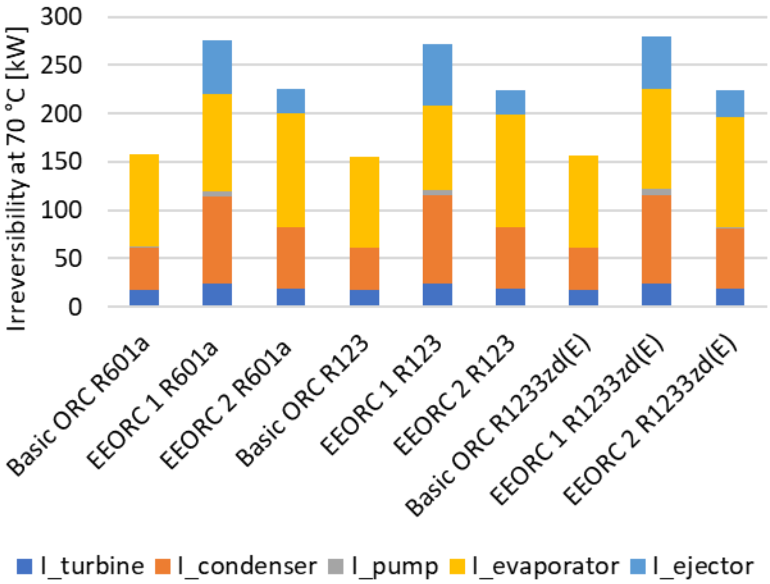

Figure 3.11. Irreversibility value of different cycle components at 70 °C

Figure 3.12 shows the variation of exergy efficiency along with waste heat inlet temperature. Exergy efficiency increases rapidly at the heat source temperature range of 60-90 °C because of the organic working fluid property. Basic ORC has higher exergy efficiency than studied ejector-enhanced cycles due to a large amount of input heat required (deduced by parametric optimization) at the same heat source temperature and thus exergy input will also increase. With the increase in heat source temperature net work output and exergy inlet will also increase and cumulatively decides how much exergy efficiency would increase. The exergy efficiency of basic and EEORC is significant at low WHT and further merges at higher WHT because of more and further less percentage increase in exergy. Basic ORC has the highest exergy efficiency and is not dependent upon working fluid used at a lower temperature range.

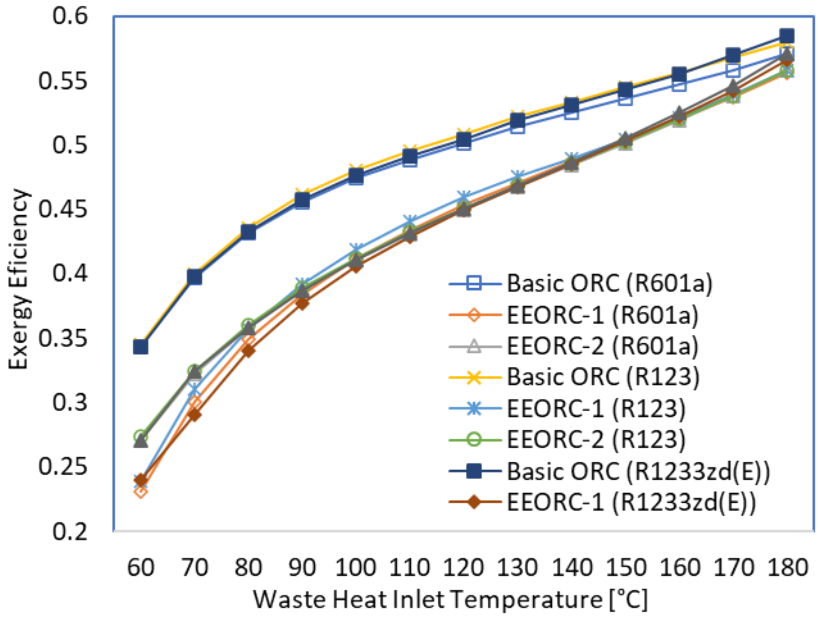

Figure 3.12. Effect on exergy efficiency with WHT for different cycles

Figure 3.13 represents the variation in size parameter with WHT. Size parameter of R123 working fluid-based cycles is the largest because of the cumulative effect of fluid property, lesser turbine isentropic enthalpy difference and higher turbine exit volume flow rate and fluid flowing through the turbine to produce maximum net work output from the shaft. From Figure 3.13, it can be concluded that the turbine size parameter is more dependent on the types of working fluid used rather than the types of cycles. The size parameter for all cases increases with increasing the WHT. The turbine size parameter directly affects the turbine cost and hence total cost consumed is the maximum for R123-based thermodynamic cycles.

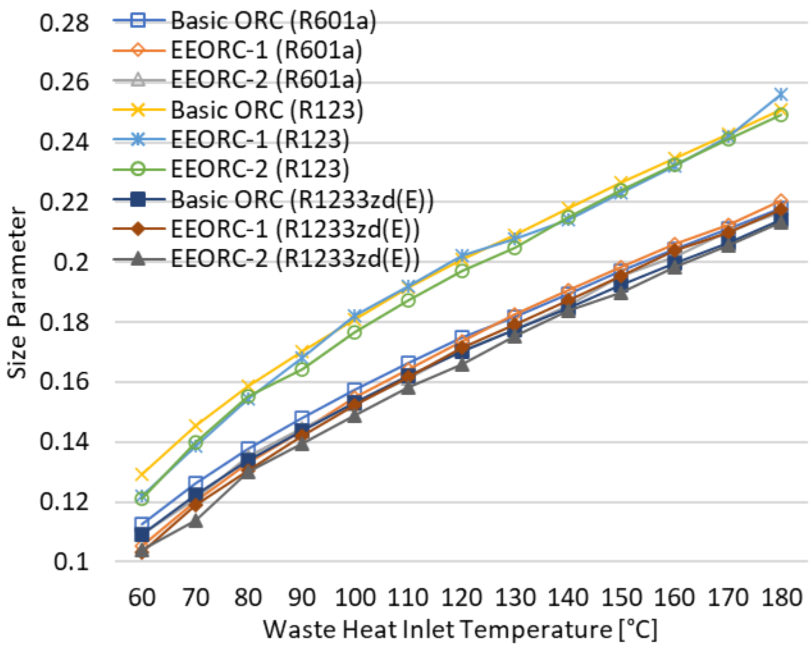

Figure 3.13. Effect on size parameter of turbine with WHT for different cycles

Figure 3.14 represents the variation in the total heat exchanger area (combined evaporator area and condenser area) with WHT. The total heat exchanger area increases with WHT. The significant deviation in the heat exchanger area at a higher heat source temperature range is due to the handling of more heat interaction in the evaporator and condenser to achieve the minimum log mean temperature difference value to maximize the net work output. This higher heat exchanger area value may bring down by appropriate judging the selling price of net work output value and capital investment in the heat exchanger. A larger area heat exchanger costs higher capital investment. EEORC-1 has a larger area because this cycle produces maximum power and so a larger heat input value requires at optimum pressure and lowest log mean temperature difference condition. Basic ORC has a lower area value because of less power production and simple thermodynamic heat exchanger design. The total heat exchanger area for EEORC-1 and EEORC-2 is dominated by the evaporator and condenser areas, respectively.

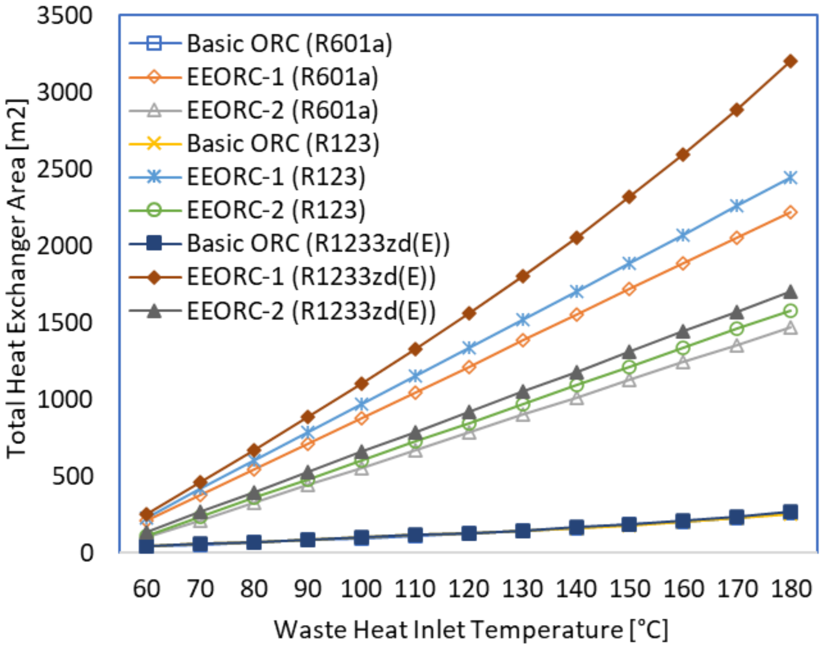

Figure 3.14. Effect on total evaporator and condenser areas with WHT for different cycles

Figure 3.15 represents the total cost consumed by different cycles for individual cycle components at 70 °C. The total cost is the sum of the capital investment, running cost and maintenance cost calculated (Table 3.4) per hour basis. As expected, the basic cycle has the lowest and EEORC-1 has the largest total cost rate due to the cost associated with the heat exchanger area and turbine size. Pump cost is significant in EEORC-1 due to more handling of working fluid mass. EEORC-1 with R1233zd(E) has the highest value due to maximum evaporator pressure and area, so the evaporator cost rate increases significantly. The available correlation [103,104] used to determine the turbine cost is for general-purpose international standards and the author feels that there is a need for some modified turbine cost correlation specially designed for waste heat recovery application for better prediction of turbine cost which will be locally manufactured.

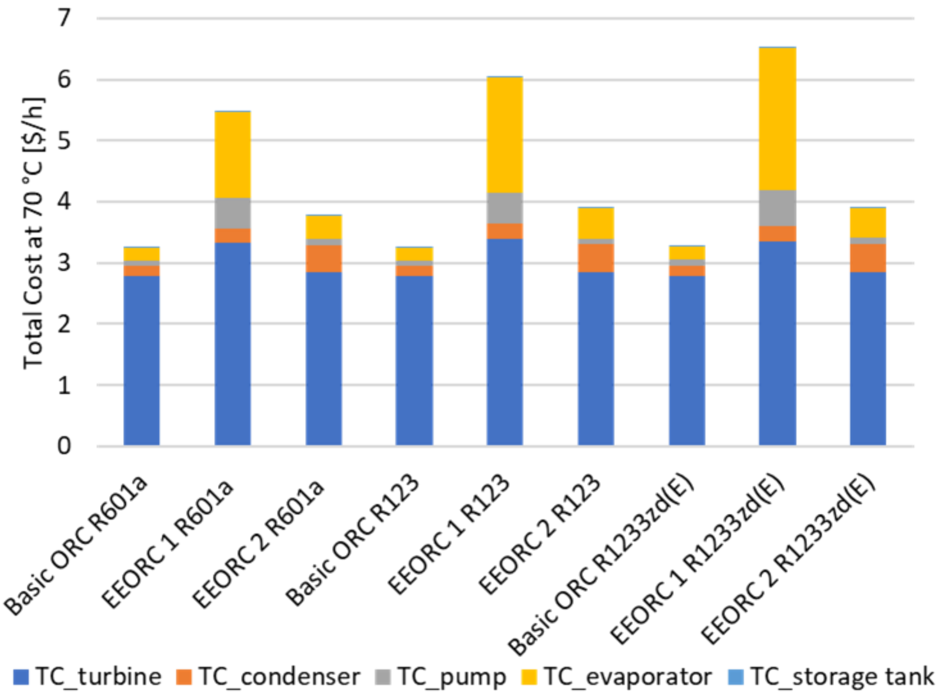

Figure 3.15. Value comparison on components cost rate of different cycles at 70 °C

Figure 3.16(a) represents the per-hour profit and per-unit selling price of three new different proposed economic models with the variation of WHT. Figure 3.16(b) represents the total annual profit for each power cycle and working fluid combination. In the figure, results show when old technology is completely replaced by new technology, then which economic model should follow so that both consumer and producer get the benefit? With the new technology, power plant production capacity will increase at the same WHT, which results in more availability (generation) of electric power. In developing countries, there is a scarcity of power due to the economy, technology and population. So, for fast development, such technology is required which can produce power at a cheaper rate with the support of the government so that more population can get benefitted from more hours of power availability but at a cheaper rate. In the current period, electricity is being sold to a consumer (country citizen) and per unit electricity price may be increased or decreased depending upon the government/industry price standard. Advancement in technology plays no role in per-unit electricity price fluctuation. Figure 3.16(a) represents the result for economic model-1 (M1) when per unit electricity selling price (SP) is the same, economic model-2 (M2) when total profit (TP) is the same, economic model-3 (M3) when unit profit (UP) is same and compare these results with the old technology having an existing economic model. In economic model

M1, the total profit rate is enhanced and maximum among other economic models at higher WHT (120-180 °C), by keeping the selling price constant with respect to the model followed by old technology. In this model, manufacturers enjoy gaining more profit, but the consumer will only get more hours of daily power availability at the same cost. In economic model M2, the total profit rate is constant but the selling price decreases with respect to the old technology economic model, so this model is favorable for the consumer as they get more hours of power availability at a cheaper rate and manufacturer's total profit remains the same. This model can be implemented by government power plants for the welfare of its citizen, especially those situated in rural areas. In economic model M3, the total profit rate is increased and the selling price decreases at a higher WHT range (95-180 °C). This model is not suitable for the lower WHT range, i.e., 60-95 °C, because of its higher value of selling price than the old technology. Figure 3.16(b) Variation on annual Net Profit with WHT for different cycles and working fluids when only existing (old) economic model is considered, among which EEORC-1 gives better results than EEORC-2. This graph serves the purpose of showing the variation in annual profit for different cycles and fluids for the old existing economic model. EEORC-1 gives maximum profit at the WHT range of 85-110 °C with a maximum of 7.32 % increment in profit by EEORC-1 (R123) at 90 °C.

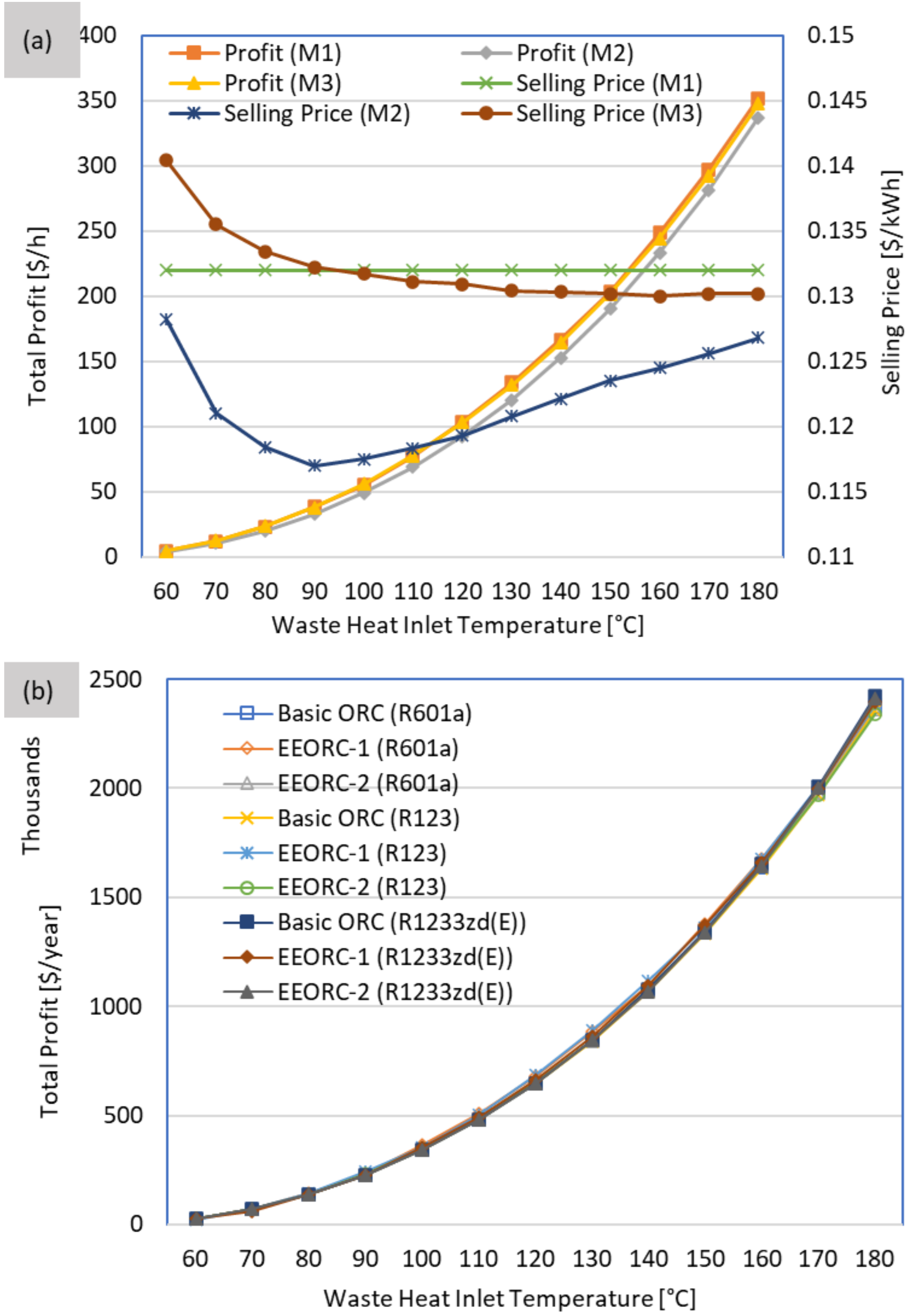

Figure 3.16. (a) Variation on total profit and selling price of EEORC-1 (R123) with WHT, (b) Variation on net annual profit with WHT for different cycles and working fluids

Figure 3.17 represents the amount of yearly CO_2 saving with the variation of WHT for different cycles. When power is produced from conventional coal-fired plants and then from boiler exhaust, a large amount of CO_2 emits, but when the same amount of power can be extracted from the waste heat source and at zero CO_2 emission, this is called CO_2 saving. There are many national and international agencies that encourage industries to emit as low as possible CO_2 and they support and encourage in terms of the monetary value of carbon credit gained. The amount of CO_2 saved converted into monetary value further adds profit to the industry. EEORC-1 saves the maximum amount of CO_2 and then EEORC-2 and basic ORC at all WHT ranges and thus add extra yearly profit.

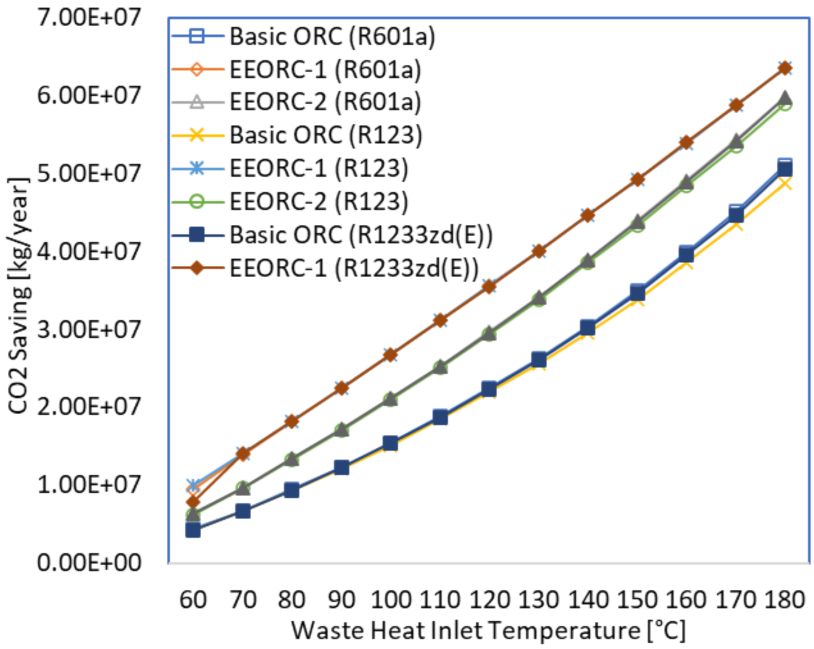

Figure 3.17. Variation of CO_2 saved with WHT for different cycles and working fluids

3.4. Important Findings

Two new ORC modification (EEORCs) are proposed and compared their 4E performances with the basic ORC for maximum net work output condition. Three economic models are chosen and used for the profit comparison of proposed cycles with the basic cycle for more power availability at a cheaper rate. By analysing the simulation results, the following conclusions are made.

(i) EEORC-1 with R123 gives maximum value for net work (122.2 kW), whereas basic ORC with R123 gives maximum thermal efficiency (3.8%), exergy efficiency (40.0%) and yearly profit (73143 $/year) at 70°C WHT.

(ii) For the studied heat source temperature range and working fluids, EEORC-1 yields maximum net work output with R123 for a lower temperature range (60-150 °C) and with R1233zd(E) for a higher temperature range (155-180°C).

(iii) Thermal and exergy efficiencies increase with WHT and are maximum for basic ORC with all studied working fluids for the whole studied range of WHT.

(iv) The heat exchanger size of EEORC is higher, whereas the size parameter is fluid-dependent (higher for all cycles with R123) for all WHT ranges and thus, the turbine cost increases significantly with cycle advancement.

(v) If economic model M1 is considered, then basic ORC with R123 will provide the highest yearly profit. Economic model M2 is the best when the industry gets subsidized by the government for new technology installation and in the reverse industry has to provide power at a lower selling price. The industry enjoys a 7.32% increase in profit with M2 model (compared with M1) when EEORC-1 (R123) is running at 90 °C WHT (some economic models are not feasible at 70 °C).

(vi) The EEORC-1 cycle saves the maximum amount of CO_2 emission, which will significantly reduce global warming. Also, CO_2 emission savings can be monetized in terms of carbon credit given by different international and governmental agencies, which can further benefit the power plant industry.

Overall, it can be concluded from this study that EEORC-1 is the best thermodynamic cycle among studied cycles as it produces maximum net power output with R123 and saves the maximum amount of CO_2 emission. The economic model M2 is the most suitable (among M1, M2 and M3), where both the industry and consumer get benefitted.

Chapter 4: Experimental Investigation

4.1. Experimentation

4.1.1. Setup Description

The experimental setup for the ORC system comprises three distinct and interconnected loops: the top hot fluid loop, the middle working fluid loop, and the bottom cold fluid loop, each serving to transfer, convert, and reject heat, respectively. The layout of an experimental setup for the organic Rankine cycle is shown in Figure 4.1. In the top hot fluid loop, a heat source supplies thermal energy to the evaporator, achieved using a 3-phase heater system with a temperature controller to simulate waste heat at a specific temperature grade. An RTD provides accurate temperature readings, ensuring a consistent heat supply to the system. Downstream of a gear pump, a pressure sensor monitors fluid pressure to maintain heat transfer efficiency and safety, while an electromagnetic mass flow meter measures the mass flow rate, regulating energy delivery to the system. The middle working fluid loop is the core of the ORC system, incorporating the evaporator, expander, condenser, and pump. A brazed plate heat exchanger functions as the evaporator, while a modified scroll compressor, adapted into a scroll expander, facilitates energy extraction. An in-house fabricated fin-type forced-air condenser handles condensation through forced convection, and a diaphragm pump enables leak-proof, fire-resistant fluid handling to prevent incidents caused by pressure surges. A high-pressure storage tank is designed to safely contain working fluid when the system is idle, preventing leaks and accommodating pressure variations. A critical component, the separator, is placed after the evaporator to divide the vapor and liquid phases of the working fluid, as fluctuations in heating load may result in mixed-phase output from the evaporator. The vaporized fluid proceeds through the scroll expander, where pressure energy is converted into mechanical work, driving a pulley that can connect to an alternator for electricity generation. This loop includes RTDs to track temperature changes at key points evaporator, expander outlet, and condenser while pressure sensors at the evaporator inlet, expander inlet and outlet, and condenser inlet monitor the pressure conditions, crucial for phase changes and cycle efficiency. A mass flow meter ensures precise measurement of the working fluid's flow rate, vital for balanced thermodynamic operation and consistent power output.

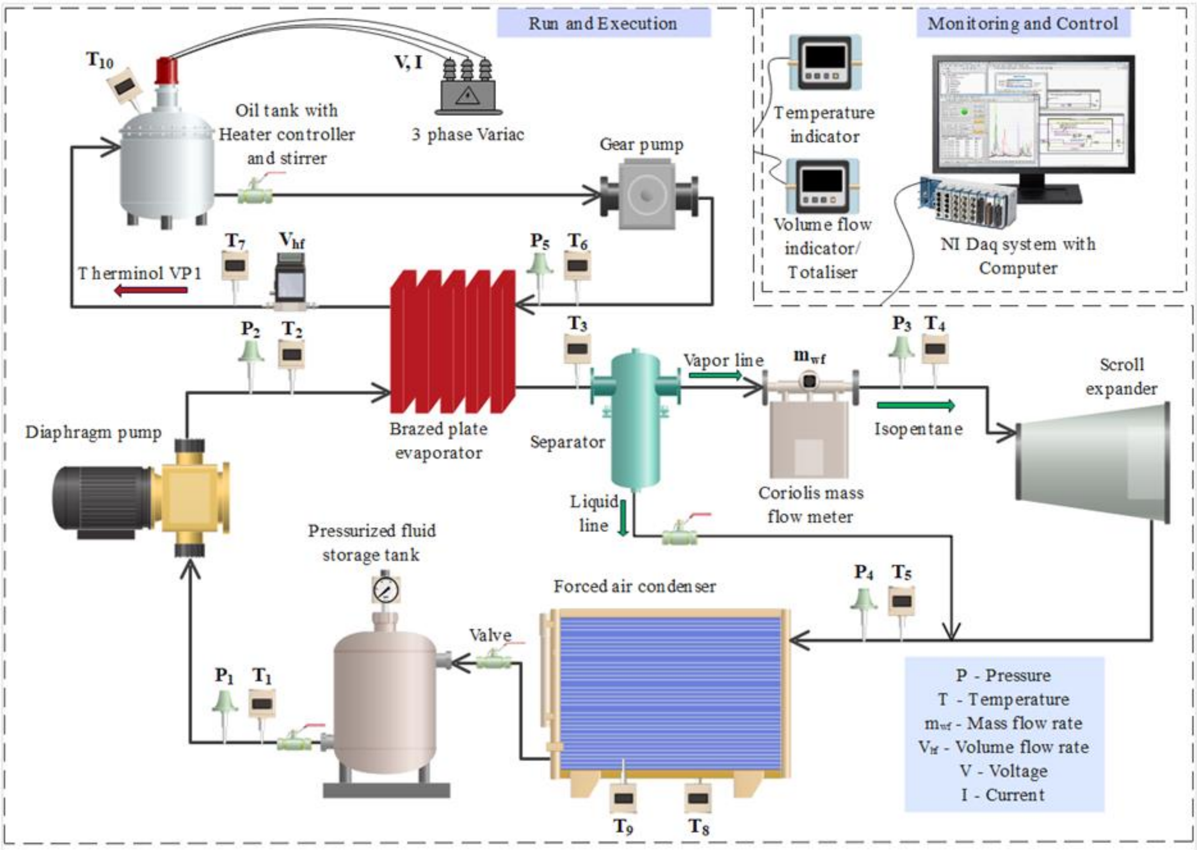

Figure 4.1. Layout of the experimental setup for the Organic Rankine Cycle

Heat is removed from the condenser in the bottom cold fluid (air) loop to achieve the necessary low-temperature conditions for effective condensation. Fan monitors temperatures before and after the condenser, ensuring sufficient heat removal, while a pressure sensor at the cooling fluid outlet provides data for flow regulation to prevent backpressure. Additionally, an air flow meter measures the cold fluid’s rate, which is critical for maintaining temperature stability and adequate heat absorption.

4.1.1.1. Fabrication and modification of Equipment’s

The fabrication of the vertical separator, as shown in Figure 4.2(a), is designed to efficiently separate liquid and vapor phases using gravity and a demister pad, having 4-inch diameter and 14-inch total height. The separator body is constructed from SS 314, a stainless-steel material known for its corrosion resistance and durability in high-temperature and high-pressure environments, making it suitable for the organic Rankine cycle. The separator consists of three ports. The top port functions as the vapor outlet, allowing separated vapor to exit the system. The middle port is the inlet for the vapor-liquid mixture, positioned so that the incoming flow can enter and begin the separation process. The bottom port serves as the liquid outlet, enabling the denser liquid phase to drain out after separation. The demister pad, positioned between the two halves of the vertical separator, is constructed from fine chicken mesh wire of 4-inch diameter and 2.5-inch height. This mesh acts as a filter, capturing any remaining liquid droplets in the vapor flow. When the vapor-liquid mixture enters the separator through the middle port, the liquid droplets are trapped by the mesh, while gravity pulls the denser liquid down to the bottom. This demister pad, secured with a metal cross-bracket, enhances the separation efficiency by ensuring that only vapor exits from the top port. The fabrication process involves first shaping and welding the stainless steel components to form a robust vertical cylinder with three distinct ports. After the cylinder body is formed, the demister pad is installed by placing it centrally between the top and bottom sections, ensuring a secure fit to handle the pressure and flow of the incoming mixture. The sections are then bolted together, compressing the demister pad and creating a gasket seal that prevents leakage. This separator setup allows gravity and the demister pad to work in tandem, ensuring effective separation of liquid and vapor phases, which is essential for maintaining system efficiency in the ORC experimental setup.

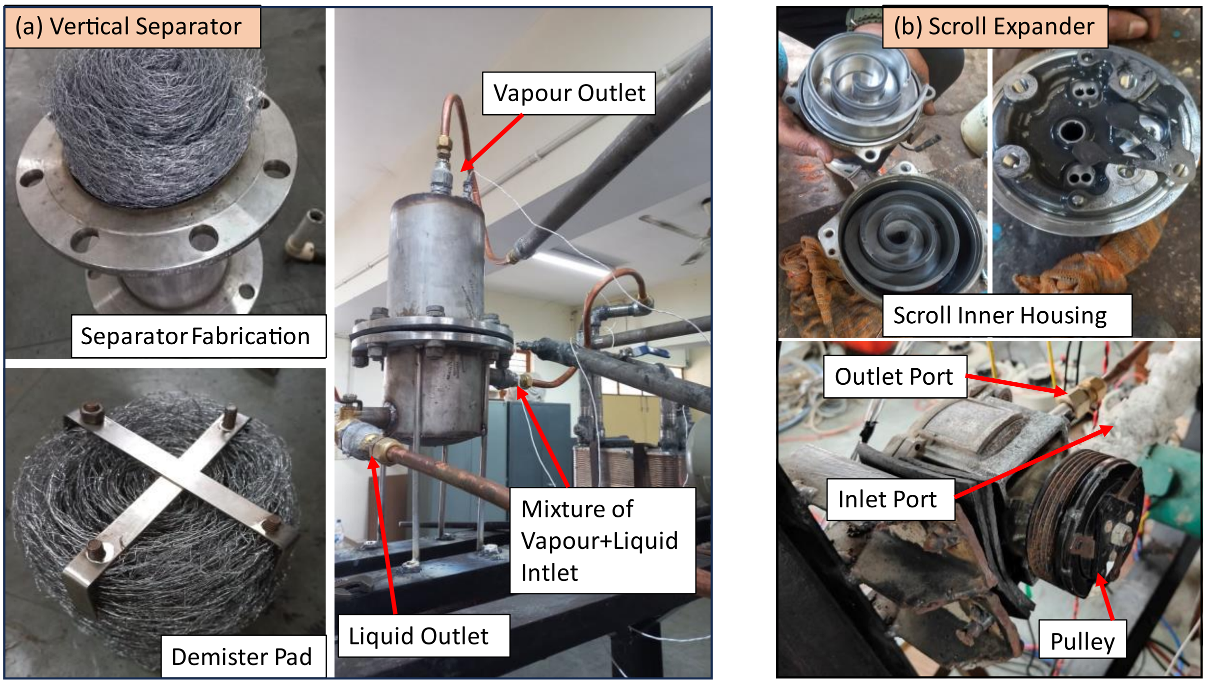

Figure 4.2. (a) Fabrication of the vertical separator and (b) modification of the scroll compressor to expander

To convert a scroll compressor into a scroll expander suitable for applications in an ORC system, several key modifications are required as shown in Figure 4.2(b). After conducting a series of trial runs on multiple scroll compressors, the authors identified the Mitsubishi-manufactured scroll compressor from the Tata Safari automobile as the most suitable choice for the application. This selection was based on its ability to handle the required volume 90 cm^3, its permissible operating speed range of 1200–1600 RPM, leak-proof design, and ease of installation, which uses R134a refrigerant and polyalkylene glycol (PAG) lubricant oil in the vehicle. Modification process allows the scroll compressor to operate in reverse, expanding a high-pressure, high-temperature working fluid into a low-pressure state while generating mechanical power. The modification begins by carefully disassembling the scroll compressor to access the internal components. This step includes separating the outer casing, removing the scroll sets, and exposing the ports. Careful documentation of the original configuration can be helpful if any reassembly guidance is needed. Once disassembled, the next step is to reverse the inlet and outlet ports. Typically, a scroll compressor has an inlet and an outlet port arranged for compressing gases. For use as an expander, these ports need to be reversed: the original compressor inlet becomes the outlet for the low-pressure expanded fluid, while the original compressor outlet serves as the new high-pressure inlet. In addition to reversing the ports, it is necessary to remove the one-way (check) valve commonly found at the compressor outlet. This valve is designed to prevent reverse flow, but in the expander configuration, it would restrict the fluid's movement, which is now intended to flow in the opposite direction. By removing this valve, the modified expander allows unrestricted fluid flow from the high-pressure inlet to the low-pressure outlet. Once the primary modifications are complete, inspect the seals and bearings to ensure they are capable of withstanding the reversed flow direction as well as any increase in temperature or pressure associated with ORC applications. In some cases, it may be necessary to upgrade these components to handle the higher temperature and pressure of ORC working fluids, which can be different from those used in conventional refrigeration systems. After all necessary modifications, reassemble the scroll expander, ensuring that each component is correctly positioned and securely fastened. Applying suitable lubricants or oils for high-temperature and high-pressure environments is advisable, as ORC systems often operate with different fluids. Before full-scale deployment, the modified scroll expander should be tested under controlled conditions to confirm proper function. During this testing phase, check for any leaks, unusual sounds, or excessive vibration that could indicate issues with the modifications. If mechanical work extraction is intended, it may be beneficial to install a pulley or coupling mechanism on the expander. This setup allows the mechanical energy produced by the expansion process to drive a generator, thereby converting thermal energy into electrical power.

The three-phase heating system depicted in Figure 4.3(a) is designed for heating oil within a storage tank, using a setup that includes dual heaters, a stirrer, and variac controllers for load adjustment. Two 5-5 kW heaters are mounted on the lid of the hot oil storage tank, providing a combined heating capacity to raise the temperature of the oil efficiently. Each heater is connected to a separate 5 kW variac, allowing precise control over the input power and heat load supplied to the heaters. The use of a three-phase system is advantageous as it helps to distribute the electrical load, reducing the current in each phase and thus making the system more efficient and safer for high-power applications. Additionally, a stirrer is installed within the tank to ensure uniform mixing of the oil, promoting even temperature distribution throughout the tank and preventing hot spots. This constant stirring action enhances the heating process and ensures that the entire volume of oil reaches the desired temperature evenly. The variacs with voltage indicators allow the operator to monitor and adjust the voltage supplied to each heater independently, providing granular control over the heating intensity. A clamp meter is used to measure the current. This combination of voltage and current provides the input heat load of the heating system. This setup is crucial for applications requiring precise thermal management and is commonly used in systems where consistent, high-temperature oil is needed as a heat transfer medium.

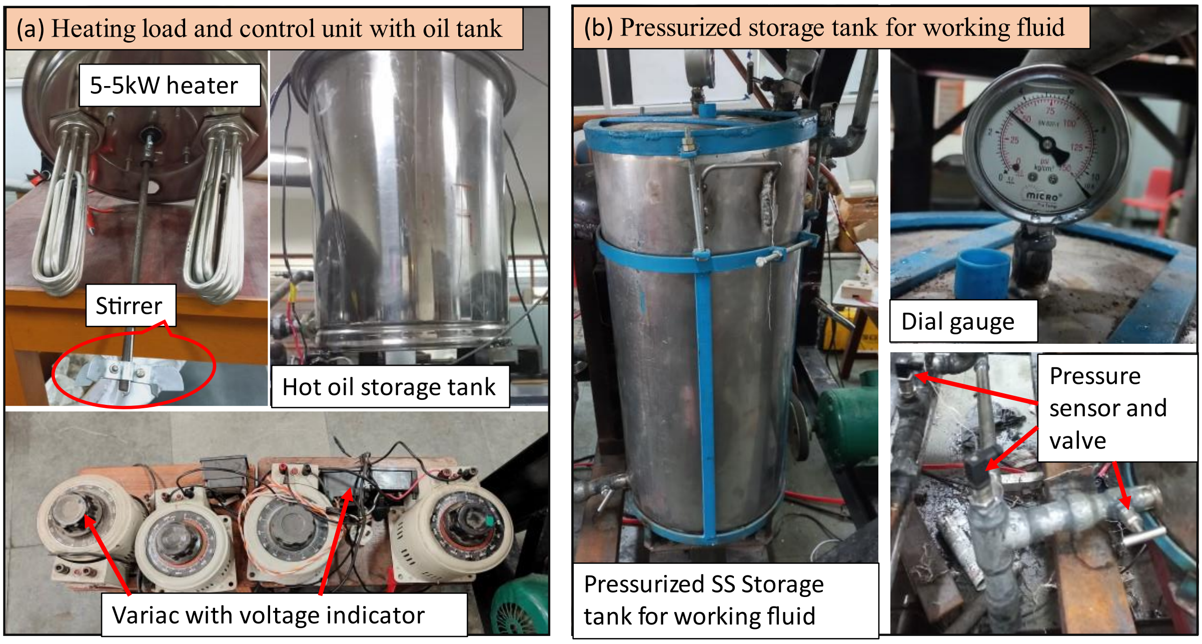

Figure 4.3. (a) Fabrication of the heating load and control unit with oil tank, (b) Pressurized storage tank for working fluid

The fabricated pressurized storage tank shown in Figure 4.3(b) is constructed from SS 314 stainless steel, designed to safely store and manage the working fluid used in the system, having 10-inch diameter and 35-inch height. The tank is equipped with three ports to facilitate the entry and exit of the circulating working fluid and to allow for the initial charging of the fluid. Each port is carefully fabricated with appropriate valves, ensuring a leak-proof design that maintains the pressurized conditions within the tank. Additionally, a pressure monitoring setup is included, with a dial gauge prominently mounted on the top for easy visibility. This dial gauge provides real-time feedback on the internal pressure levels, ensuring safe operating conditions. This robust construction ensures that the tank can handle high-pressure demands and maintain the integrity of the working fluid circulation within the system.

Other than fabricated components, ORC's main components description and technical details are tabulated in Table 4.1 for clear understanding. Table 4.1 contains the type, make, model and dimensions, along with the cost of the components.

Table 4.1. ORC component description and technical details

Component	**Type**	**Make**	**Model**	**Size and Capacity**	**Cost (USD)**	**Application**
Evaporator	Brazed	Alfa Laval	CB40	Heat transfer area: 1 m^2, Number of plates: 40 Capacity: 13.7 kw	249.14	Evaporation of working fluid
Expander	Scroll	Mitsubishi heavy industries, Purpose: Compressor of Tata Safari Storme	5DR 2.2L VX 4X2	Volume flow rate: 90 cm^3	973.81	Modified to serves as turbine to generate electricity by pulley rotation

Condenser	Forced air fin type	Gireesh Condensers	-	Heat transfer area: 1.7 m^2	207.14	To condense the working fluid to liquid state
Pump	Hydraulic diaphragm pump with rupture detection	Grosvenor	GP-Z-C	Head: 10 kg/cm^2 Capacity: 1000 LPH	1136.25	To pump the working fluid to the evaporator
	Gear pump	Dhara	DP-40	Head: 1 kg/cm^2 Capacity: 1500 LPH	261.01	To pump the hot oil to the evaporator

4.1.1.2. Instruments and Sensors

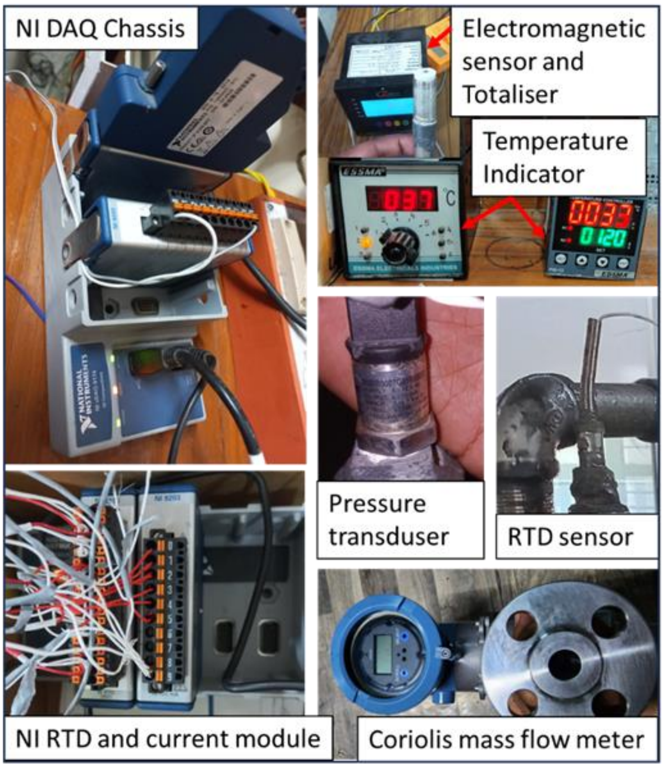

Figure 4.4. Installation of instruments and sensors to ORC setup

The instrumentation setup for the ORC experiment includes a variety of sensors and data acquisition tools that are critical for accurate measurement and data logging, as shown in Figure 4.4. An NI DAQ Chassis (National Instruments Data Acquisition System) with modules for RTD (Resistance Temperature Detector) and current measurement serves as the core for data collection. This DAQ system allows for real-time monitoring and logging of various parameters in the ORC system. The RTD sensors are used to accurately measure temperatures at different points in the system, providing crucial data for evaluating heat transfer efficiency and thermodynamic performance. A pressure transducer is installed to measure the pressure at key points, ensuring that the pressure levels are within safe operational limits and aiding in the calculation of energy transformations within the cycle. A Coriolis mass flow meter is employed for flow measurement. This sensor provides precise mass flow rate data, which is essential for balancing the thermodynamic equations and for the efficiency analysis of the ORC system. An electromagnetic sensor with a totalizer is used to measure the cumulative flow of the hot oil fluid, providing additional insights into fluid dynamics over time. Additionally, a temperature indicator is used to display temperature readings from the thermocouples placed at the entry and exit of the forced air condenser system, giving immediate feedback for on-site monitoring and adjustments. These instruments collectively enable accurate and comprehensive data collection, allowing for detailed performance analysis and optimization of the ORC system.

Table 4.2 shows the typical range and associated accuracies of the instruments used for data reduction from the ORC setup. This information is useful for analyzing the sensor's placement and accuracy in measuring the data.

Table 4.2. ORC sensors description, along with technical details

Sensor	**Type**	**Make**	**Working Range**	**Accuracy**	**Position**
Pressure Transducer	Piezoelectric Type	Gem	0-5 bar, 0-10 bar (2 nos), 0-15 bar and 0-25 bar	±0.25% of the reading	P_1, P_2, P_3, P_4 and P_5
Temperature Transducer	RTD	Airex	0–850°C	±0.2°C	T_1, T_2, T_3, T_4, T_5, T_6 and T_7

	J-type	Thermonic	0–750°C	±1.5°C or ±0.75% of the reading	T_8, T_9 and T_{10}
Mass Flow Meter	Coriolis	Shanghai Yinou-LZYN	0–50 kg/min	±0.29–2.5% of reading	Working fluid side ($\dot{m}_{wf}$)
Volume Flow Meter	Electromagnetic	Ztech	25–160 lpm	±1.5% of reading	Hot oil side ($\dot{V}_{hf}$)
Data Acquisition System (DAQ)	-	National Instrument	-	±0.05% of the reading	Computer
Voltage and Current Meter	Clamp	Unity	0–750V; 0–1000A	±1% for current, ±1% for voltage	Oil Tank with Heater

4.1.1.3. Assembly of different equipment in the setup

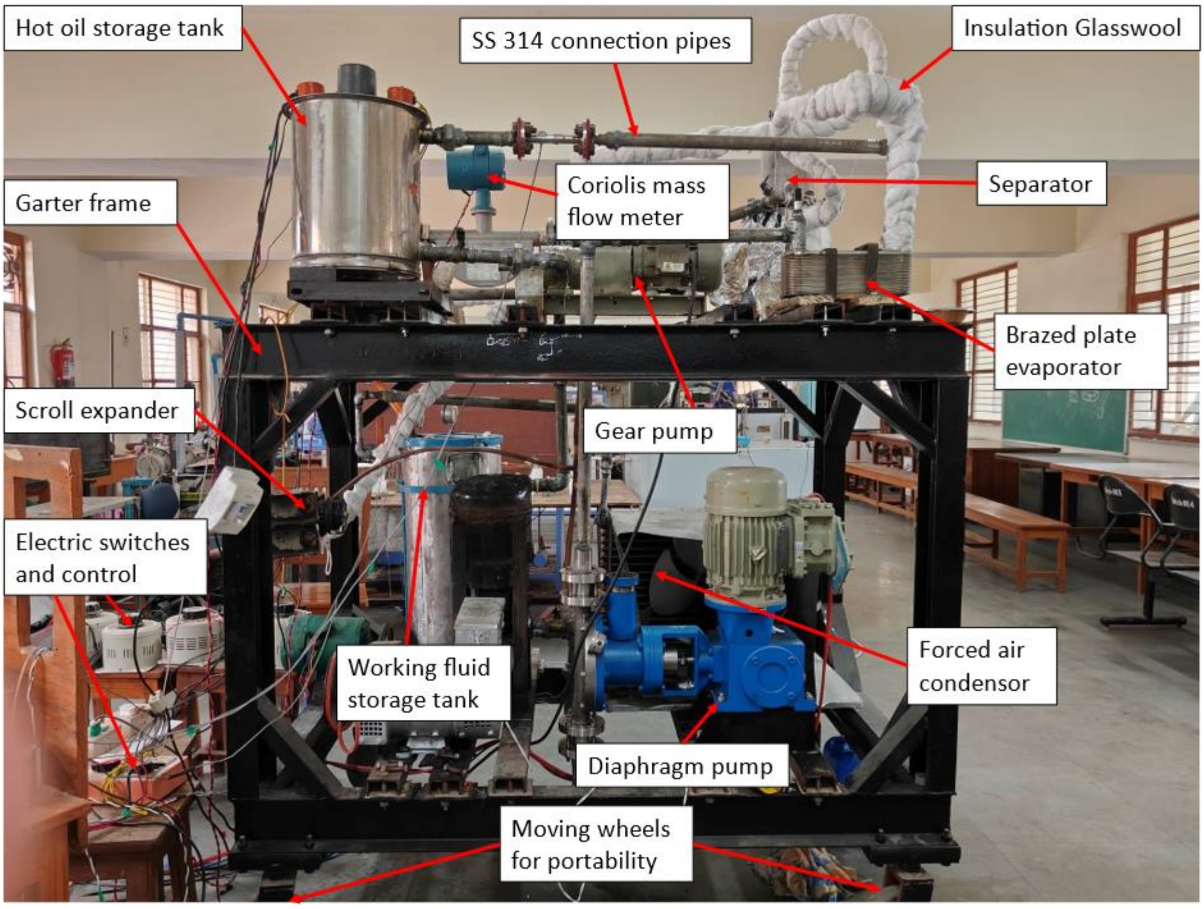

Figure 4.5. Lab-scale ORC experimental setup

The ORC experimental setup shown in Figure 4.5 consists of various components and systems assembled to enable the generation of power from low-grade thermal energy sources. The main components include a hot oil storage tank, scroll expander, working fluid storage tank, evaporator, condenser, pumps, meters, and control systems. This setup is designed to test and analyze the ORC's performance in converting thermal energy into mechanical or electrical energy. The fabrication of this ORC setup starts with building a sturdy foundation using a garter frame, typically made from steel and welded together to provide stability during operation. Moving wheels are attached to the frame base for portability, allowing the setup to be easily relocated within the laboratory or workshop. Several key components, including the hot oil storage tank, are fabricated from stainless steel (SS 314) to ensure durability and resistance to high temperatures. This storage tank is designed to store and supply thermal oil to heat the working fluid in the system. Stainless steel (SS 314) connection pipes are used to link different components, chosen for their corrosion resistance and ability to handle high temperatures. The evaporator, designed to vaporize the working fluid by transferring heat, and the separator, which removes residual liquid from the vapor, are fabricated using SS 314 materials that can withstand high temperatures. Critical components such as the connection pipes and evaporator are wrapped with insulation glass wool to minimize heat loss, thereby improving the efficiency of the ORC system. The assembly process involves setting up a pump and flow control system, heat exchange and vaporization system, expansion and condensation system, and a control panel. The setup includes a gear pump and diaphragm pump; the gear pump circulates thermal oil from the hot oil storage tank to the evaporator, while the diaphragm pump circulates the working fluid throughout the ORC system. A Coriolis mass flow meter is placed on the working fluid line to monitor and measure the mass flow rate, which is essential for system performance analysis. In the heat exchange system, the hot oil storage tank supplies heated oil to the brazed plate evaporator, where heat is transferred to the working fluid, vaporizing it. The separator, positioned after the evaporator, ensures that only vapor enters the scroll expander. The vaporized working fluid then flows into the scroll expander, where it expands, converting thermal energy into mechanical energy. The scroll expander has been modified to operate in an expansion mode rather than compression. After expansion, the working fluid enters a forced air condenser, where it releases heat and condenses back into a liquid before returning to the storage tank. An electric control panel with switches manages the operation of pumps, flow rates, and other critical parameters, enabling precise control and safe operation during testing. Following assembly, the ORC setup undergoes testing and calibration. A system leak test is performed on all connections, including the SS 314 pipes, pumps, and the evaporator, to ensure there are no leaks, as leaks could lead to inefficiencies and safety hazards. The Coriolis mass flow meter and control systems are calibrated to ensure accurate readings of mass flow rate and other operational parameters, enhancing the reliability of data collected during testing. The heating system, comprising the hot oil storage tank and circulation system, is tested to confirm that the thermal oil reaches the required temperature for effective heat transfer, and the effectiveness of insulation is also verified. The setup is then subjected to a trial run to assess its operational performance. During initial startup, the pumps are activated to circulate both the working fluid and thermal oil through the system, with the heated oil vaporizing the working fluid in the evaporator. This vaporized fluid is directed into the scroll expander, which begins to rotate and generate mechanical energy. Key parameters, such as mass flow rate, temperature, and pressure, are continuously monitored using the Coriolis mass flow meter and other sensors, providing essential data for evaluating the system's performance and efficiency. The condenser’s performance is observed to ensure the working fluid fully condenses before returning to the storage tank. Data collected during the trial run is used to analyze the ORC's efficiency, heat transfer effectiveness, and the mechanical output of the expander, allowing for further adjustments and optimizations if necessary.

This experimental ORC setup provides a practical approach to harnessing low-grade heat for power generation, demonstrating the effectiveness of the ORC in converting thermal energy into mechanical energy. Through careful fabrication, assembly, testing, and operational adjustments, this setup provides valuable insights into the ORC's efficiency and effectiveness for energy conversion applications.

Figure 4.6. Isometric view and running condition of ORC experimental setup

4.1.2. Experimental Procedure

To conduct an experiment on the ORC setup, the following procedure has been developed, which integrates the detailed setup description, assembly, and testing process with the provided checklist instructions for startup, operation, and shutdown. Figure 4.6 shows the isometric view and running condition of the ORC experimental setup. Safety measures are emphasized throughout the process to ensure accurate data recording while avoiding accidents.

i. **Preparation and Initial Checks:** Begin by conducting a comprehensive check of the entire ORC system to ensure that all components are correctly installed and ready for operation. Inspect the garter frame for stability, and confirm that the moving wheels are locked to prevent any unintentional movement during the experiment. Carefully inspect all stainless steel (SS 314) connection pipes for any signs of leakage or weak joints, particularly at critical points around the hot oil storage tank, working fluid storage tank, gear pump, and diaphragm pump. Verify that all valves are correctly installed and can open and close smoothly.

ii. **Wiring and Electrical System:** Examine all electrical wiring and connections to the control panel and electric switches. Ensure that all wires are securely connected and safely organized to avoid contact with heated components. Put on hand gloves and a mask as an additional safety precaution before beginning any operations involving electricity or heat.

iii. **Power On and Initial System Setup:**

- Turn on the Main MCB (Main Circuit Breaker), then switch on all sensors and NI DAQ system.
- Turn on the main heater and stirrer switch to initiate uniformly heating of the oil in the hot oil storage tank. Subsequently, turn on the gear pump and open its corresponding valve to start the circulation of thermal oil towards the brazed plate evaporator.

iv. **Data Acquisition System Setup:** Connect the NI DAQ A-type cable to the computer to facilitate data logging. Run the NI code, initializing it by turning on the RTD channel and current channel within the software code. Ensure that all columns necessary for data recording, including time, heater load, hot tank temperature, hot oil mass flow rate, condenser inlet temperature, and condenser outlet temperature, are pre-set in an encoded Excel sheet and a diary to log observations manually as well.

v. **Safety Measures Before Operation:** Verify that all safety measures are in place, such as wearing hand gloves, masks and fire extinguisher, to protect against burns or inhalation of fumes. Double-check and open all valves of hot oil side and working fluid side for flow freely during the experiment.

vi. **System Start-Up:**

- Turn on the diaphragm pump and verify that its valve is open to allow fluid movement through the ORC system.
- Activate the condenser fan to ensure adequate cooling for the condensation process after expansion.

- Closely monitor the heater ampere and voltage reading to avoid overheating, and carefully observe any signs of leaks around the high-temperature areas and connections.

vii. **Data Collection and Observation:**

- As the system reaches operational temperature, data recording begins. Monitor and log all readings continuously in the Excel sheet linked to the NI system code, which captures data on temperature, pressure, and mass flow rates.
- Observe the scroll expander for any signs of abnormal vibration or noise, which may indicate issues in the expansion process.
- Ensure that all data is being correctly recorded automatically and manually to track the performance and efficiency of each component in real time.

viii. **Cautious Data Recording:**

- To avoid potential accidents, keep a safe distance from the high-temperature components like the hot oil storage tank and evaporator while observing the readings.
- Be vigilant in checking for any leaks around the piping or valves, and do not attempt to tighten or adjust any components while the system is pressurized and hot.
- Regularly inspect the condenser for proper cooling, as failure in the cooling process could result in overheating and potential hazards.

ix. **Shut Down Procedure:**

- Close the working fluid storage tank outlet valve immediately after the experiment is complete. Allow the diaphragm pump to run for an additional 0.5 minutes to circulate any remaining fluid within the system.
- Close the hot fluid valve and allow the gear pump to run for 1 minute to flush any residual hot oil, which helps in preventing leakage, overheating of the storage tank or gear pump post-operation.
- Conduct a final inspection of all connections, checking for any leaks, and ensure that all valves are securely closed.
- Turn off all switches and finally turn off the Main MCB to cut off power to the entire system.

x. **Final Data Logging and Clean-Up:** Record any final observations in the diary regarding the setup's performance, anomalies encountered, and the overall data trends observed. Save and back up the collected data from the Excel sheet to ensure no loss of information.

This ORC experiment procedure is designed to facilitate a safe and structured approach to operating and analyzing the ORC system. The startup and shutdown checklists are followed rigorously, with particular attention to inspecting connections, monitoring leakage, and ensuring all valves and wiring are in place before initiating any heating. Data reading is carefully monitored to maintain distance from high-temperature components, and any signs of leakage are dealt with by immediately halting operations. Through this controlled procedure, the ORC setup can be tested effectively while minimizing risks and providing accurate data on the system's performance.

4.1.3. Data Reduction

This section details the methodology for analyzing the ORC's thermodynamic performance based on experimentally measured data. Using temperature, pressure, and flow rate data collected from the ORC setup, thermodynamic properties are required to evaluate cycle performance metrics such as heat input, work output, and thermal efficiency. The required thermodynamic equations, (2.1 - 2.19) are taken from chapter 2.

The heat input through a 3-phase heater is calculated by,

$$Q_{in} = V \times I \tag{4.1}$$

Where V is 3-phase voltage and I is current.

ORC experiment has been performed on the above setup and the data reduced is tabulated below in Table 4.3 for the mean condition of cold air inlet temperature (33°C) and volume flow rate of hot oil (50 litre/min) for different heat input loads. Table 4.3 contains all the important input and output parameters of experimental data.

Table 4.3. ORC experimental data at various heat loads and mean input condition

Parameter	**Unit**	**Experimental data**				
***Heat Input**	(kW)	5	6.5	8	10	11.5
***Cold air inlet temperature**	(°C)	33.2	32.8	32.6	33.3	32.8
***Volume flow rate of hot fluid**	(litre/min)	50.34	50.21	49.92	49.49	49.60
Pump inlet pressure	(bar)	1.73	1.75	1.76	1.76	1.77
Pump outlet pressure	(bar)	4.10	5.09	8.32	12.62	17.85
Turbine inlet pressure	(bar)	3.75	4.55	7.60	11.73	16.72
Turbine outlet pressure	(bar)	2.02	2.10	2.17	2.24	2.30
Evaporator's hot fluid inlet pressure	(bar)	2.06	2.03	2.06	2.07	2.07
Mass flow rate of working fluid	(kg/sec)	0.0053	0.0062	0.0066	0.0077	0.0079

Hot fluid inlet temperature	(°C)	100.9	107.4	127.6	150.2	172.2
Hot fluid outlet temperature	(°C)	95.9	101.0	119.7	140.8	161.5
Pump inlet temperature	(°C)	34.9	35.0	34.9	34.8	35.0
Pump outlet temperature	(°C)	35.1	35.4	35.5	35.6	36.2
Turbine inlet temperature	(°C)	87.4	93.4	112.8	132.2	150.6
Turbine outlet temperature	(°C)	75.9	78.1	85.6	93.2	101.8
Pump isentropic efficiency	(%)	58.81	63.09	67.20	67.60	66.66
Turbine isentropic efficiency	(%)	67.75	71.68	77.27	80.30	77.05
Evaporator effectiveness		0.81	0.81	0.83	0.83	0.82
Net power output	(kW)	0.123	0.189	0.387	0.670	0.939
Pump power	(kW)	0.004	0.005	0.011	0.018	0.026
Turbine power	(kW)	0.127	0.194	0.397	0.688	0.966
Cycle efficiency	%	2.34	2.91	4.75	6.67	8.08
Specific Work Output	(kJ/kg)	23.17	30.58	59.03	87.41	118.81

*Input parameters used to investigate the performance on other parameters (Table 4.3)

As the heat input increased from 5 kW to 11.5 kW, pump and turbine pressures, working fluid mass flow rate, and system temperatures rose accordingly, reflecting the system's response to higher loads. The turbine and pump pressures increased with heat input, driving higher fluid flow and power output. This was accompanied by an increase in working fluid mass flow through the evaporator. Pump and turbine isentropic efficiencies also improved, indicating better thermodynamic performance. The evaporator maintained stable effectiveness, ensuring consistent heat exchange. Net power output grew from 0.123 kW to 0.939 kW, with cycle efficiency rising from 2.34% to 8.08%, demonstrating a more efficient conversion of heat into mechanical power. Specific work output also increased, enhancing system performance under higher heat conditions. While a techno-economic analysis on a lab-scale experimental setup may not provide a precise representation of large-scale implementation, it offers valuable insights into scalability and technology validation. Considering a waste heat input of 11.5 kW, the system can generate approximately 1 kW of net power. The estimated setup costs include approximately $3,000 (₹2,60,000) for equipment, $5,500 (₹4,80,000) for instrumentation, and $1,700 (₹1,50,000) for working fluids. Assuming an annual operation of 7,000 hours, the system would produce 7,000 kWh of electricity, generating a revenue of ₹70,000 ($805) at ₹10 per kWh. Based on this, the total investment of \$10,200 (₹8,90,000) can be recovered in approximately 13 years all while producing energy without burning fossil fuels.

4.1.4. Uncertainty Analyses

The ORC net power and cycle efficiency are primarily dependent on temperature, pressure, mass flow rates and electrical power. Each measured parameter has its own uncertainty. Using the partial derivative approach (root-sum-square method), propagate uncertainties for key calculated parameters using equation (4.2) given by (Kline and McClintock, 1953).

$$U_Z = \left[\left(\frac{\partial Z}{\partial X_1} U_{X_1}\right)^2 + \left(\frac{\partial Z}{\partial X_2} U_{X_2}\right)^2 + \cdots \ldots \ldots + \left(\frac{\partial Z}{\partial X_n} U_{X_n}\right)^2\right]^{\frac{1}{2}} \quad (4.2)$$

Where, Z is a function of the independent variables X1, X2, X3,…,Xn are the uncertainties of the independent variables. The maximum uncertainties of the calculated parameters are listed in Table 4.4.

Table 4.4. Uncertainty analyses of major input and output parameter

Parameters	**Uncertainty Calculation Formula**	**Uncertainty value (%)**
Heat Input (kW)	$\mathrm{U_{Q_{in}}} = \left[\left(\frac{\partial \mathrm{Q_{in}}}{\partial \mathrm{V}} \mathrm{U_V}\right)^2 + \left(\frac{\partial \mathrm{Q_{in}}}{\partial \mathrm{I}} \mathrm{U_I}\right)^2\right]^{\frac{1}{2}}$	±4.2
Net Power (kW)	$\mathrm{U_{W_{net}}} = \left[\left(\frac{\partial \mathrm{W_{net}}}{\partial \dot{\mathrm{m}}_{\mathrm{wf}}} \mathrm{U}_{\dot{\mathrm{m}}_{\mathrm{wf}}}\right)^2 + \left(\frac{\partial \mathrm{W_{net}}}{\partial \mathrm{h_{t,i}}} \mathrm{U_{h_{t,i}}}\right)^2 + \left(\frac{\partial \mathrm{W_{net}}}{\partial \mathrm{h_{t,o}}} \mathrm{U_{h_{t,o}}}\right)^2\right]^{\frac{1}{2}}$	±5.6
Cycle Efficiency (%)	$\mathrm{U_{\eta_{th}}} = \left[\left(\frac{\partial \eta_{\mathrm{th}}}{\partial \mathrm{W_{net}}} \mathrm{U_{W_{net}}}\right)^2 + \left(\frac{\partial \eta_{\mathrm{th}}}{\partial \mathrm{Q_{in}}} \mathrm{U_{Q_{in}}}\right)^2\right]^{\frac{1}{2}}$	±4.7

4.1.5. Optimization and Prediction

In the optimization and prediction of ORC performance, Response Surface Methodology (RSM) coupled with Analysis of Variance (ANOVA) plays a critical role. The design of experiments (DOE) through RSM enables the investigation of the relationship between independent input variables and the response variables, such as net power output and cycle efficiency. By employing statistical models, RSM aids in optimizing performance and predicting outcomes under various conditions.

The experiments for this study were constructed using central composite design (CCD), a common approach in RSM, which allows for a systematic variation of process parameters and evaluation of their impact on the performance of the ORC. The experimental data for the ORC was derived from controlled tests and tabulated in Table 4.5, where key operating parameters such as heat load, volume flow rate of hot oil, and cold air inlet temperature were varied. The objective was to maximize both the net power output and the cycle efficiency.

Table 4.5. Design of Experiment Table by Central Composite Method

	Factor 1	**Factor 2**	**Factor 3**	**Response 1**	**Response 2**
Run	**A: Heat Input (kW)**	**B: Cold Air Inlet Temperature (°C)**	**C: VFR of Hot Oil (litre/min)**	**Net Power (kW)**	**Cycle Efficiency (%)**
1	11.5	37	60	0.864	7.52
2	5	37	40	0.135	2.70
3	11.5	29	60	0.831	7.23
4	8.25	33	40	0.383	4.64
5	8.25	33	50	0.422	5.12
6	11.5	33	50	0.940	8.17
7	8.25	33	50	0.424	5.14
8	11.5	37	40	0.906	7.88
9	5	29	60	0.092	1.84
10	5	37	60	0.109	2.18
11	8.25	33	50	0.422	5.12
12	5	33	50	0.123	2.46
13	5	29	40	0.120	2.39
14	8.25	33	50	0.421	5.11
15	8.25	33	50	0.422	5.11
16	8.25	33	50	0.423	5.12
17	8.25	33	60	0.399	4.84
18	11.5	29	40	0.874	7.60
19	8.25	29	50	0.436	5.28
20	8.25	37	50	0.397	4.81

The results from ANOVA were tabulated in Table 4.6, with the F-value, p-value, mean, standard deviation, adjusted R^2, and predicted R^2 provided in a structured format. Table 4.6 serves as a key tool for assessing the adequacy of the developed models and ensuring they can be used reliably for optimization.

Table 4.6. ANOVA coefficients and fit statistics of the model

	Response 1: Net Power	**Response 2: Cycle Efficiency**
Model	Quadratic	Quadratic
F-value	406.36	167.86
P-value	< 0.0001	< 0.0001
Mean	4.57	5.01
Standard deviation	0.2034	0.2193
Adjusted R2	0.9948	0.9875
Predicted R2	0.9789	0.9491
Adequate Precision	56.795	39.1257

The F-value tests the overall significance of the model. A higher F-value suggests that the model is significant and that the variation in the data is well-explained by the independent variables. The Model F-value for net power is 406.36 and for cycle efficiency is 167.86, which implies that the model is significant. There is only a 0.01% chance that an F-value this large could occur due to noise. The p-value indicates the probability that the observed F-value occurs by chance. P-values less than 0.0500 indicate model terms are significant. The Predicted R^2 is in reasonable agreement with the Adjusted R^2 for both responses; i.e., the difference is less than 0.2. Adequate precision measures the signal-to-noise ratio and the value greater than 4 is desirable. Thus, this model can be used to navigate the design space.

Regression equations (4.3) and (4.4) used for the prediction of net power and cycle efficiency based on the above RSM-ANOVA model are illustrated below, on heat input [A], 5-11.5 kW; cold air inlet temperature [B], 29-37 °C; and volume flow rate of hot oil [C], 40-60 litre/min. The Validity range of net power and cycle efficiency are 0.092-0.94 kW and 1.84-8.17 % respectively.

$$\begin{aligned} Net\ Power\ =\ &+0.4228 + 0.3836A + 0.0058B - 0.0123C + 0.0041AB \\ &- 0.0039AC + 0.0004BC + 0.1081A^2 - 0.0069B^2 - 0.0324C^2 \end{aligned} \tag{4.3}$$

$$\begin{aligned} Cycle\ Efficiency \\ &= +5.11 + 2.68A + 0.0753B - 0.1617C - 0.0092AB \\ &+ 0.0424AC + 0.0040BC + 0.2151A^2 - 0.0542B^2 - 0.3597C^2 \end{aligned} \tag{4.4}$$

Where A, B and C indicate independent variable Heat input, Cold air inlet temperature and Volume flow rate of hot oil, respectively.

The Predicted vs. Actual graph for ORC's net power and cycle efficiency responses in RSM-ANOVA is crucial for assessing model accuracy and shown in Figure 4.7. It compares the model's predicted values from the regression equation as illustrated above, with actual experimental results. A strong correlation, where points align closely to the diagonal line, indicates that the model reliably captures the relationship between the input variables and the responses. Deviations from this line suggest model inaccuracies or the presence of outliers. Overall, this graph helps validate the model's predictive net power and cycle efficiency, ensuring it can be used confidently for optimization and performance forecasting of the ORC experiment setup.

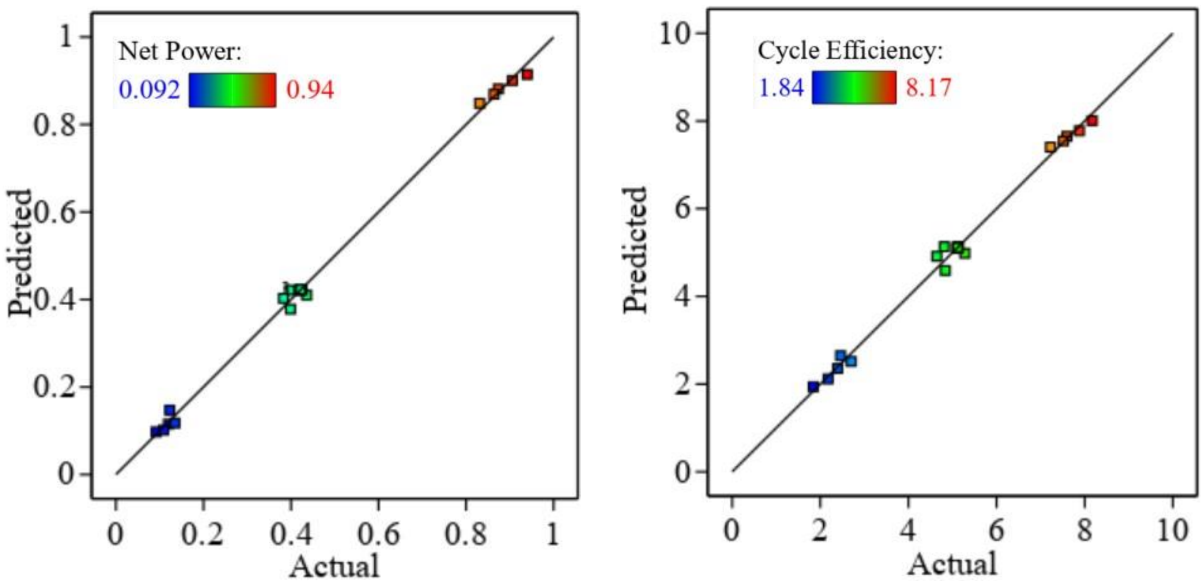

Figure 4.7. Normal plot of variation between predicted and actual value of net power and cycle efficiency

4.2. Results and Discussion

4.2.1. Effect on operating and performance parameters

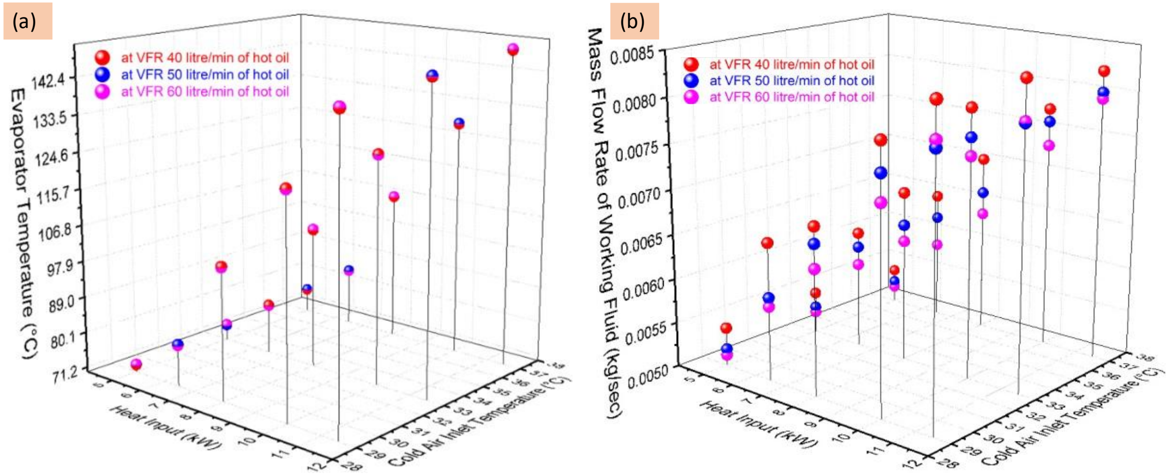

Figure 4.8. Effect on (a) Evaporator temperature and (b) Mass flow rate of working fluid

Figure 4.8(a) illustrates the relationship between heat input, VFR of hot oil, and cold air inlet temperature on the evaporator temperature in an ORC system. Data points are color-coded to indicate different VFRs, as mentioned previously, to help make a straightforward visual comparison of how variations in the hot oil flow rate impact the evaporator temperature under different conditions of heat input and cold air inlet temperatures. The plot shows a clear trend where an increase in heat input results in a corresponding rise in the evaporator temperature. This is an expected outcome, as a higher energy input elevates the thermal load in the evaporator, thus raising its temperature. Furthermore, within each level of heat input, an increase in the VFR of hot oil generally leads to a slightly higher evaporator temperature. This suggests that higher flow rates enhance the heat absorption capacity of the hot oil, improving the energy transfer efficiency in the evaporator. The VFR effect on the evaporator's temperature is not realised from the figure because of both a slight increase in the evaporator's temperature and instrument uncertainty. Additionally, the effect of cold air inlet temperature is significant in this figure. At higher cold air inlet temperatures, the evaporator temperature also tends to be higher, indicating reduced cooling effectiveness in the system. This is likely due to the decreased temperature gradient between the working fluid and the condenser air, which limits the cooling capacity and results in a warmer evaporator.

Figure 4.8(b) provides a comprehensive visualization of the relationship between the mass flow rate of the working fluid (in kg/sec) with heat input (in kW), the cold air inlet temperature (in °C) under varying VFR of hot oil in an ORC experimental setup. From the graph, it is evident that the mass flow rate of the working fluid generally increases with a rise in both heat input and cold air inlet temperature across all tested flow rates of hot oil. For instance, at a lower heat input and colder inlet temperatures, the mass flow rate is minimal, particularly for the 60 LPM flow rate, indicating a lower thermodynamic efficiency in transferring heat to the working fluid. However, as the heat input increases, a noticeable rise in the working fluid's mass flow rate can be observed, especially at lower VFRs of 40 and 50 LPM. This trend suggests that decreasing the hot oil flow rate enhances the heat transfer capacity, thereby driving a higher mass flow rate of the working fluid in the ORC system. Moreover, the graph highlights that the impact of cold air inlet temperature on the mass flow rate becomes more pronounced at lower VFRs. This correlation indicates that a higher VFR of hot oil enhances the system’s responsiveness to changes in cold air inlet temperature, likely due to improved heat exchange efficiency at elevated flow rates. Overall, the interrelationship between heat input, cold air inlet temperature, and hot oil VFR underscores the dynamic response of the ORC system under different operating conditions.

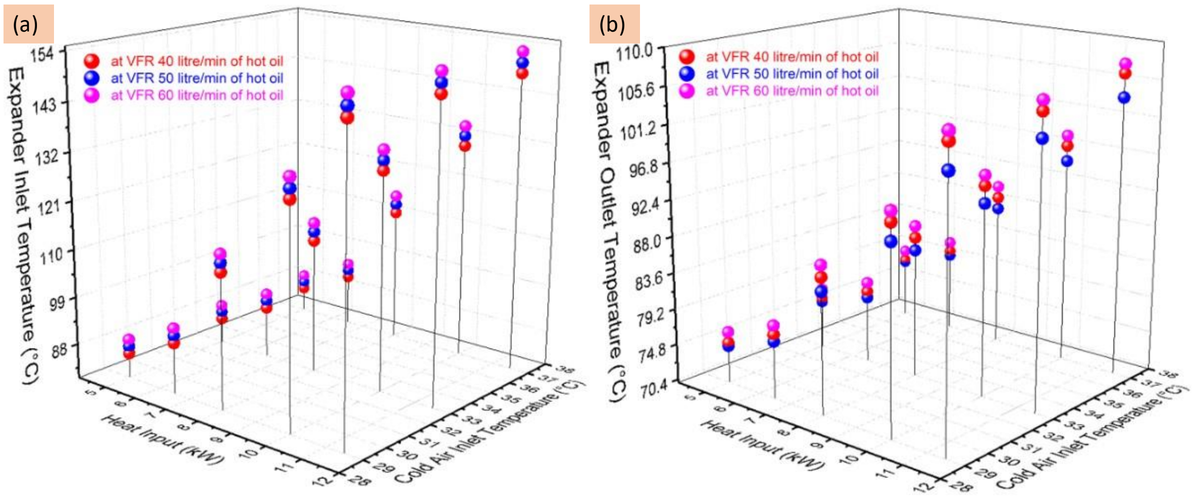

Figure 4.9. Effect on (a) expander inlet temperature and (b) expander outlet temperature

Figure 4.9(a) illustrates the expander inlet temperature variations against the heat input, cold air inlet temperature, and different volumetric flow rates of hot oil (40, 50, and 60 liters per minute). As the heat input increases, a corresponding increase in the expander inlet temperature is observed, which is consistent across all volumetric flow rates. This trend suggests that the heat input plays a dominant role in raising the working fluid’s temperature before it enters the expander, thereby contributing directly to the system's thermal efficiency. At each heat input level, the expander inlet temperature also exhibits a slight variation based on the cold air inlet temperature, implying a secondary effect where lower cold air temperatures might allow better heat retention in the system. However, the effect of varying the volumetric flow rate of hot oil is more pronounced. For instance, at higher flow rates (60 litres per minute), the expander inlet temperature reaches slightly higher values compared to lower flow rates (40 litres per minute), suggesting that increased flow rates enhance the heat transfer process, allowing more heat to be absorbed by the working fluid.

Figure 4.9(b) graph shows the expander outlet temperature as a function of the same parameters: heat input, cold air inlet temperature, and varying flow rates of hot oil. Similar to the inlet temperature behaviour, the outlet temperature also rises with an increase in heat input. However, the difference between the inlet and outlet temperatures at each flow rate and heat input provides insight into the expander's effectiveness in extracting work from the working fluid. A notable observation is that at higher volumetric flow rates, the outlet temperature tends to be higher, indicating that the expander releases less heat under these conditions. This behaviour could imply that at elevated flow rates, the working fluid has less residence time within the expander, resulting in a lower degree of expansion and heat extraction. Conversely, at lower flow rates (40 litres per minute), the working fluid undergoes a more extensive expansion, leading to a lower outlet temperature, which could be more favourable for work extraction efficiency in certain ORC configurations.

The heat input primarily drives the inlet temperature, which subsequently influences the outlet temperature depending on the flow rate and cooling conditions. Increased flow rates generally lead to higher inlet and outlet temperatures, potentially maximizing the ORC's thermal output at the expense of expansion effectiveness. On the other hand, optimizing the flow rate at each heat input level can enable better control over the expander's thermal and mechanical output, leading to potentially improved efficiency.

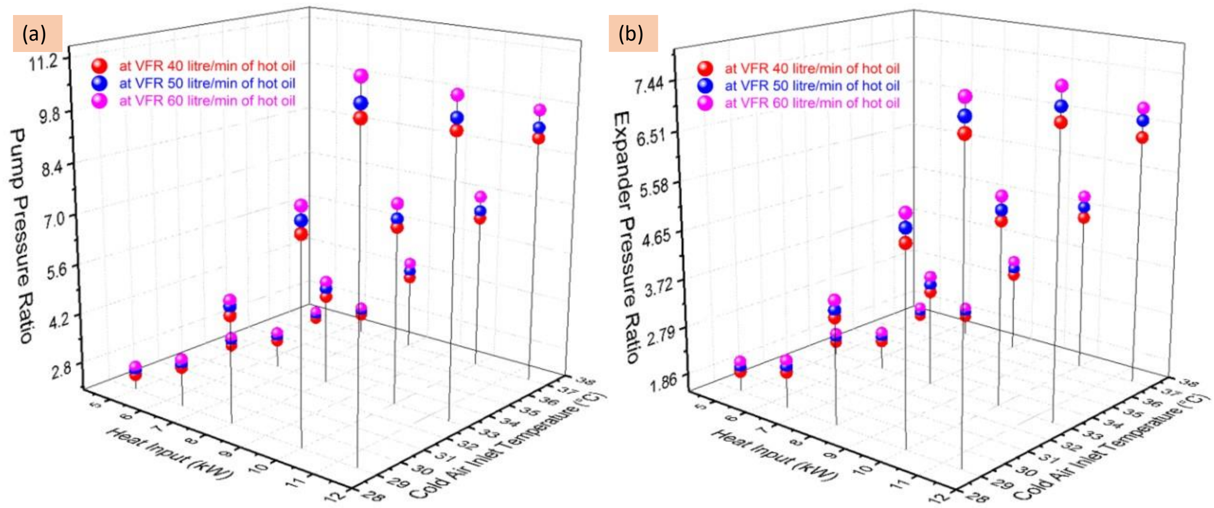

Figure 4.10. Effect on pressure ratio of (a) pump and (b) expander

Figure 4.10(a) illustrates the pump pressure ratio as it varies with heat input, cold air inlet temperature, and different VFRs of hot oil. The pump pressure ratio, representing the pressure increase across the pump, is a critical factor for ensuring the effective circulation of the working fluid. The graph shows that the pump pressure ratio increases as the heat input increases. This trend is logical because a higher heat input results in a greater thermal energy input to the working fluid, elevating its vapour pressure. As a result, the pump needs to operate at a higher pressure ratio to maintain circulation. Interestingly, the pump pressure ratio decreases with an increase in the inlet temperature of cold air. This inverse relationship may be due to the reduced cooling effect at higher cold air temperatures, which leads to a slightly higher temperature of the working fluid exiting the condenser. The volumetric flow rate of hot oil also affects the pump pressure ratio. At a higher VFR (e.g., 60 litres per minute), the pump pressure ratio is generally higher at each level of heat input and cold air temperature. This is because a higher hot oil flow rate improves heat transfer to the working fluid, raising its vapour pressure at the pump inlet. Consequently, the pump requires a higher pressure ratio to drive the fluid through the cycle effectively.

Figure 4.10(b) illustrates the expander pressure ratio under different conditions of heat input, cold air inlet temperature, and hot oil flow rate. The expander pressure ratio is critical for converting thermal energy into mechanical work and reflects the difference in pressure across the expander. Similar to the pump pressure ratio, the expander pressure ratio increases with higher heat input. This behaviour is expected as more heat input raises the pressure of the vapor entering the expander, thereby increasing the pressure ratio across it. Notably, the expander pressure ratio also decreases with an increase in the cold air inlet temperature. This trend occurs for similar reasons as seen in the pump pressure ratio. With a higher inlet temperature of cold air, the condenser's cooling efficiency is reduced, leading to a higher outlet temperature of the working fluid from the condenser. This results in lower condensation pressure, thereby reducing the overall pressure differential across the expander and subsequently the expander pressure ratio. The volumetric flow rate of hot oil has a pronounced impact on the expander pressure ratio as well. Higher flow rates, such as 60 litres per minute, lead to increased expander pressure ratios across all levels of heat input and cold air inlet temperatures. This is due to enhanced heat transfer from the hot oil, which elevates the working fluid's pressure at the expander inlet. Thus, a higher hot oil flow rate increases the pressure difference across the expander, enhancing the potential for mechanical work extraction.

Increasing heat input positively impacts both pump and expander pressure ratios, which is beneficial for energy conversion efficiency. However, the cold air inlet temperature should ideally be kept low to maintain high pressure differentials across both the pump and the expander. Lower cold air inlet temperatures improve condensation efficiency, which helps sustain higher pressure ratios in the system and ultimately enhances the overall cycle efficiency. The volumetric flow rate of hot oil is another critical parameter. A higher VFR improves heat transfer, leading to increased pressure ratios, especially under higher heat inputs. However, it is essential to manage the flow rate to ensure the system operates within safe pressure limits.

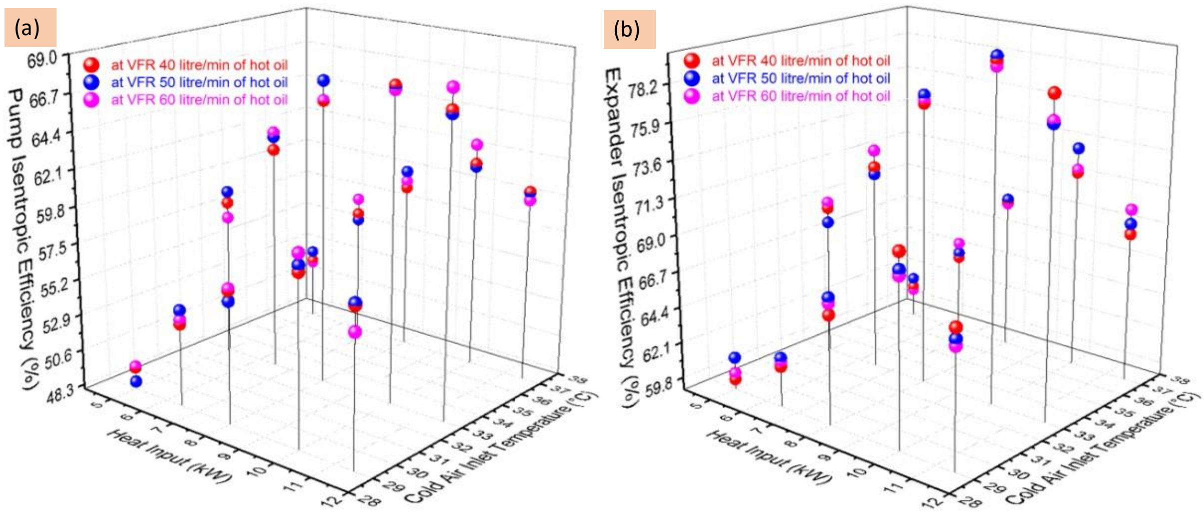

Figure 4.11. Effect on isentropic efficiency of (a) pump and (b) expander

Figure 4.11(a) illustrates the interrelationship between various parameters affecting the isentropic efficiencies of the pump in an ORC system. Specifically, these 3D plots display the pump and expander isentropic efficiencies as functions of heat input and cold air inlet temperature, with data segmented by VFR of the hot oil at 40, 50, and 60 litres per minute. In the first plot, which represents the pump's isentropic efficiency, it can be observed that at lower heat inputs (5–10 kW), the efficiency generally remains lower and shows minor variations with changes in air inlet temperature. As the heat input increases, the pump's isentropic efficiency becomes more sensitive to the air inlet temperature, particularly at higher flow rates of 50 and 60 litres per minute. This relationship indicates that under higher heat input conditions, the performance of the pump improves as the system handles increased thermal energy more effectively.

Figure 4.11(b), depicting the expander's isentropic efficiency, shows a similar trend with a stronger correlation between higher heat input and efficiency improvements. However, the expander efficiencies are notably higher than those of the pump across the heat input range, particularly at the highest flow rate (60 litres per minute). This suggests that the expander performs more optimally under elevated thermal loads and increased flow rates, likely due to enhanced working fluid expansion under these conditions. The expander's efficiency also demonstrates greater responsiveness to variations in air inlet temperature, emphasizing the role of cooling efficiency in maintaining optimal performance.

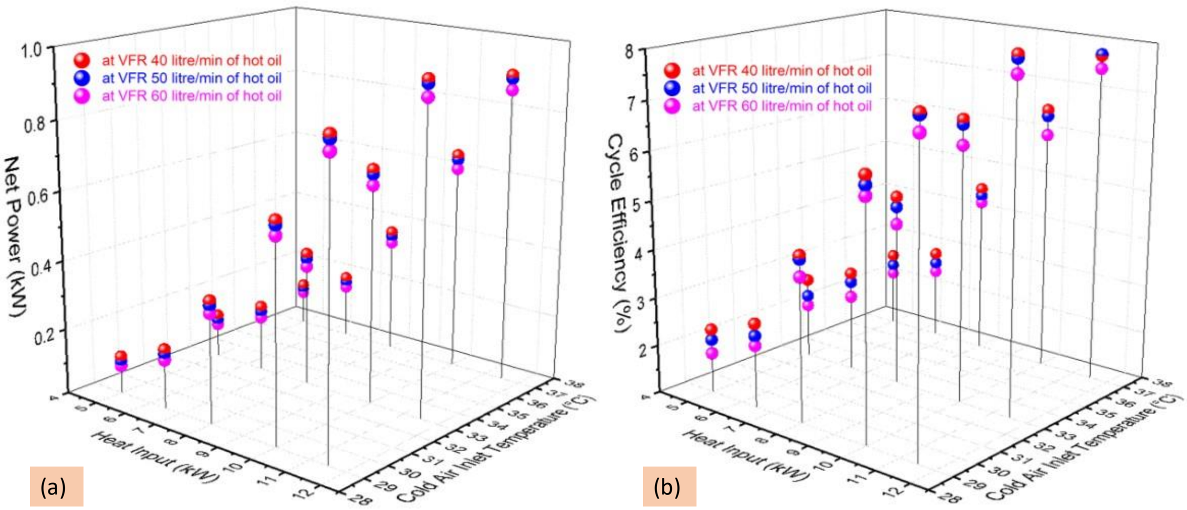

Figure 4.12. Effect on (a) net power output and (b) cycle efficiency

Figure 4.12 illustrates the interrelationships between heat input (kW), cold air inlet temperature (°C), and volumetric flow rates (VFR) of hot oil (40, 50, and 60 LPM) on two key performance parameters in the ORC system: net power output (kW) and cycle efficiency (%). These parameters are critical for evaluating the thermodynamic performance of the ORC system under various operating conditions. Figure 4.12(a) presents the net power output of the

ORC system as a function of heat input and cold air inlet temperature at each of the three tested hot oil flow rates. A clear trend is observed, where an increase in heat input and cold air inlet temperature generally corresponds to an increase in net power output across all flow rates. For example, at lower heat inputs and colder air temperatures, the net power output is relatively low for all VFR levels, indicating limited energy conversion. However, as the heat input rises, a more significant increase in net power output is seen, especially for higher VFRs (50 and 60 LPM). This suggests that greater flow rates of hot oil enhance the heat transfer effectiveness, enabling the working fluid to extract more thermal energy and convert it into mechanical power. Notably, the net power output at 60 LPM reaches peak values at high heat input levels, confirming that increased VFR contributes to higher net power outputs under optimal thermal conditions.

Figure 4.12(b) displays the cycle efficiency, which is similarly influenced by heat input, cold air inlet temperature, and hot oil VFR. Here, the ORC efficiency follows a trend similar to that observed in net power output, with efficiency increasing alongside higher heat inputs and warmer air inlet temperatures. However, a distinct observation is that the impact of VFR on cycle efficiency appears to be more complex. At lower heat inputs, the cycle efficiency is relatively comparable across all flow rates, suggesting the limited influence of VFR on efficiency under low thermal conditions. As heat input increases, however, a divergence in efficiency emerges, with the highest cycle efficiency values observed at the 40 LPM flow rate. This indicates that, beyond a certain threshold, higher VFRs may not proportionally increase efficiency due to increased parasitic losses associated with pumping and thermal resistance.

Both graphs offer valuable insights into the performance dynamics of the ORC system. They reveal that while increased VFR of hot oil enhances net power output, optimal cycle efficiency may be achieved at moderate flow rates under high heat inputs, indicating a trade-off between maximizing power output and achieving thermal efficiency. This analysis provides essential guidelines for selecting appropriate operational parameters in ORC systems to balance power generation and energy efficiency based on specific application requirements.

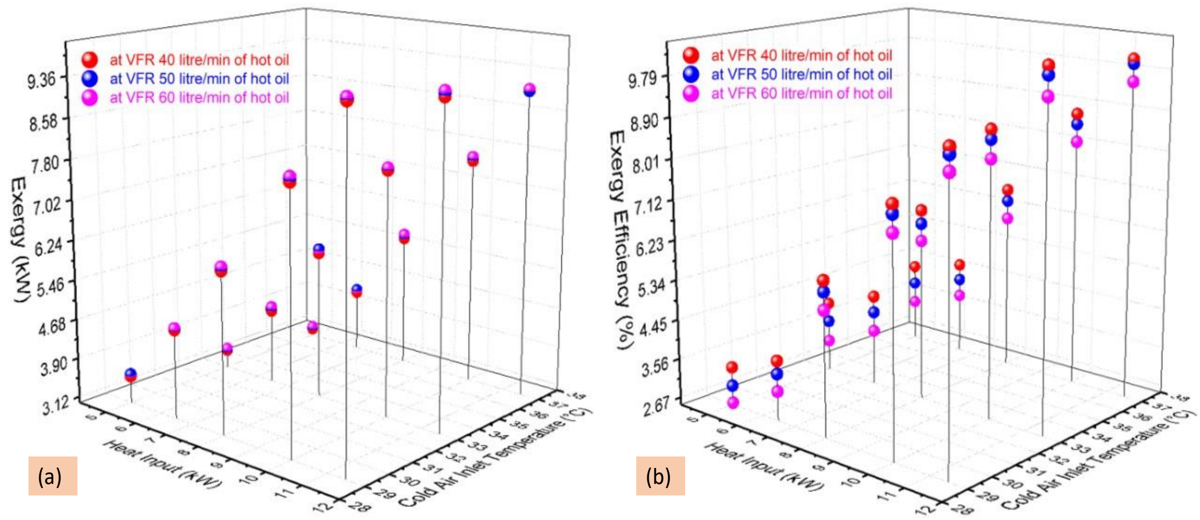

Figure 4.13. Effect on (a) exergy and (b) exergy efficiency

Figure 4.13 illustrates the influence of heat input, cold air inlet temperature, and the VFR of hot oil on the exergy and exergy efficiency. In Figure 4.13(a), the exergy (kW) is plotted against heat input (kW) and cold air inlet temperature (°C) for three different VFRs of hot oil: 40, 50, and 60 L/min. As observed, the exergy output increases with rising heat input, regardless of the VFR. This trend suggests that higher thermal energy input directly enhances the exergy available for conversion, likely due to an improved temperature gradient across the ORC system. Additionally, at a constant heat input, higher cold air inlet temperatures tend to result in a marginally lower exergy output. This effect could be attributed to reduced thermal efficiency at elevated condenser temperatures, limiting the potential for work extraction.

In Figure 4.13(b), the exergy efficiency (%) is plotted similarly against heat input and cold air inlet temperature for the three VFR levels. The results show that exergy efficiency improves with increasing heat input across all flow rates. This efficiency gain is primarily due to enhanced system performance under higher energy availability, which allows more effective utilization of the working fluid's thermodynamic potential. Notably, lower VFRs (e.g., 40 L/min) tend to yield slightly higher exergy efficiencies than higher VFRs at comparable conditions. This observation may be explained by the reduced heat transfer losses at lower flow rates, which improves overall energy utilization efficiency.

These graphs demonstrate that optimizing heat input and controlling the VFR of hot oil are essential for enhancing both exergy and exergy efficiency in ORC systems. Elevated heat input levels promote higher exergy outputs and efficiencies, while a moderate flow rate may be preferable for achieving optimal exergy efficiency. These findings provide valuable insights into the operational parameters that can maximize ORC performance under varying conditions, paving the way for more efficient waste heat recovery in practical applications.

4.2.2. ANOVA model for optimization and prediction

The following constraints were taken into consideration while ORC's experimental data is being optimized by the RSM-ANOVA method for maximum net power and cycle efficiency. Equal weightage is given to both factors as the condition is described in the following Table 4.7. Independent variables A, B and C is being tested for all its range to find the optimum condition of A, B and C at which both net power and cycle efficiency is maximum.

Table 4.7. ANOVA optimization constraints

Name	Goal	Lower Limit	Upper Limit	Lower Weight	Upper Weight	Importance
A: Heat Input (kW)	is in range	5	11.5	1	1	3
B: Cold Air Inlet Temperature (°C)	is in range	29	37	1	1	3
C: VFR of Hot Oil (litre/min)	is in range	40	60	1	1	3
Net Power (kW)	maximize	0.092	0.940	1	1	3
Cycle Efficiency (%)	maximize	1.843	8.170	1	1	3

Functions with the highest desirability are selected to maximize both the net power and cycle efficiency. Desirability plays a crucial role in optimizing net power and cycle efficiency in RSM-ANOVA by providing a single metric to balance multiple responses, as shown in Figure 4.14. It translates both objectives, maximizing net power and cycle efficiency, into a scale between 0 (undesirable) and 1 (most desirable). By combining these desirability, the optimization process identifies operating conditions that achieve the best overall system performance, ensuring an effective trade-off between the competing responses. This helps to find the optimal settings for maximization of both power output and cycle efficiency simultaneously by heat input, cold air inlet temperature, and VFR of hot oil.

Figure 4.14 illustrates the desirability analysis, shown at the top, which measures how well the selected parameter values satisfy both objectives. The highest heat input value of 11.5 kW significantly increases net power output and cycle efficiency, with a near-perfect desirability of 0.978, indicating that this heat input is optimal for system performance. At this input, net power reaches 0.92 kW, and cycle efficiency climbs to 8.037%, reflecting the system's improved energy conversion efficiency. On the other hand, the cold air inlet temperature, optimized at 35.611°C, and the hot oil VFR at 48.031 litre/min, show a relatively flat response in terms of desirability. This suggests that these two parameters are less sensitive to variations and have a minor influence on improving performance compared to heat input. The flat curves in these two plots indicate that slight deviations from their optimal points may not drastically affect system performance, unlike heat input, which plays a more dominant role.

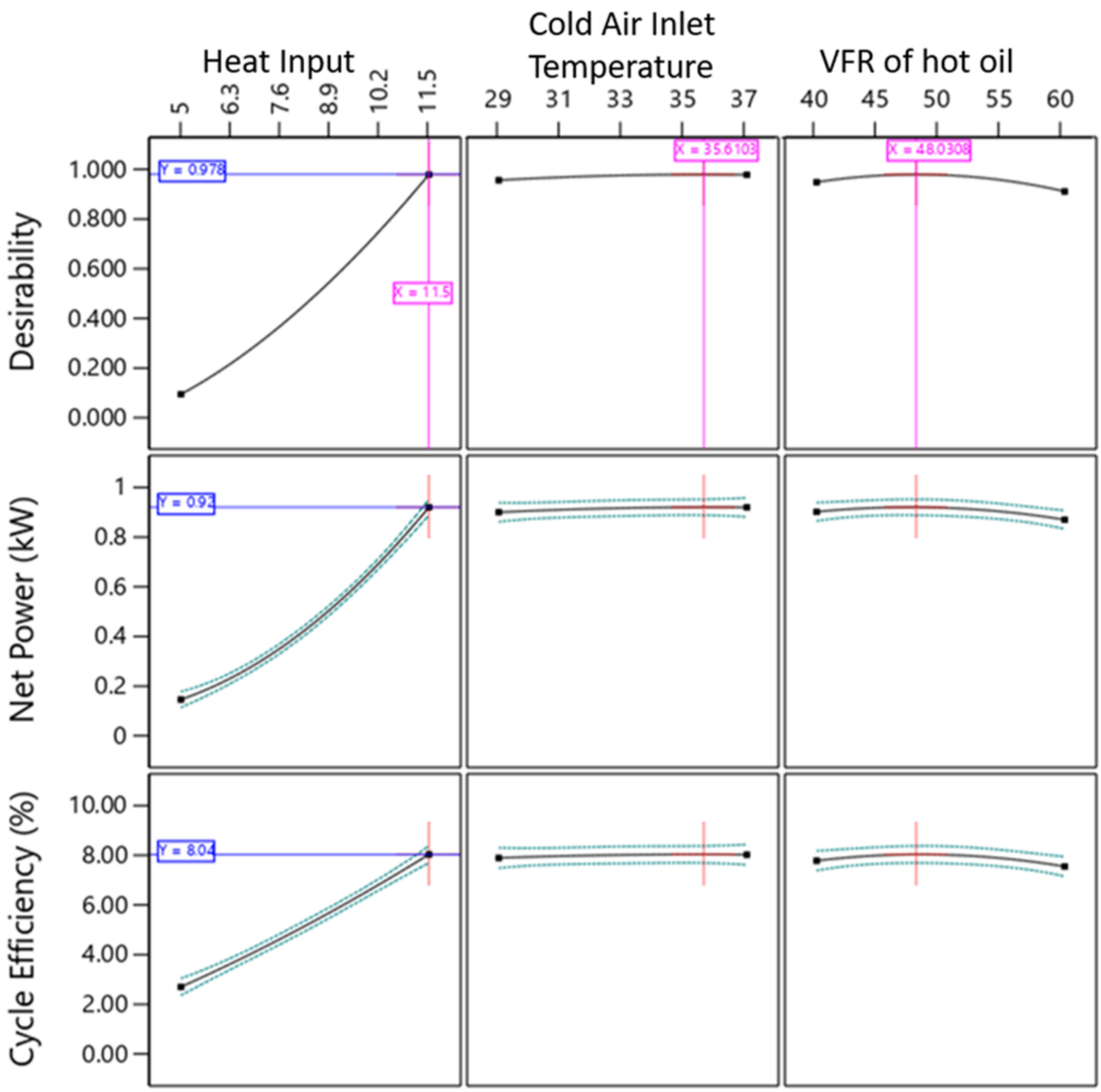

Figure 4.14. Desirability for net power and cycle efficiency for prediction analysis

Table 4.8 presents the optimized conditions for the independent variables heat input, cold air inlet temperature, and VFR of hot oil that achieves a balance between maximizing net power output and cycle efficiency. These optimized settings were validated through experimental testing under nearly identical conditions. The heat input was set to 11.5 kW, with a cold air inlet temperature of 35°C, and a VFR of hot oil at 48 litre/min. In the experimental test run, the actual net power output was found to be 0.906 kW, which is close to the optimized prediction of 0.920 kW, resulting in a minor error of 1.55%. Similarly, the experimental cycle efficiency was 7.878%, compared to the predicted 8.037%, with an error of 2.01%. These small discrepancies between the optimized and actual values are within acceptable limits, demonstrating that the model's optimization is reliable and accurate. The low error percentages confirm the effectiveness of the optimization process in predicting real-world ORC system performance under the given conditions.

Table 4.8. Validation of optimized condition output result with the experimental run at same optimized condition

		Optimized	Test Run	Error (%)
Independent Variable	Heat Input (kW)	11.5	11.5	-
	Cold Air Inlet Temperature (°C)	35.611	35	-
	VFR of Hot Oil (litre/min)	48.031	48	-
Dependent Variable	Net Power (kW)	0.920	0.906	1.55
	Cycle Efficiency (%)	8.037	7.878	2.01

Table 4.9 presents predicted data for net power and cycle efficiency in an ORC system, highlighting both experimental and theoretical predictions. The analysis considers key input parameters heat input (kW), cold air inlet temperature (°C), and the VFR of hot oil (litre/min) to assess their impact on system performance, with statistical calculations performed at a 95% confidence level, 99% population coverage, and a tolerance level of 0.99. The model incorporates a standard deviation of 20.34 for net power and 0.22 for cycle efficiency, which offers insight into the variability of these outputs under the specified experimental conditions. For the first five rows, predictions for net power and cycle efficiency are generated based on specific input parameters, such as heat input, cold air inlet temperature, and VFR of hot oil, and validated through simultaneous test runs to observe prediction error. In these rows, prediction accuracy improves at higher heat inputs, as evidenced by the lower error values, which indicates reliable model performance in these conditions. For instance, at a heat input of 11.5 kW and 50 LPM (S.N. 5), the predicted mean was 0.917 kW, close to the observed 0.864 kW, showing a -6.15% prediction error. Cycle efficiency also follows this trend, with minimal error between predicted and observed values, particularly at moderate to high heat inputs and VFRs, indicating stable predictive accuracy. Several entries (S.N. 6–10) lack observed values, providing useful benchmarks for future validation. These cases demonstrate the model's

potential to predict system performance under varied conditions. The data suggests that the model is more accurate at higher heat inputs irrespective of cold air inlet temperatures and VFRs, making it a valuable tool for further outcome predictions under high thermal load. This analysis confirms the model's robustness, especially for high heat input scenarios, and its utility for optimizing ORC performance across diverse operating conditions.

Table 4.9. Predicted data for net power and cycle efficiency in an ORC system, highlighting both experimental and theoretical predictions

	Input Parameters for Predictions			**Predicted Response 1: Net Power (kW)**				**Predicted Response 2: Cycle Efficiency (%)**			
S. N.	**A: Heat Input (kW)**	**B: Cold Air Inlet Temp (°C)**	**C: VFR of Hot Oil (litre/min)**	**Predicted Value**	**Standard Error of Prediction**	**Observed Value**	**Prediction and Observed Error (%)**	**Predicted Value**	**Standard Error of Prediction**	**Observed Value**	**Prediction and Observed Error (%)**
1.	5	33	40	0.123	0.018	0.137	10.15	2.49	0.2	2.75	9.45
2.	8.25	29	60	0.365	0.018	0.411	11.18	4.46	0.2	4.93	9.53
3.	10	33	50	0.661	0.01	0.671	1.49	6.62	0.11	6.71	1.34
4.	10	37	60	0.616	0.018	0.611	-0.70	6.14	0.19	6.11	-0.49
5.	11.5	37	50	0.917	0.018	0.864	-6.15	8.02	0.2	7.52	-6.65
6.	6	36	45	0.204	0.012	-	-	3.39	0.13	-	-
7.	7	34	54	0.282	0.01	-	-	4	0.11	-	-
8.	9	32	40	0.496	0.016	-	-	5.51	0.17	-	-
9.	10	35	55	0.648	0.011	-	-	6.48	0.11	-	-
10.	11	30	50	0.814	0.014	-	-	7.45	0.15	-	-

Table 4.10. Advantages of current developed system with previously developed systems

Criteria	This Study	Previous Studies
Working Fluid & Cycle Configuration	R601a (Isopentane) – Experimentally validated, operated with a saturated vapor inlet for maximum power output	Mostly R123, R245fa, R134a, with a focus on superheated ORC, which results in lower power output at the same pressure [32,67,77,86–88]

Expander & Component Innovation	Modified scroll compressor as an expander; custom-built separator for saturated vapor condition	Scroll, screw, rolling piston, and turbo expanders; no reported use of a dedicated separator [29,30,35,37,60,66,71,74,75,77]
Optimization & Validation	RSM-ANOVA used for performance prediction and optimization, validated with minimal error (1.55% for power, 2.01% for efficiency)	No prior ORC study optimized conditions using RSM-ANOVA; limited optimization studies focused on individual parameters [63,81]
Experimental Parameters & Operating Conditions	Simultaneous variations in heat input (5–11.5 kW), cold air inlet temperature (29–37°C) and volume flow rate of hot oil (40–60 LPM),	Most studies varied only one or two parameters; experiments generally conducted below 10 kW heat input [29,30,32,40,60,88,89]
Performance (Net Power & Efficiency)	Maximum net power: 0.939 kW, Maximum thermal efficiency: 8.08%	Power output: 0.3 – 2.5 kW, Efficiency: 3–7% [32,37,74,86–89]
Application Scope	Suitable for waste heat recovery from 95–180°C sources, including geothermal, solar collectors, and industrial waste heat	Mostly focused on specific temperature ranges and applications [29,40,60,80]

Table 4.10 shows the advantages and comparison of this manuscript ORC experimental setup with previous developed ORC systems. This experimental setup provides maximum thermal efficiency that no one has achieved so far due to novel R601a working fluid and operating condition. This ORC system is designed to operate with any waste heat source within a temperature range of 95–180 °C. As such, it is well-suited for applications including geothermal energy recovery, solar collector systems, industrial waste heat utilization, and the harnessing of exhaust heat. The ORC system faces limitations in utilizing nanofluid-based novel working fluids because the existing heat exchanger design requires significant modifications. Additionally, adapting large-scale scroll expanders from standard scroll compressors presents challenges for small-scale production. These obstacles could be overcome with further design optimizations and economies of scale in a commercial application.

4.3. Important Findings

The experiments have been performed on the fabricated lab-scale basic ORC system to analyze the thermal performance, which is a significant parameter in generating electricity. The input parameter heat load is varied from 5kW to 11.5kW, cold air inlet temperature is varied from 29°C to 37°C and the volume flow rate of hot fluid (oil) is varied from 40 litre/min to 60 litre/min. The variation effect of input parameters in being analyzed on systems temperature, pressure and mass flow rate. The following outcomes are deduced from the results.

(i) Increased heat input positively influenced both net power output and cycle efficiency. As heat input rose from 5 to 11.5 kW, net power significantly increased, reaching a peak of 0.939 kW, while cycle efficiency improved from 2.34% to 8.08%.

(ii) Optimal cycle efficiency was achieved at the highest heat input of 11.5 kW and moderate volume flow rates, suggesting that increasing VFR beyond a certain point can diminish efficiency gains due to parasitic losses.

(iii) Exergy output increased with higher heat inputs, as more thermal energy provided a greater potential for conversion. However, the exergy efficiency was highest at moderate flow rates (e.g., 40 litre/min), as excessive flow rates reduced energy utilization efficiency due to higher heat losses.

(iv) Cold air inlet temperature inversely impacted exergy output, as elevated condenser temperatures reduced the cooling gradient, limiting work extraction potential.

(v) Evaporator effectiveness ranged from 0.78 to 0.84, with improved efficiency at higher heat inputs and VFRs of hot oil, showcasing the system's enhanced heat transfer capability.

(vi) The expander demonstrated optimal isentropic efficiency under high thermal load, with notable performance improvements at elevated VFRs due to increased fluid expansion.

(vii) Mass flow rate of the working fluid rose with higher heat inputs and cold air inlet temperatures, particularly at low VFRs, where heat transfer was maximized.

(viii) The optimization achieved using Response Surface Methodology (RSM) and Analysis of Variance (ANOVA) was validated by experiments, showing low error margins (e.g., 1.55% for net power and 2.01% for cycle efficiency), confirming model accuracy.

(ix) Desirability analysis confirmed that maximizing heat input had the greatest impact on performance, while adjustments in cold air inlet temperature and hot oil VFR had smaller effects. This suggests that, while important, these parameters can vary slightly without significantly affecting performance, whereas optimizing heat input is crucial.

Experiment working prototype setup Video link (drive):
https://drive.google.com/file/d/1Yx6cehR4Ft3RagchZ2eJOHpyopIi-Rk7/view?usp=drive_link.

Chapter 5: Case Study for Nuclear Power Plant

5.1. Selection of Location – Feasibility Study

The real data of working NPP, provided by BRNS, India, have been used for analysis. The possible waste heat locations are mentioned in Table 5.1.

A steam and feed water system are a device that enhances a steam turbine's ability to control a feedwater pump and plant operation characteristics when water is delivered slowly. The main feedwater duct on the discharge side of the feedwater pumps is equipped with a cut-off valve and is connected parallel with a bypass duct containing a pressure-compensated flow control valve in a nuclear power plant where the reactor's feedwater pumps are driven by a steam turbine. This system allows water to be fed to the reactor through the main feedwater duct from feedwater pumps powered by the steam turbine when the rate of feedwater is high and the cut-off valve is closed when the rate is low. In this system, the main steam condenser is the essential component in which steam is condensed and the feed water pump is used to supply a sufficient amount of feed water by steam and feed water system.

The purpose of the Main Heat Transport (MHT) purification system is to maintain high reactor water purity in order to minimize the reduction of heat transfer in the nuclear reactor core by minimizing the deposition of water impurities on the fuel surfaces and to minimize secondary sources of beta and gamma radiations by removing the corrosion products, fission products and impurities in the primary system. The purification system comprises of pumps, heat exchangers such as regenerative coolers, isolation heat exchanger, non-regenerative coolers, filters, ion exchange columns and strainers storage tank and the associated instrumentation, piping and valves. The purification flow from MHT is passed through heat exchangers to cool it before passing it through an ion-exchange column and filters for purification and returned back to MHT after reheating in non-regenerative coolers.

The moderator in a nuclear power plant is a material, usually heavy water or graphite, that slows down neutrons, enabling nuclear reactions to occur in a controlled manner. The moderator is a crucial component of a nuclear reactor, and it is essential to maintain its temperature within a safe range. The moderator cooling system is responsible for removing heat generated by the nuclear reaction and maintaining the moderator's temperature. The moderator cooling system typically uses a closed-loop cooling system, which circulates water or another coolant through the moderator vessel to remove heat. The system comprises a moderator vessel, a heat exchanger, pumps, and a cooling tower. The moderator vessel is the primary component of the cooling system, where the moderator is located. The vessel is made of a suitable material, such as stainless steel, and is designed to withstand high temperatures and pressures. The coolant circulates through the vessel, removing heat from the moderator. The heat exchanger is another critical component of the moderator cooling system. The heat exchanger transfers heat from the coolant to the secondary coolant, which carries heat away from the power plant. The secondary coolant can be air, water, or another suitable fluid. Pumps are used to circulate the coolant. One of the critical challenges in the moderator cooling system is maintaining the temperature of the moderator within a safe range. If the moderator's temperature is too high, it can cause the nuclear reaction to become unstable, leading to a potential nuclear meltdown. Conversely, if the moderator's temperature is too low, it can reduce the efficiency of the reactor. To prevent these issues, the moderator cooling system is designed to maintain the moderator's temperature within a safe range.

The author has done a feasible study with the help of necessary input data and identified locations provided by BRNS (Board of Research in Nuclear Sciences). Within nine waste heat sources, the feasible cases to use ORC have been discussed in the Table 5.2.

Table 5.1. Waste heat disposal components and its temperature of Indian NPP data provided by BRNS

System	Component	Waste Heat Source [MWth]	Hot fluid inlet temperature [°C]	Hot fluid outlet temperature [°C]	Cold fluid inlet temperature [°C]	Cold fluid outlet temperature [°C]	Hot fluid flow rate [kg/s]	Cold fluid flow rate [kg/s]
Steam and Feed Water System	Main Steam Condenser	635	Heat Source Temp: 42.3 °C Steam condenses at a temp. of 42.3 °C at a pressure of 62.5/0.085 mm Hg/ kg/cm^2.		29	36	323	21600
MHT Purification System	Isolation Heat Exchanger	4.2	98	68	65	78	33.33	77
	Non-regenerative Heat Exchanger	3.2	68	45	35	42	33.33	110
Main Moderator Cooling System	Moderator Active Process Water Heat Exchanger No-1	25	75	50	35	47	235.5	498
	Moderator- Active Process Water Heat Exchanger No-2	25	75	50	35	47	235.5	498

Table 5.2. Input condition data to check the feasibility of running ORC

S.No.	System and component for waste heat source	Modification required in existing system or not	Source of Input condition	Comment
1.	Main steam condenser of steam and feed water system	Modification not required	$T_{hf,i}$=36 °C, $\dot{m}_{hf}$=21600 kg/s	(Cycle can not run) Hot fluid inlet temperature is very less (below condenser temperature). No cycle is possible at this condition.
2.	Main steam condenser of steam and feed water system	Modification required	$T_{hf,i}$=42.3 °C, $T_{hf,o}$=42.3 °C, P_{hf}=8.33 kPa, $\dot{m}_{hf}$=323 kg/s	(Cycle can not run) Hot fluid inlet temperature is very less to produce any work output from given condition. No cycle is possible at this condition.
3.	Isolation heat exchanger of MHT purification system	Modification not required	$T_{hf,i}$=78 °C, $\dot{m}_{hf}$=77 kg/s	(Cycle can not run) This case is technically not possible because waste heat from isolation condenser is taken in use for producing desalination water. Thus no direct waste heat is available to produce the power. Thus, no cycle is possible at this condition.
4.	Isolation heat exchanger of MHT purification system	Modification required	$T_{hf,i}$=98 °C, $T_{hf,o}$=68 °C, $\dot{m}_{hf}$=33.33 kg/s	**Case-1 (Cycle can run)** Cycle can run on the given condition to produce the work due to availability of hot fluid inlet temperature in adequate

				amount. Cycle is possible at this condition.
5.	Non-regenerative heat exchanger of MHT purification system when isolation heat exchanger is not considered	Modification required	$T_{hf,i}$=98 °C, $T_{hf,o}$=42 °C, $\dot{m}_{hf}$=33.33 kg/s	(Cycle can not run) Boiler pressure is lowered to the maximum possible (near lowest condenser temperature, i.e., 37°C) value to achieve 42°C boiler hot fluid (water) outlet temperature, but not. Further, by decreasing condenser temperature below 35°C, boiler hot fluid (water) outlet temperature 42°C is achieved by small amount of work output. At 35°C condenser temperature, corresponding cold fluid (water) inlet temperature of condenser must be below 27°C, which is hard to maintain ambient temperature in India throughout the year.
6.	Non-regenerative heat exchanger of MHT purification system	Modification not required	$T_{hf,i}$=42 °C, $\dot{m}_{hf}$=110 kg/s	(Cycle can not run) Hot fluid inlet temperature is very less to produce any work output from given condition. No cycle is possible at this condition.
7.	Non-regenerative heat exchanger of MHT purification system	Modification required	$T_{hf,i}$=68 °C, $T_{hf,o}$=45 °C, $\dot{m}_{hf}$=33.33 kg/s	(Cycle can not run) Hot fluid outlet temperature is very low, so to achieve 45°C boiler hot fluid (water) outlet temperature, evaporator pressure falls below 40°C saturation condenser temperature. If further condenser temperature is

				decreased then small amount of work can be obtained which serves no purpose. Hence, no cycle is possible at this condition.
8.	Moderator active process water heat exchanger of main moderator cooling system (when No-1 and No-2 both in use)	Modification not required	$T_{hf,i}$=47 °C, $\dot{m}_{hf}$=996 kg/s	(Cycle can not run) Hot fluid inlet temperature is very less to produce any work output from given condition because of evaporator temperature becomes equal to condenser temperature after applying PPTD value of heat exchanger. If further condenser temperature is decreased then small amount of work can be obtained which serves no purpose. Hence, no cycle is possible at this condition.
9.	Moderator active process water heat exchanger of main moderator cooling system (when No-1 and No-2 both in use)	Modification required	$T_{hf,i}$=75 °C, $T_{hf,o}$=50 °C, $\dot{m}_{hf}$=471 kg/s	**Case-2 (Cycle can run)** Cycle can run on the given condition to produce the work due to availability of hot fluid inlet temperature in sufficient amount. Also, hot fluid outlet temperature value is favorable for lower condenser temperature condition in which evaporator temperature can have enough value to produce work after considering PPTD. There will be no/very small amount of work output if condenser temperature is increased which serves no purpose. Cycle is possible at

				given condition but at lower condenser temperature (below general value of condenser).

The feasibility of using ORC for all nine locations is discussed in Table 5.2. Two potential locations (cases 1 and 2) are thermodynamically identified based on the feasibility study for direct application of simple ORC to generate extra power. A few systems and components have been identified that require modification but can not run on simple ORC. To run this system, further changes have to be implemented in the heat exchanger system to get the desired boiler pressure.

Isopentane, R245fa and R236ea are taken as working fluids and water is used as a hot and cold fluid. Input parameters are as follows: General Condenser temperature = 40°C, Ambient temperature = 29°C, Cold fluid inlet temperature = 29°C, PPTD of the plate type evaporator and condenser = 7°C [114,123], Isentropic reciprocating pump efficiency = 0.8 , Isentropic scroll turbine efficiency = 0.6 [124], Alternator mechanical efficiency= 0.96 [123], Electricity cost = 0.078 USD/kWh [125,126] and Annual running time = 7000 h.

5.2. Modelling and Simulation

The feasible location of waste heat recovery from the real operating NPPs data can be identified based on the thermodynamics (mass, momentum and energy equations) point of view. After identifying a feasible location and system's component, it is very necessary to check its viability from economic and environmental points of view. The required thermodynamic and design mathematical modelling equations, (2.1 - 2.27) are taken from chapter 2. Other than the above, additional equations and correlations are mentioned below.

5.2.1. Mathematical Modelling

Table 5.3 shows the market price of the alternators of different capacities and different manufacturers. This cost data, along with capacity, will be helpful in building a correlation for an alternator that can be used to convert mechanical energy into electrical energy.

Table 5.3. The market price of the alternator of different capacities and different manufacturer

Company (Manufacturer)	**Capacity (kVA)**	**Capacity (kW)**	**Market Price (INR)**	**Market Price (USD)**
Start Up Atop	5	4	22,800	274.5995

Prem	5	4	22,500	270.9864
MD Bharat	5	4	15,500	186.6795
Bharat Ac Alternator	7.5	6	23,500	283.0302
Tech Power	7.5	6	27,500	331.2056
Sunfield	10	8	27,000	325.1837
Kirloskar	10	8	22,500	270.9864
Ashok	15	12	44,000	529.9289
Gravis	20	16	49,500	596.1701
Power Gold	25	20	42,000	505.8413
Electron	25	20	42,000	505.8413
Start Up Atop	25	20	48,500	584.1262
Kishanmaster	25	20	42,000	505.8413
Mahima Enterprise	25	20	44,000	529.9289
Ms Power	35	28	56,000	674.455
Crompton	35	28	58,000	698.5427
Chandra Agriculture Industry	40	32	58,000	698.5427
Mahima Enterprise	50	40	60,000	722.6304

A trendline analysis of the 3-phase alternator's capital cost correlation has been done with capacity (kW) and cost (USD), as shown in Figure 5.1. The general value of the power factor is taken as 0.8 to convert alternator capacity kVA to kW. The R^2 value is accepted as 0.9085 because of the market price difference for the same capacity and different manufacturers.

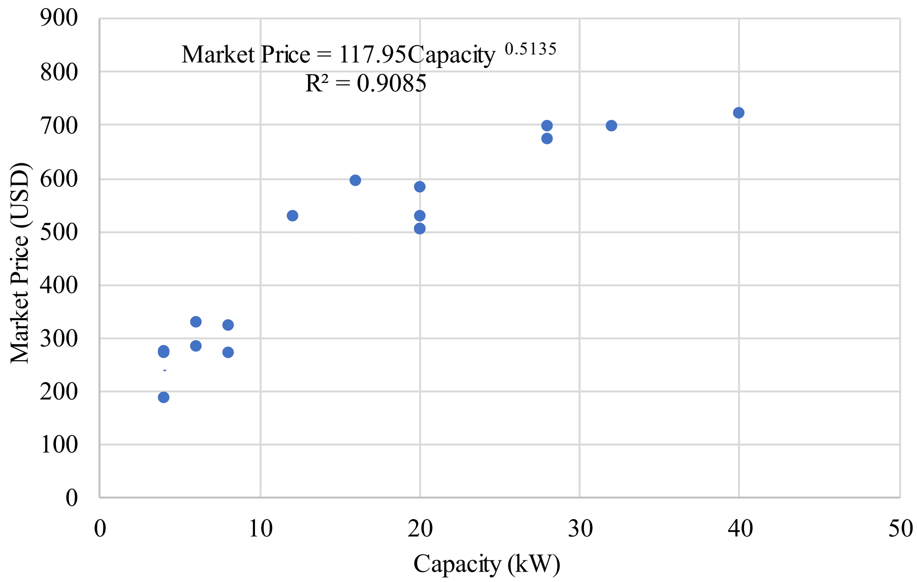

Figure 5.1. Alternator's capital cost correlation by trendline analysis between capacity (kW) and market price (USD)

Alternator's capital cost correlation is deduced from Figure 5.1 as:

Capital investment (USD),

$$Z_{alt}^{CI} = 117.95(W_{net})^{0.5135} \qquad (5.1)$$

5.2.2. Simulation and Validation

While simulating the ORC systems to identify and evaluate the possible location to generate power, input and ambient thermodynamic parameters are chosen based on the problem defined and NPPs data (Table 5.1). PPTD is defined effectively when designing evaporator and condenser [114]. The simulation is done using EES software [127]. All physical and thermodynamic properties of the different fluids are calculated using the REFPROP function built into EES. DPP, LCOE, NPV, and IRR are calculated using the formula given on the spreadsheet. The heat exchanger area is calculated by Muley's and Yan-Lin's correlations [102] to determine the capital investment. Figure 5.2 represents the flow chart followed in the simulation process. Validation is the same as discussed in chapter 2.

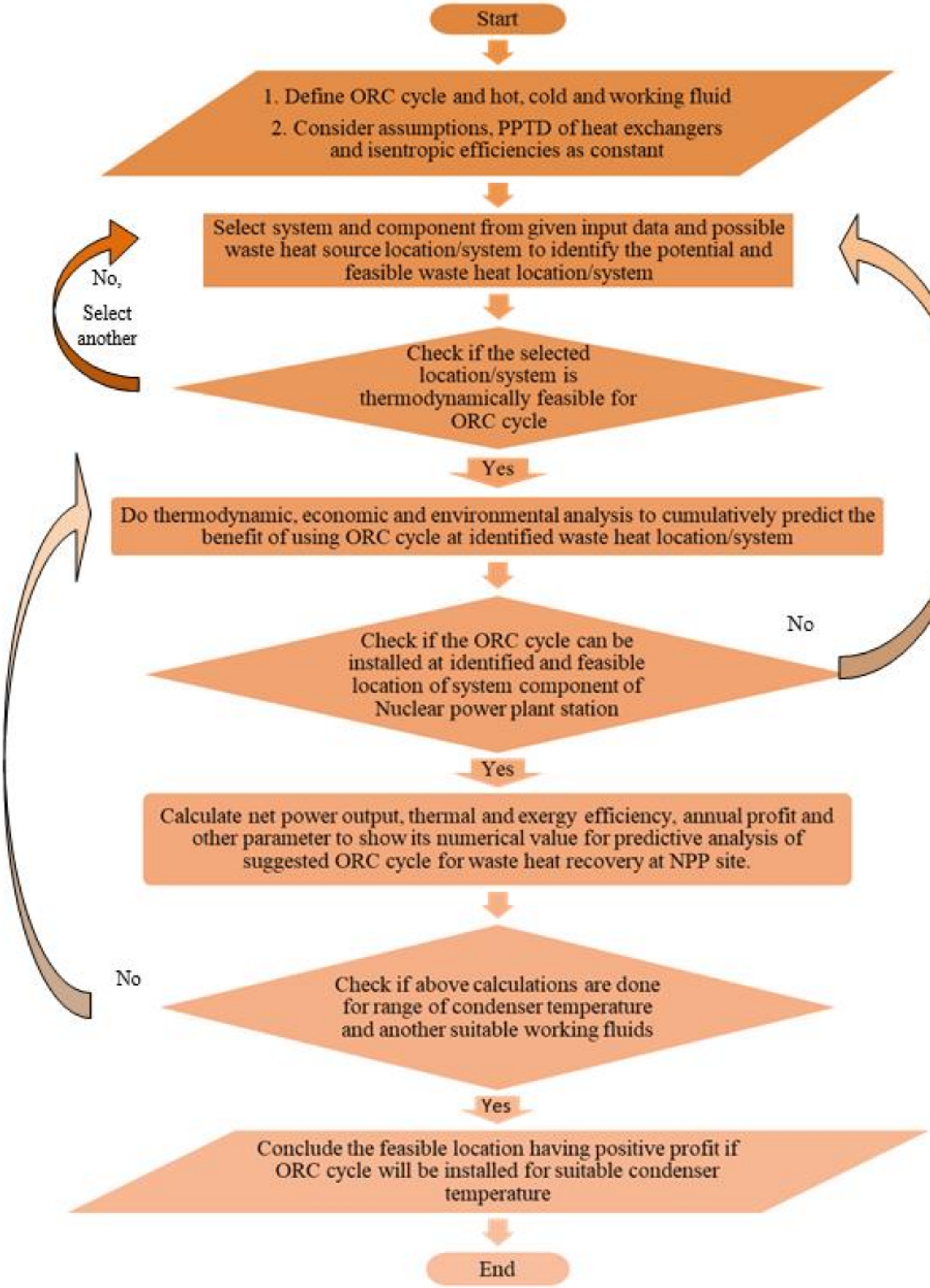

Figure 5.2. Flowchart of simulation process for feasible location in NPP to install ORC

5.3. Result and Discussion

5.3.1. Comparison of two feasible cases

The two waste heat source locations are identified by a feasibility test on EES (Engineering equation solver) for ORC applicability based on the data and drawings provided by BRNS for the nuclear power plant's waste heat recovery installation. The above 2 cases are suggested for ORC installation and recommended for the nuclear power plant's waste heat recovery, based on the requirement. The above two cases are selected without altering the existing system and components, as well as for thermal performance and cost-to-profit analysis. These two cases will be recommended for the upgrading of existing nuclear power plants to generate more electricity with the consideration of profit and the environment. Figure 5.3 shows the schematic diagram of the suggested component to be installed at NPP waste heat recovery site for further electricity generation. To upgrade the existing nuclear power plant, the following equipment is mentioned in Table 5.4, are designed and recommended for upgradation purposes to harness waste heat into electricity generation.

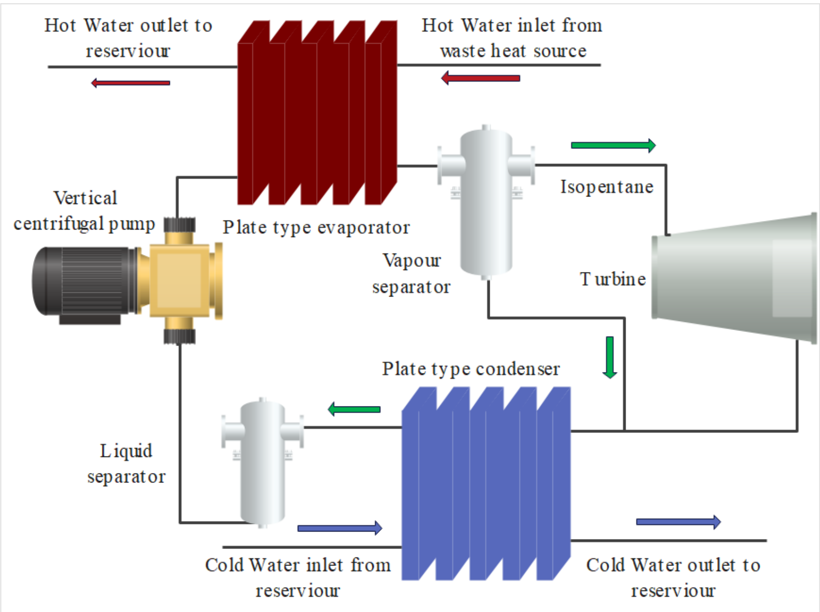

Figure 5.3. Schematic diagram of suggested ORC to be installed at NPP waste heat recovery site

Table 5.4. Recommended component design and specification for ORC installation

Sr. No.	Equipment	Type	Case-1: Design and Cost Specification	Case-2: Design and Cost Specification

1.	Pump	Vertical centrifugal pump	Capacity: 4.5 kW, Liquid flow rate: 1,128 litre/min, Cost: ₹ 7,94,724	Capacity: 6.1 kW, Liquid flow rate: 14,587 litre/min, Cost: ₹ 9,98,592
2.	Turbine	Case 1: Radial (Centrifugal), Case 2: Axial	Capacity: 199 kW, Vapour flow rate: 73,922 litre/min, Cost: ₹ 1,90,13,904	Capacity: 374 kW, Vapour flow rate: 1,760,566, litre/min, Cost: ₹ 2,96,45,112
3.	Evaporator	Plate heat exchanger	Heat transfer Area: 21m^2, Design pressure: 3.21 bar, Capacity: 4,194 kW, Cost: ₹ 7,45,584	Heat transfer Area: 136.1m^2, Design pressure: 1.7 bar, Capacity: 49,262 kW, Cost: ₹ 32,15,856
4.	Condenser	Plate heat exchanger	Heat transfer Area: 32m^2, Design pressure: 1.52 bar, Capacity: 4,024 kW, Cost: ₹ 10,25,304	Heat transfer Area: 232.3m^2, Design pressure: 1.52 bar, Capacity: 48,954 kW, Cost: ₹ 48,78,468
5.	Liquid vapour separator	Vertical cylinder	Separation velocity: 1.2 m/s, Capacity: 0.34 m^3, Cost: ₹ 1,87,120	Separation velocity: 0.97 m/s, Capacity: 10.12 m^3, Cost: ₹ 10,43,645

Table 5.5. Various input and output parameters for case 1 and case 2

Output Parameter	**Case -1**	**Case -2**
Net power (work) [kW]	167.8	318.4
Thermal efficiency (%)	4	0.65
Pump work [kW]	4	5.5
Turbine work [kW]	178.8	337.2
Condenser pressure [kPa]	151.3	151.3
Boiler pressure [kPa]	321.1	169.4
Exergy efficiency (%)	26.5	6.5
Exergy in [kW]	633.8	4896

Total irreversibility [kW]	459	4564
Condenser cold fluid (water) mass flow rate [kg/s]	224.1	2898
Working fluid mass flow rate (cold side of boiler and hot side of condenser) [kg/s]	11.3	145.7
*Boiler hot fluid (water) mass flow rate [kg/s]	33.3	471
Heat inlet from boiler [kW]	4199	49286
*Hot fluid (water) inlet temperature [°C]	98	75
*Hot fluid (water) outlet temperature [°C]	68	50
Cold fluid (water) inlet temperature [°C]	29	29
Cold fluid (water) outlet temperature [°C]	33.3	33
Condenser area [m^2]	31.5	232.3
Evaporator area [m^2]	21	136.1
Capital investment Cost [in thousand USD]	259.42	464.32
NPV of total cost (CI and O&M for 40 years) [in thousand USD]	472.26	845.27
NPV of total energy output (for 40 years) [GWh]	12.86	24.41
Total capital and O&M cost [USD/h]	3.29	5.89
Total revenue earned [USD/h]	13.09	24.83
Yearly profit (in thousand USD)	68.56	132.58
Payback period [years]	6.15	5.86
Discounted payback period [years]	8.67	8.08
LCOE (USD/kWh)	0.037	0.035
Internal rate of return (%)	17	17
Annually saving in CO_2 emission from NPP [ton]	21.14	40.12

*Selected input parameters of the feasible location of NPP for waste heat recovery

For fixed operating conditions (Table 5.2), all necessary input and output parameters are tabulated in Table 5.5 for both cases. Comparison is made easy from thermal and economic points of view. For the analysis, two feasible cases (case-1 and case-2) are deduced. Case-2 produces maximum power because of the availability of a high hot fluid mass flow rate in the cycle, but due to the availability of waste heat at a lower grade, it has the lowest efficiency. Case-1 has the highest thermal efficiency because it operates at a higher boiler temperature when compared to case-2. LCOE obtained a value of 0.038 USD /kWh for case-1 and 0.036 USD /kWh for case-2, which is lower than the electricity selling cost (0.061 USD/kWh) from power generated from Indian NPPs. So, for both cases, ORC upgradation is worth venturing into the current NPP site. It is worth noting that ORC's built-up cost in India is calculated as 1.20-1.51 thousand USD/kWe, which is the lowest among South Korea, China, Japan, Russia, and many more countries [28]. It is clear that ORC installation cost for the upgradation of the current NPP site for case -1 is 1.46 thousand USD/kWe and for case-2 is 1.38 thousand USD/kWe, which is lower and in the range of India's expected per kWe expense.

T-s diagram is shown in Figure 5.4 for both cases discussed in Table 5.5. It is clearly shown that case-1 has the maximum turbine enthalpy difference, but power output is maximum for case-2 because of the high mass flow rate of working fluid (Table 5.5). Figure 5.4 also shows the exact temperature and specific entropy node value at different stages of the ORC power plant for both cases.

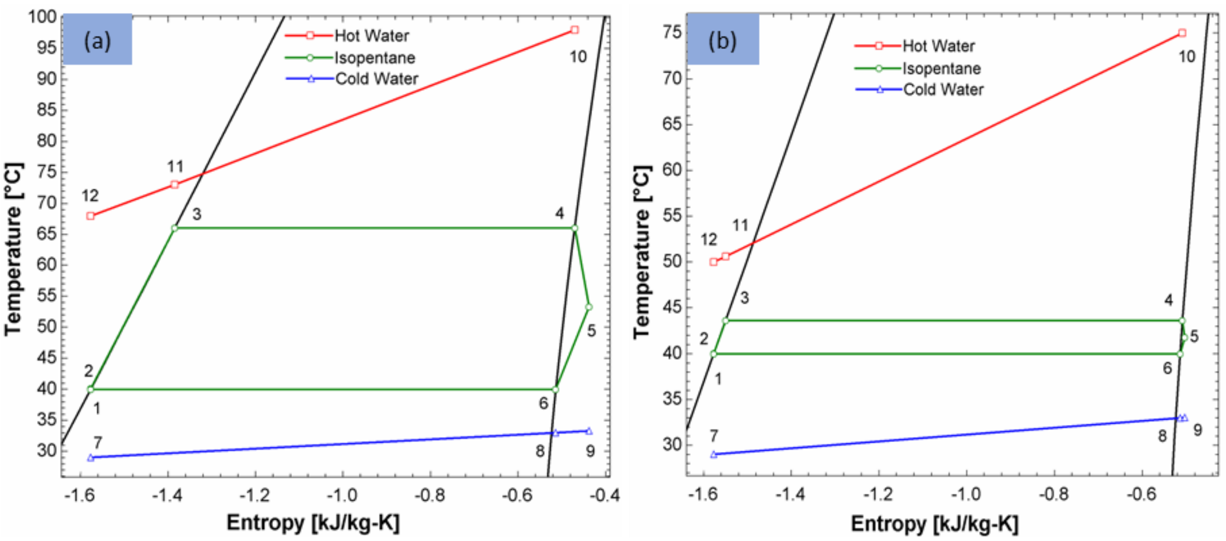

Figure 5.4. (a) ORC T-s diagram of case-1, (b) ORC T-s diagram of case-2

5.3.2. Working fluid behaviour on the output parameter

Table 5.6 shows the working fluid behaviour for different output parameters for both feasible cycles. Results show that R245fa performed better for case-1 and R236ea performed better for case-2 in terms of yearly profit when compared with R601a (Isopentane) working fluid. Other necessary parameters are compared and tabulated in Table 5.6.

Table 5.6. Effect on output parameter with working fluid for both feasible cases

Output Parameter	Case -1				Case -2			
	R601a	R245fa	R236ea	R123	R601a	R245fa	R236ea	R123
Net power (work) [kW]	167.8	169.5	169.5	168.1	318.4	321.7	329.8	314.8
Thermal efficiency (%)	4.01	4.03	4.03	4.00	0.65	0.65	0.67	0.64
Boiler pressure [kPa]	321.1	554.9	737.3	334.9	169.4	281.4	380.4	173.7
Exergy efficiency (%)	26.50	26.74	26.74	26.53	6.5	6.57	6.74	6.43
Capital investment [in thousand USD]	259.42	267.21	275.10	259.53	464.32	473.83	489.86	460.83
Yearly profit (in thousand USD)	68.56	68.79	68.07	68.74	132.58	133.54	136.55	130.92
NPV of the total cost [in thousand USD]	472.26	486.43	500.80	472.45	845.27	862.57	891.75	838.90
Discounted payback period [years]	8.67	8.87	9.19	8.65	8.08	8.18	8.26	8.12
LCOE (USD/kWh)	0.037	0.037	0.039	0.037	0.034	0.035	0.035	0.034

5.3.3. Parametric study

The net work output of the cycle will be increased when condenser temperature and cold fluid inlet temperature are lowered, as shown in Figure 5.5. Amount of work obtained for different cases will vary with evaporator and condenser pressure that is directly affected by waste heat source input temperature and condenser temperature. From Figure 5.5, it can be observed that case-1 cycle work production capacity does not much changes with condenser temperature as it drastically changes with case-2 due to the amount of working fluid mass flow rate. Case-2 produces maximum power when both condenser temperature and cold fluid inlet temperature are lowered because of the large amount of working fluid mass flow rate and turbine enthalpy difference. All graphs have some missing values because PPTD criteria cannot be met at some condenser temperature and cold fluid inlet temperature values.

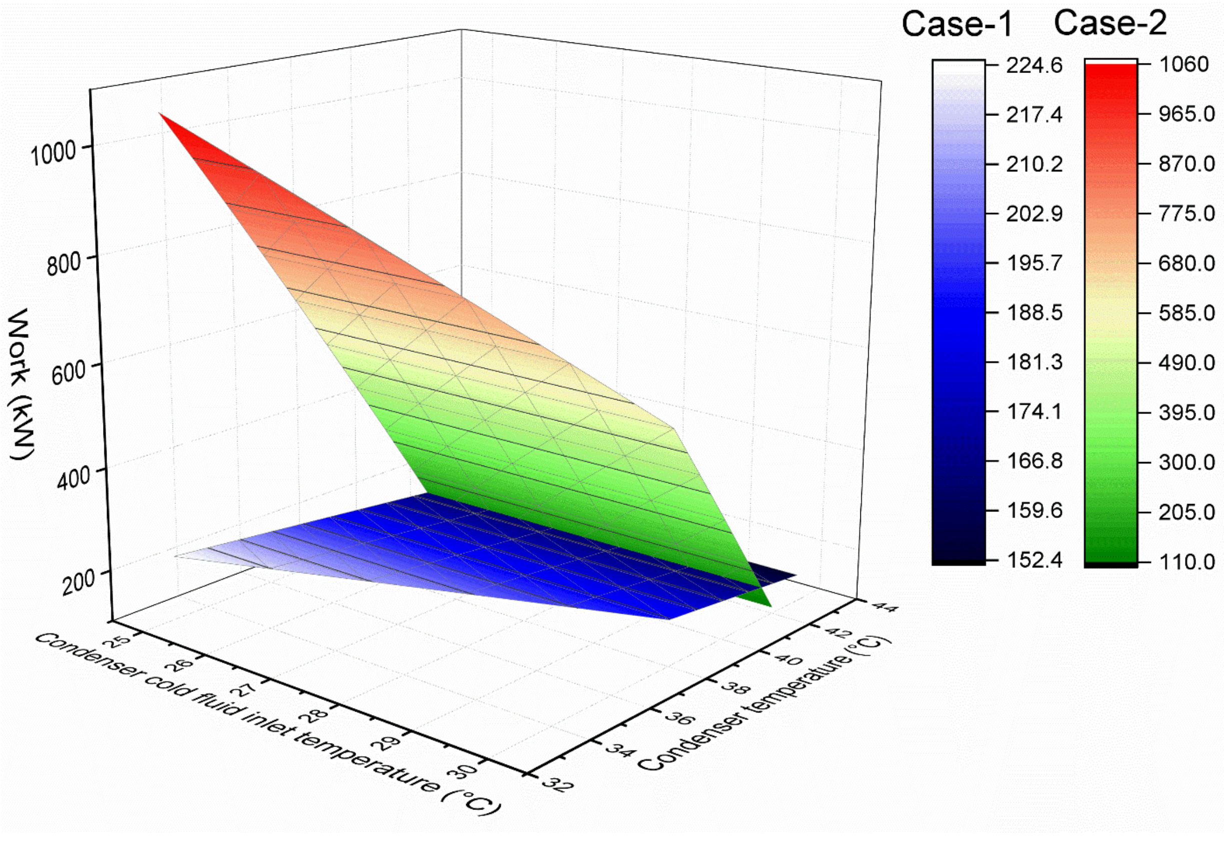

Figure 5.5. Effect of condenser and cold fluid inlet temperatures on net work output

Thermal efficiency is dependent on the type of working fluid used and the pressure ratio of the power cycle. The temperature grade of the heat source plays a significant effect on thermal efficiency. High grade of evaporator /waste heat source temperature gives higher thermal efficiency. Case-1 cycle has maximum thermal efficiency because of its high-pressure ratio of evaporator and condenser when compared to case-2, as shown in Figure 5.6. Both cases show the same decremental trend in thermal efficiency when the condenser temperature increases. Thermal efficiency is not significantly affected by the variation in the condenser's cold fluid inlet temperature.

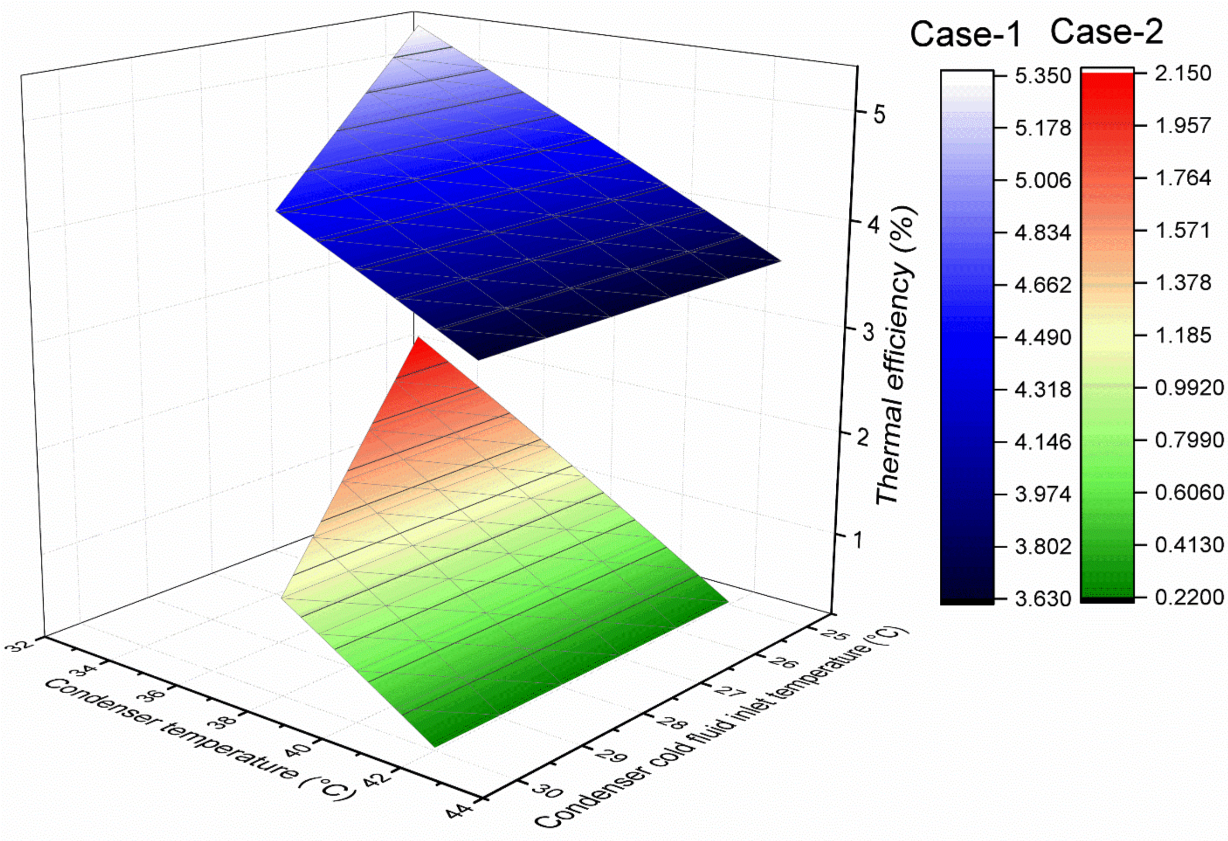

Figure 5.6. Effect of condenser and cold fluid inlet temperatures on thermal efficiency

The total investment cost is affected by the sum of individual components' capital cost and their maintenance cost up to the project lifespan, which is further dependent on the intensive property (pressure and temperature) and extensive property (mass flow rate) of the fluid. Capital cost is directly influenced by material and manufacturing costs, whereas operation and maintenance costs are dependent on the raw material used (fuel) and labor expenses for successive years. In successive years, labor and other expenses will not be the same and the time value of money also comes into the picture when calculating project feasibility at present time. To withstand the component at higher pressure and temperature, thick material is used and to handle more mass flow rate, a large size component is used. Figure 5.7 shows variations in total capital investment and O&M cost (operation and maintenance cost) for the 20-year lifespan of both cases, with variations in condenser temperature and cold fluid inlet temperature. If condenser temperature and cold fluid inlet temperature are lowered, then both cycles will produce higher work output at a larger pressure ratio; thus, net present value (NPV) of total investment becomes maximum for both cases, Figure 5.7. NPV of total investment is larger for case-2 due to big size component requires for higher mass flow rates. Due to the PPTD design constraint of condenser temperature, the difference of cold fluid inlet and outlet temperature will be less and so, more amount of cold fluid mass flow rate will be required for the same amount of heat rejection. At lower condenser temperatures, condenser size will be increased for the same mass flow rate due to lower LMTD.

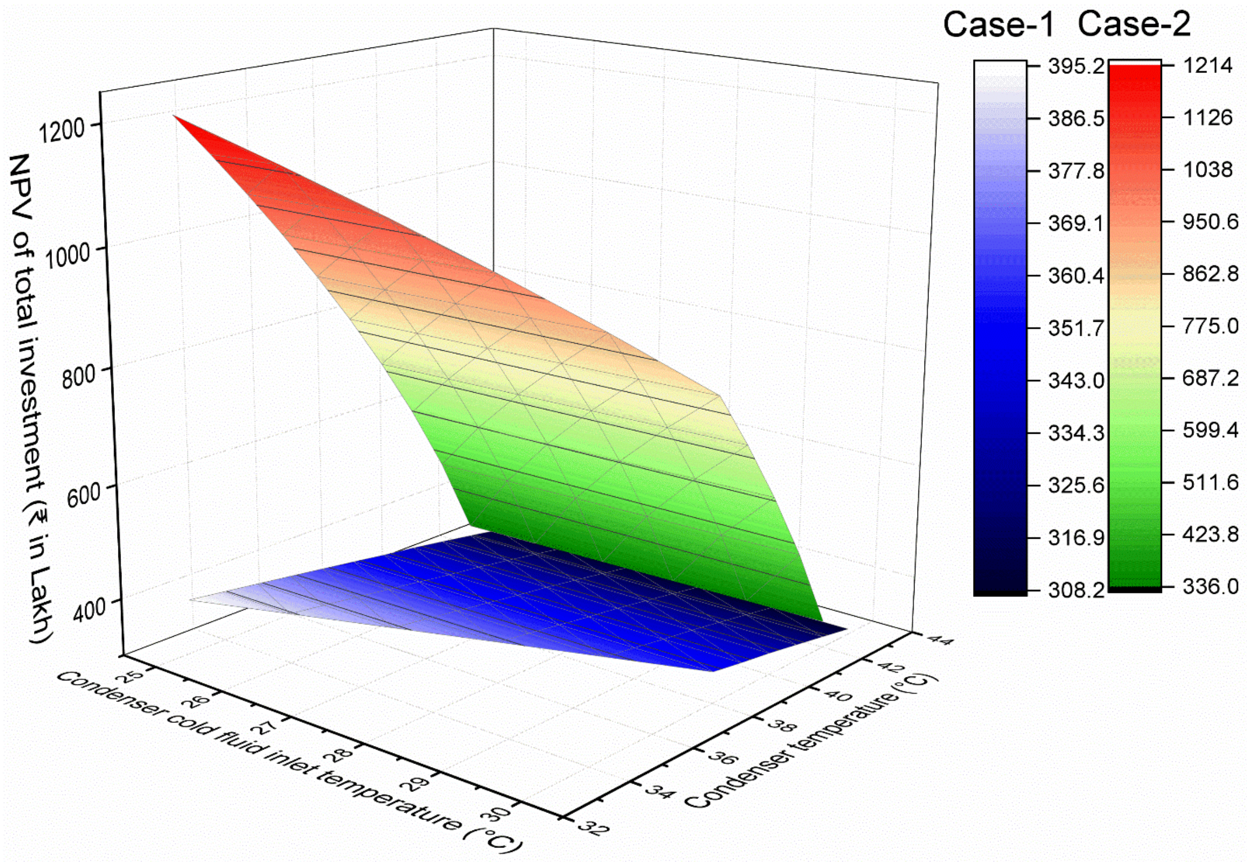

Figure 5.7. Effect of condenser and cold fluid inlet temperatures on NPV of total investment

Although case 2 has the highest capital investment and NPV of total investment, it also possesses the highest net annual profit at the same input condition due to the maximum production of the net work. Figure 5.8 shows that the annual profit increment trend with condenser temperature and cold fluid inlet temperature is the same as the work production trend because of its relative dependencies on work output and capital investment. Case-2 is not favourable concerning case-1 at a condenser temperature higher than 41°C. Although case-2 has a lower pressure ratio and thermal efficiency because of increased mass flow rate, it gives the best profit for a condenser temperature below 41°C.

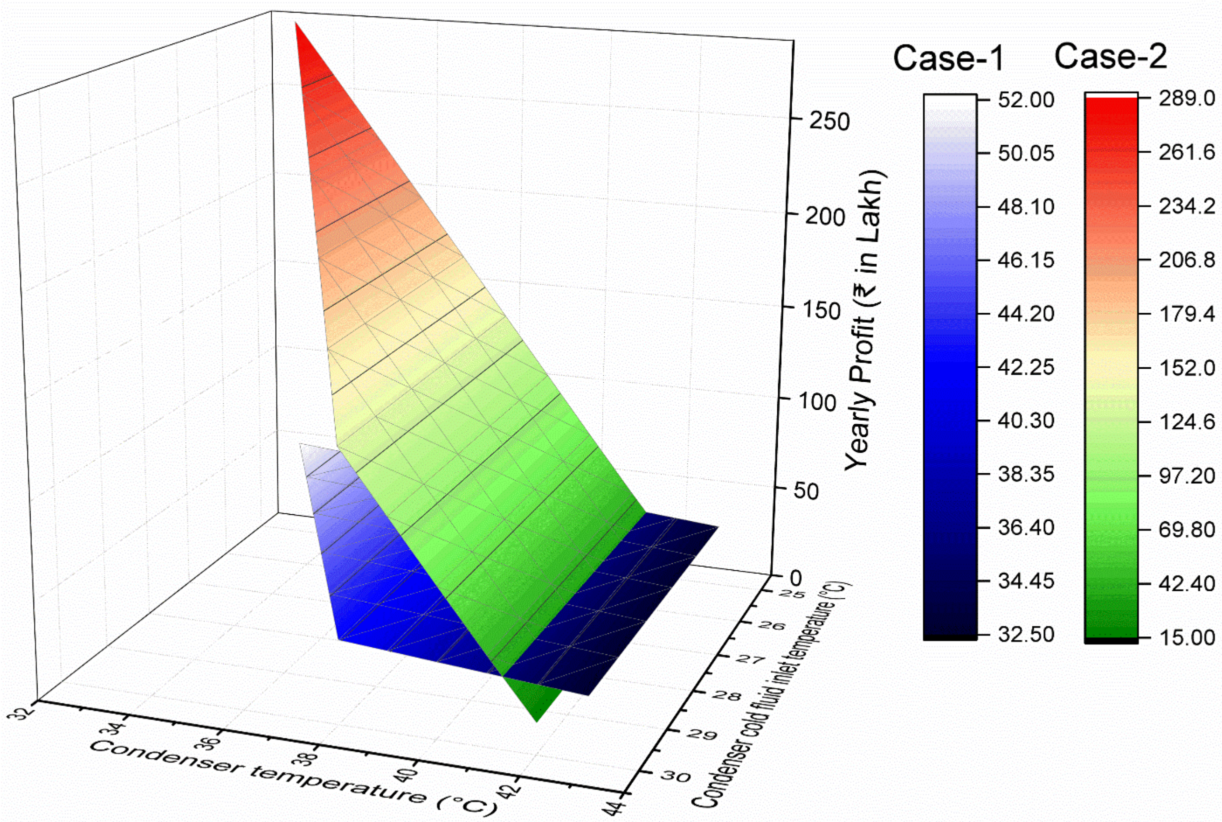

Figure 5.8. Effect of condenser and cold fluid inlet temperatures on yearly profit

The lower value of LCOE is favorable for the selection of power plant projects. Figure 5.9 shows the effect of condenser temperature and cold fluid inlet temperature on LCOE for different case cycles. Figure 5.9 clearly shows that case-1 will be worth venturing at above 41°C condenser temperature and case-2 will be worth venturing at below 41°C condenser temperature. LCOE value is quite low, thus favorable for the case-2 cycle when operating below 41°C condenser temperature. At a high value of LCOE, the discounted payback period may be greater than the project lifespan, which means the project will surely be in loss-making.

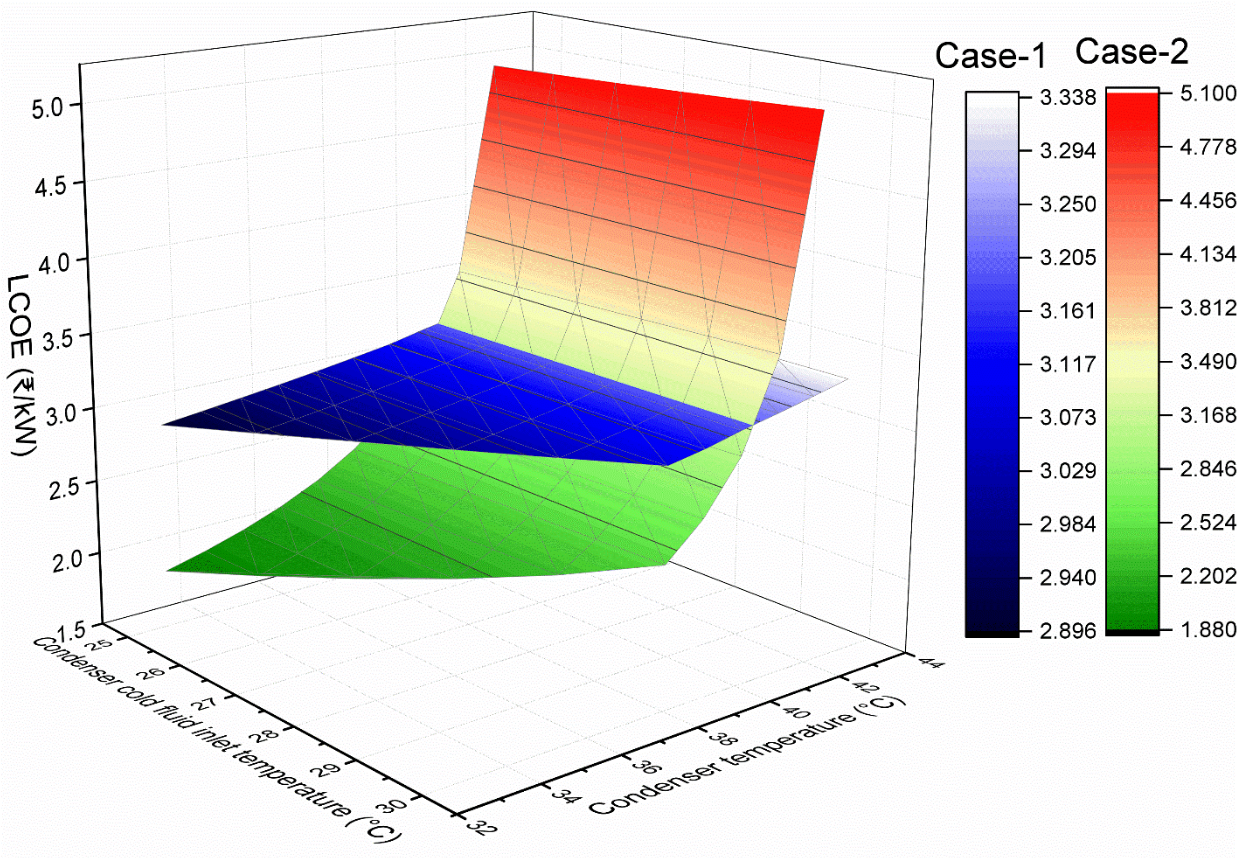

Figure 5.9. Effect of condenser and cold fluid inlet temperatures on LCOE

Discounted payback period reveals how fast invested money can be paid back when the time value of money is considered. Lower DPP is favorable for identifying potentially benefited projects. Figure 5.10 shows that case-2 is favorable for condenser temperature operating below 41°C. Figure 5.10 has some missing values of case-2 for condenser temperature operating above 41°C because, at that temperature intersection, DPP will be greater than the estimated life span of the project (40 years).

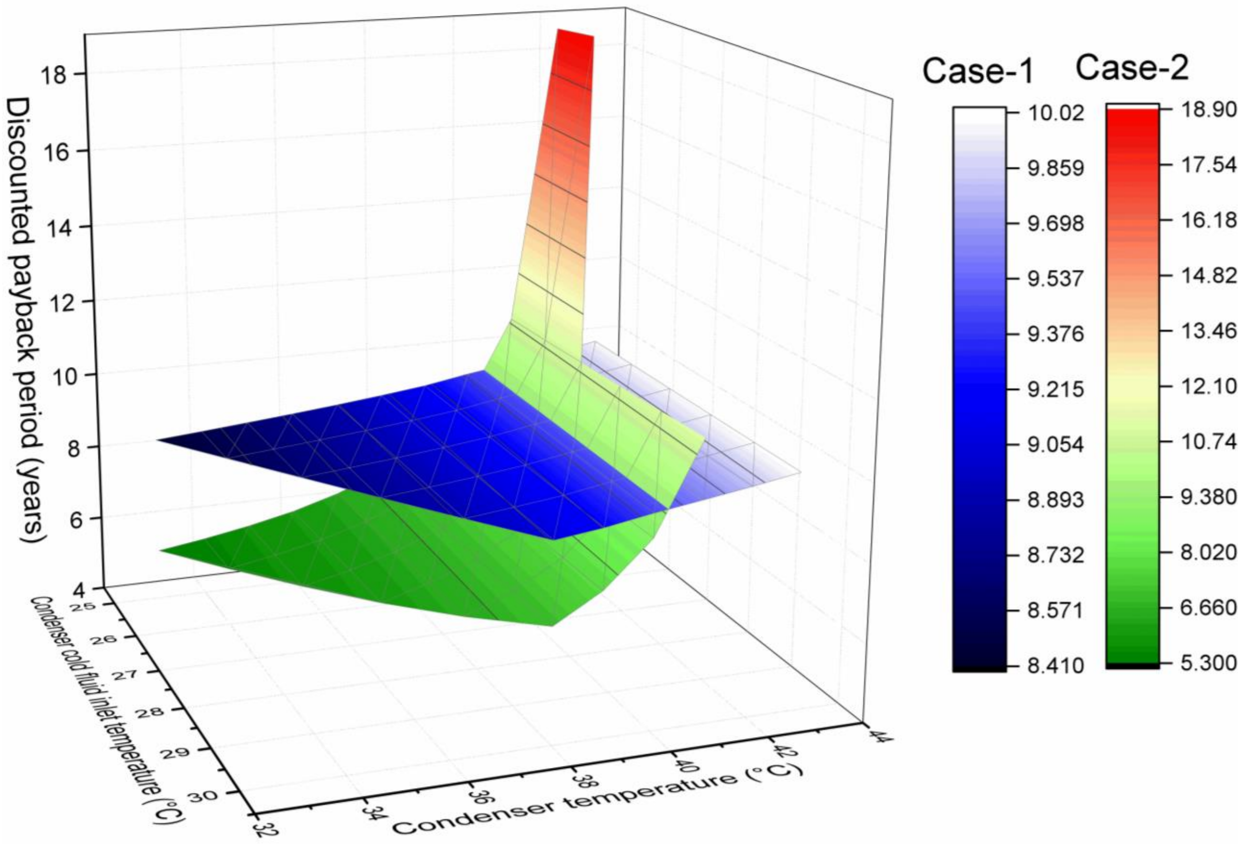

Figure 5.10. Effect of condenser and cold fluid inlet temperatures on DPP

To decide whether the project should be taken or not, internal rate of return (IRR) plays an important role in decision-making. If IRR> discounted rate (8%), then the project can be profitable. The decision is further dependent on IRR value and other parameters also (LCOE, DPP). It is clear from Figure 5.11 that case-1 would be feasible to opt at a condenser temperature less than 43°C and case-2 would be feasible to opt at a condenser temperature less than 42°C. The higher value of IRR is favorable when choosing between two projects. It is clearly shown in Figure 5.11 that the project below 41°C condenser temperature case-2 and above 41°C condenser temperature case-1 is worth venturing for all ranges of condenser cold fluid inlet temperature.

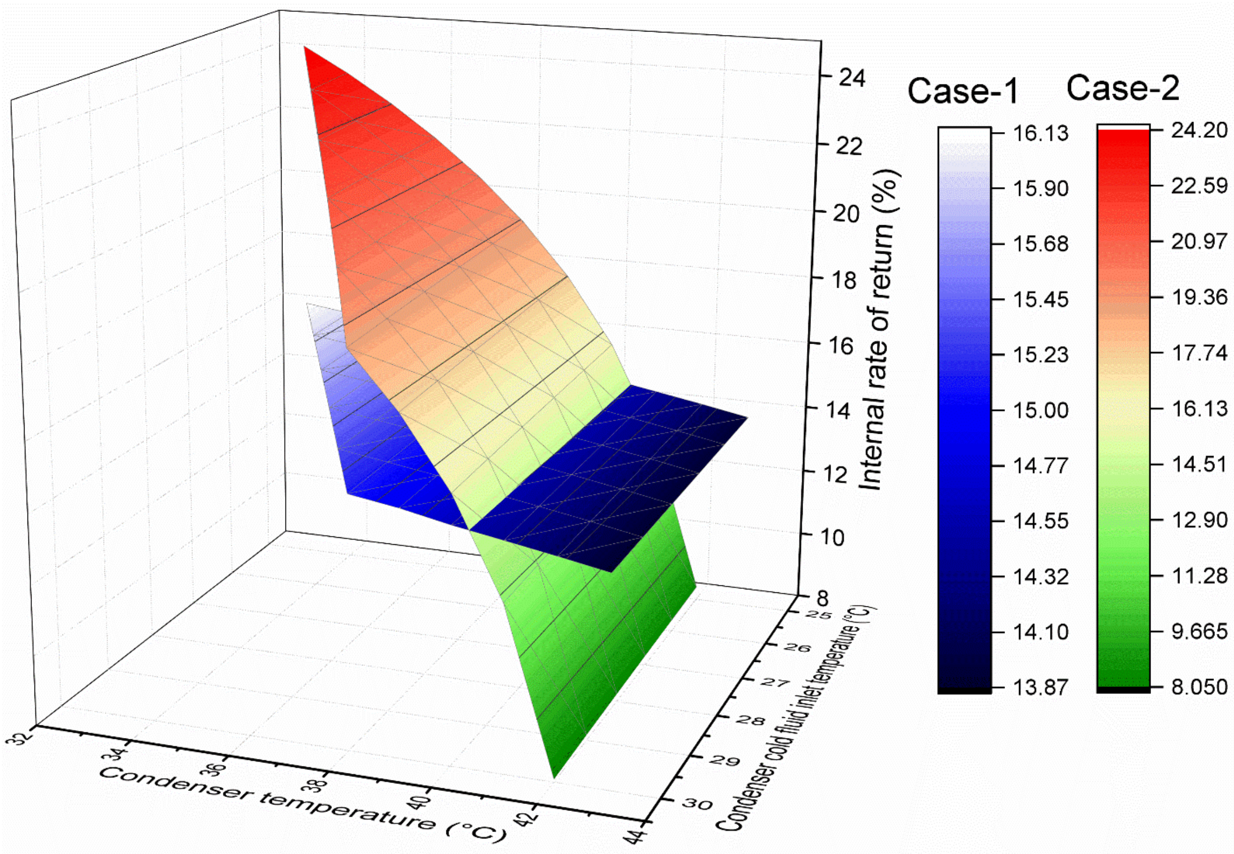

Figure 5.11. Effect of condenser and cold fluid inlet temperature on IRR for different case cycles

Although CO_2 saving from NPP is much lower than that of conventional power plants (coal-based power plants), it is worth mentioning when compared with renewable-based power plants (solar, hydro, wind). Figure 5.12 shows the effect of condenser temperature and cold fluid inlet temperature on annual CO_2 saving for both case cycles. It is clearly shown in Figure 5.12 that the project below 42.5°C condenser temperature case-2 and above 42.5°C condenser temperature case-1 will save the maximum amount of CO_2 emission for all ranges of condenser cold fluid inlet temperature. This CO_2 emission comes into the picture when the same amount of additional power generated is achieved from ORC upgradation at the NPP site and not from the NPP itself.

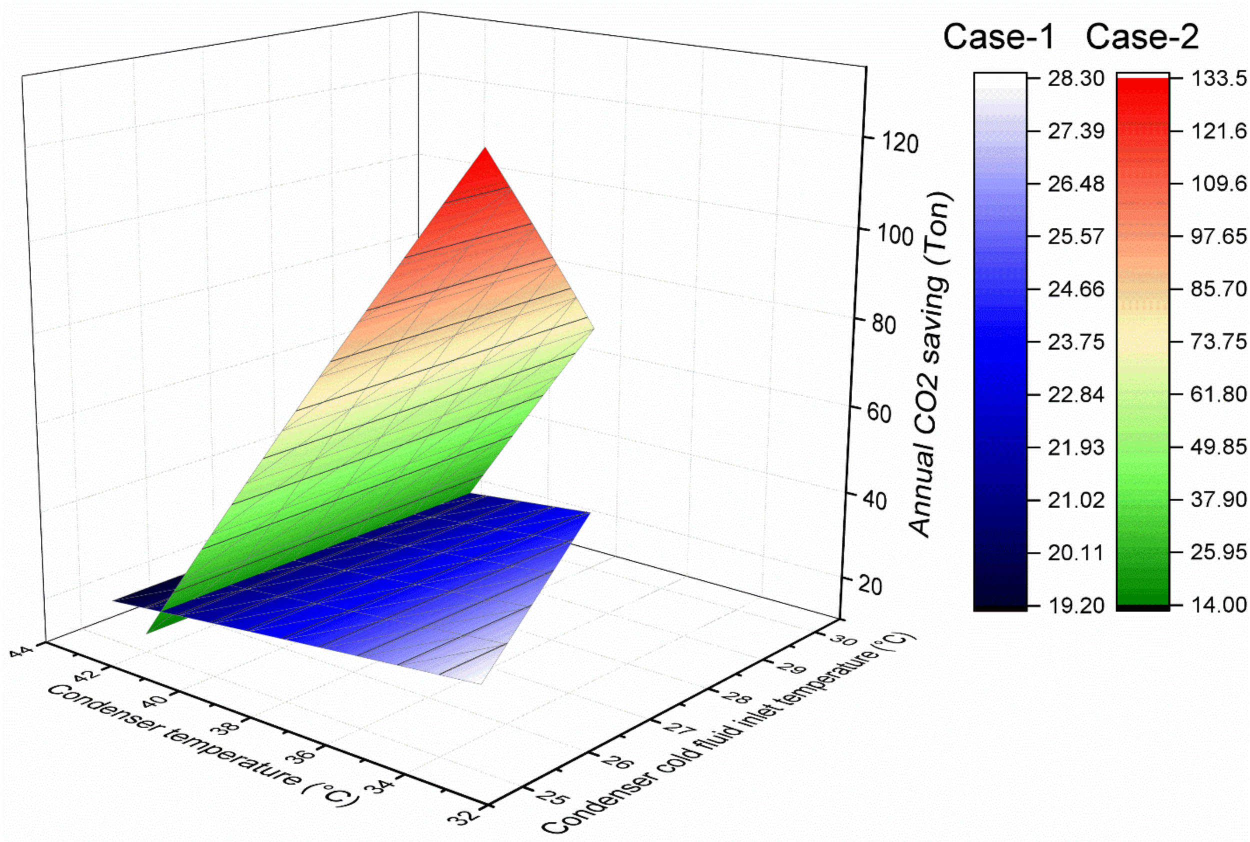

Figure 5.12. Effect of the condenser and cold fluid inlet temperature on annual CO_2 emission saving

5.3.4. Simulation vs Experimental

The simulation and experimental variation of data provided by BRNS for NPP upgradation and feasibility studies are tabulated in Table 5.7 for case-1 and Table 5.8 for case-2. For simulation conditions, cold fluid is taken as water, while for experimental purposes, the air is taken as cold fluid to avoid further complexities of water supply, drainage and leak. The hot fluid inlet temperature was matched with simulation data (data provided by BRNS, Table 5.1) by adjusting the heating load for both cases. The mean condition of the volume flow rate was taken, and the mass flow rate value for therminol VP1 was obtained.

Table 5.7. Simulation and experimental variation of Case-1 NPP

Case-1		
Parameter	**Simulation**	**Experimental**
***Hot fluid Inlet Temperature [°C]**	98.00	98.72
***Cold fluid inlet temperature [°C]**	29.00 (Air)	28.82 (Air)

Hot fluid Outlet Temperature [°C]	68.00	96.10
***Mass flow rate of hot fluid [kg/s]**	33.33 (Water)	0.833 (Therminol VP1)
Mass flow rate of working fluid [kg/s]	11.26 (Isopentane)	0.0052 (Isopentane)
***Heat Input [kW]**	4199	5
Net Work [kW]	174.8	0.106
Thermal efficiency (%)	4.2	2.13
Pump inlet pressure [bar]	1.51	1.60
Pump outlet pressure [bar]	3.21	4.12
Turbine inlet pressure [bar]	3.21	3.76
Turbine outlet pressure [bar]	1.51	1.89
Pump inlet temperature [°C]	40.00	30.92
Pump outlet temperature [°C]	40.10	31.19
Turbine inlet temperature [°C]	66.08	87.45
Turbine outlet temperature [°C]	53.32	74.61

*Selected input parameters

Table 5.8. Simulation and experimental variation of Case-2 NPP

Case-2		
Parameter	**Simulation**	**Experimental (Threshold condition)**
***Hot fluid Inlet Temperature [°C]**	75	90.7**
***Cold fluid inlet temperature [°C]**	29 (Air)	29.32 (Air)
Hot fluid Outlet Temperature [°C]	50	88.88
***Mass flow rate of hot fluid [kg/s]**	471 (Water)	1.003 (Therminol VP1)
Mass flow rate of working fluid [kg/s]	145.6 (Isopentane)	0.0050 (Isopentane)
***Heat Input [kW]**	49286	4.0
Net Work [kW]	318.4	0.09449 (94.49 W)
Thermal efficiency (%)	0.65	2.34
Pump inlet pressure [bar]	1.51	1.63
Pump outlet pressure [bar]	1.69	3.68

Turbine inlet pressure [bar]	1.69	3.35
Turbine outlet pressure [bar]	1.51	1.88
Pump inlet temperature [°C]	40.0	30.8
Pump outlet temperature [°C]	40.01	31.01
Turbine inlet temperature [°C]	43.63	81.67
Turbine outlet temperature [°C]	41.79	71.9

*Selected input parameters

**Current fabricated and installed ORC experimental setup in HMT lab of IIT BHU has design constraint (Evaporator undersize) due to which turbine movement with desired RPM is only possible at above 90°C heat source inlet temperature condition. If evaporator size is increased then it can be possible to run the experimental setup at 75°C heat source inlet temperature condition. Moreover, operating condition (Fixed hot fluid outlet temperature) is also mazor constraint to get more power at higher thermal (cycle) efficiency.

Table 5.7 and Table 5.8 show the input and output condition of both selected feasible cases and based on that, scalability scope can be identified to get installed at the site location for further generation of electricity. If desired hot fluid outlet temperature (for case-1, 68°C and for case-2, 50°C) can be maintained separately after the ORC evaporator, then by optimizing at given condition, more turbine power and cycle efficiency can be obtained.

5.3.5. Nanofluid-enhanced WHR for ORC

Waste heat-driven ORC using nanofluid as a recovery medium is taken as a case study. ORC can convert low-to-medium-temperature waste heat into useful work. Incorporating nanofluids as the hot fluid in the ORC enhances heat transfer efficiency, potentially boosting the cycle's overall performance, as shown in Figure 5.13. The studied system includes the following key components: evaporator, organic working fluid, nanofluid, turbine, condenser, and pump. The nanofluid behaviour on ORC affects the performance parameter. Hot fluids such as water and therminol VP1 are taken for comparison purposes with Al_2O_3 nanoparticles. This hot side nanofluid behaviour is analyzed with six organic fluids. The following table shows the properties of nanofluid and organic fluids used.

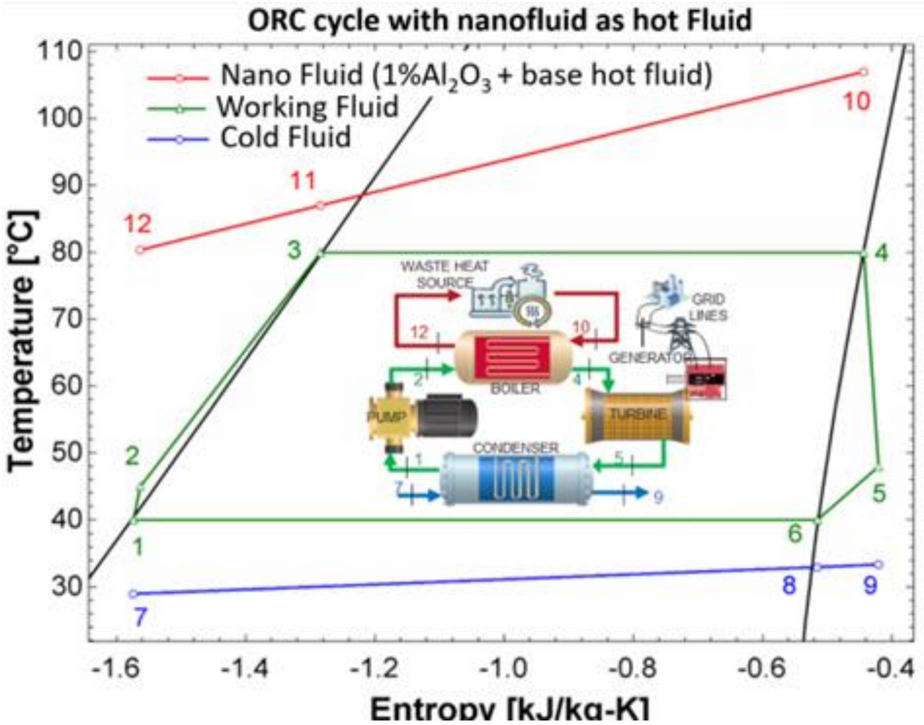

Figure 5.13. T-s Diagram and layout of nanofluid based ORC

The simulation code based on the above model has been developed on the EES platform. The input parameters are listed in Table 5.1. These feasible input parameters (Table 5.2) help in the simulation for performance comparison of waste heat recovery ORC for various nanofluid and organic working fluid combinations. The properties of used nanofluids (Al_2O_3/water and Al_2O_3/Thermonol-VP1) have been calculated using suitable correlations [128] based on individual data given in Table 5.10. Table 5.11 shows the properties of organic working fluids.

Table 5.9. Input parameters used

Input parameter	Value	Input parameter	Value
Alternator efficiency	0.96	Plate heat exchanger's length	150 mm
Cold fluid inlet	29°C	Dimension of storage tank	30 cm × 70 cm
Condenser temperature	40°C	Operational year	40 year
Hot (Nanofluid) inlet	75°C	PPTD	7°C
Hot (Nanofluid) outlet	50°C	Electricity cost	0.078 $/kWh
Nanofluid mass flow rate	471 kg/s	Yearly working hour	7000 h

Nanoparticle volume percentage	1%	Turbine efficiency	0.6
Pump efficiency	0.8		

Table 5.10. Thermophysical properties relevant to nanofluids [99,128]

Thermophysical property	Water	Therminol VP1	Al_2O_3
Density (kg/m^3)	998.2	1059	3970
Dynamic viscosity (Pa.s)	0.001003	0.003599	-
Specific heat (J/kgK)	4182	1565	765
Thermal conductivity (W/mK)	0.6	0.1357	40

Table 5.11. Organic working fluid properties

Working fluid	Isopentane	R123	R236fa	R236ea	R141b	R143m
Global warming potential	4	77	9,810	1370	725	4800
Normal boiling point value [°C]	27.85	27.78	-1.492	6.105	32.06	-23.57
Critical temperature [°C]	187.2	183.7	124.9	139.3	204.2	104.8
Ozone depletion potential	0	0.02	0	0	0.12	0
Critical pressure [bar]	33.7	36.68	32	34.29	42.49	36.35

Figure 5.14 compares the net work obtained with different hot fluids and working fluids viz. R143m, R141b, R236ea, R236fa, R123 and R601a. Water-based nanofluid and water show greater value for net work because of greater specific heat value, same temperature difference and hot fluid mass flow rate, which ultimately requires a very large amount of heat (almost 250% higher) to be used to operate the turbine and thus large turbine work is obtained. It has been clearly shown in the figure that net work output performance for nanofluid is lower than respective base fluid (hot fluid) for all organic working fluids because nanofluid lowers the specific heat value for nanofluid, which ultimately lowers the amount of heat transfer to the

boiler for same temperature difference (input condition constraint). Further, a lower amount of heat interaction requires less organic working fluid mass flow rate, which results in lower turbine work being obtained. Generally nanofluid application requires redesigning of the heat exchanger and PPTD go down for nanofluid applied boiler. From the organic working fluids, R236fa showed the best performance while R141b showed the lowest.

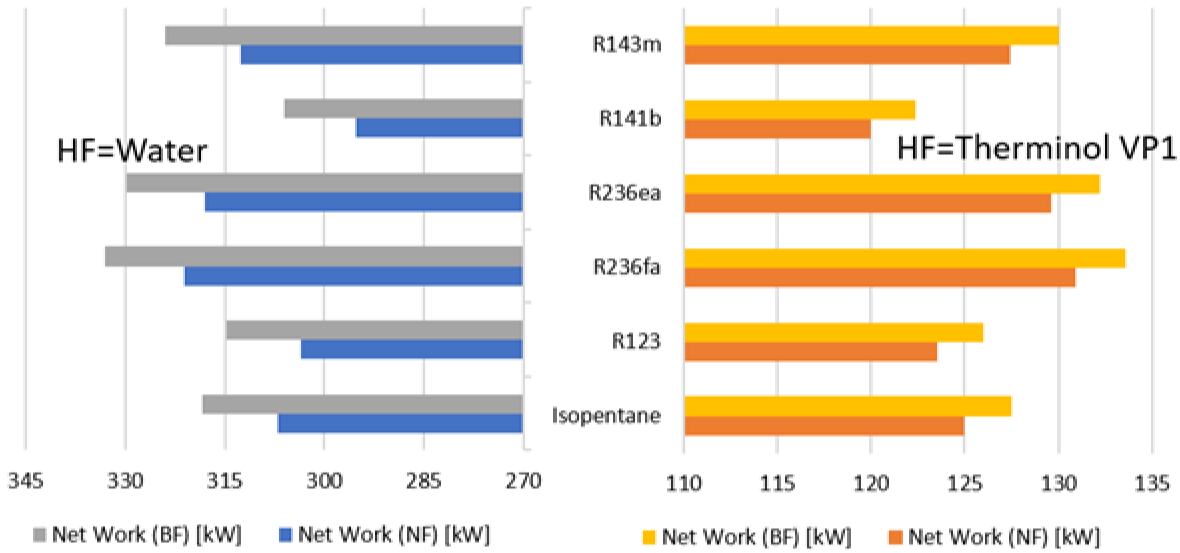

Figure 5.14. Net work comparison with different hot fluids and working fluids

Figure 5.15 compares the thermal efficiency obtained using both base hot fluids and nanofluids. Thermal efficiency depends upon net work and boiler's heat interaction. The study found that water and therminol-VP1 showed almost the same thermal efficiency with little increment with therminol-VP1 base fluid and nanofluid. Interaction of therminol-VP1-based nanofluid showed almost same or little increase in thermal efficiency with its base fluid, while water and its nanofluid slowed adverse effect. This is because of the mutual interaction between net work and boiler's heat value. Redesigning the heat exchanger is generally needed for nanofluids to optimize performance and thus, PPTD will affect the other parameters' performance. It can also be concluded that among the organic working fluids, R236fa gives the best thermal efficiency, while R141b performs the worst.

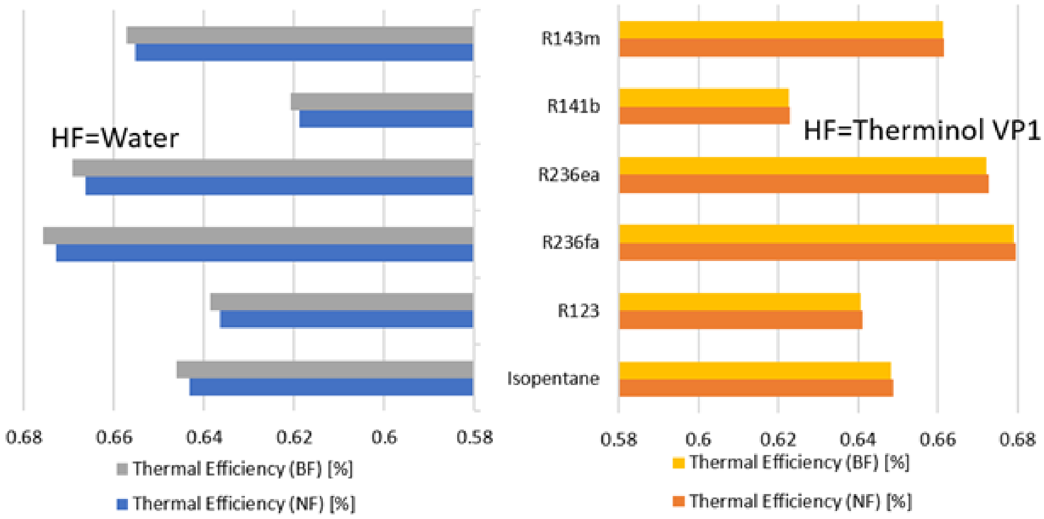

Figure 5.15. Thermal efficiency comparison with different hot fluids and working fluids

Water-based nanofluid shows a greater working fluid mass flow rate than therminol-based nanofluid due to their higher specific heat. Figure 5.16 demonstrates that the working fluids mass flow rate output for nanofluids is lower than their respective base fluids across all organic working fluids, as nanofluids lower the specific heat value, reducing heat transfer to the boiler under the same conditions. This results in a lower mass flow rate of organic working fluid and, consequently, lower turbine work. The PPTD value remains constant because the same heat exchanger is used. Generally, nanofluid applications necessitate heat exchanger redesign, reducing the PPTD for nanofluid-applied boilers.

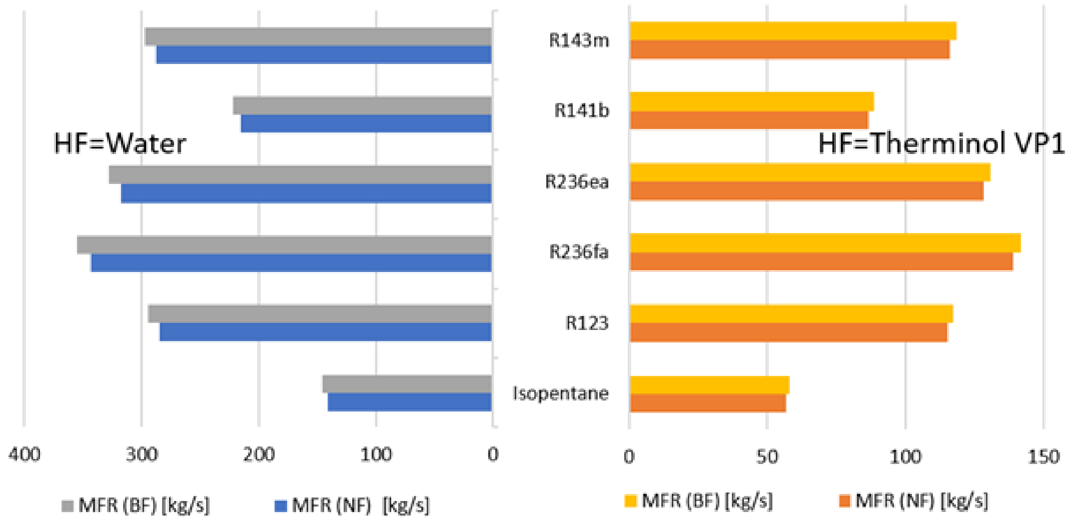

Figure 5.16. Working fluid mass flow rate comparison with different hot fluids and working fluids

Figure 5.17 compares the capital investment using base hot fluids and nanofluids with six different organic working fluids. Water-based nanofluid and water as base fluid yield higher capital investment due to greater specific heat of water which requires large size of heat exchangers (boiler and condenser) to handle large amount of heat. Figure 5.17 also shows, the capital investment value for nanofluids is lower than for their respective base fluids because nanofluids have lower specific heat and higher thermal conductivity than base fluid which affects the higher heat transport coefficient for nanofluid-based heat exchangers. Among the organic working fluids, R143m requires the largest capital investment, and R141b requires the lowest for both base hot fluid and its nanofluid combination.

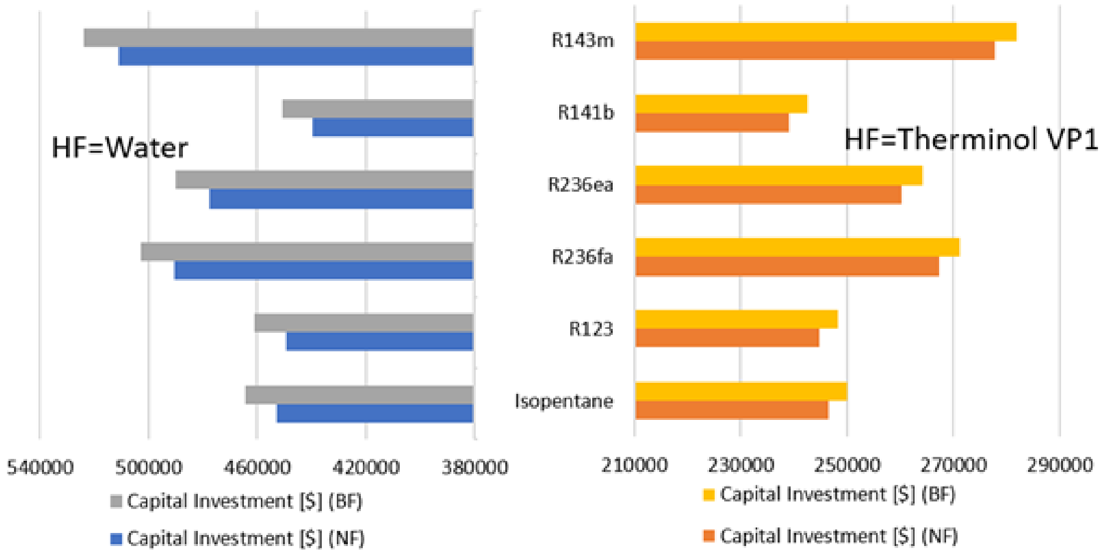

Figure 5.17. Capital investment comparison with different hot fluids and working fluids

Figure 5.18 illustrates the earned profit ($) comparison of ORC when water and therminol-VP1 hot fluid and its nanofluid are used with six different organic working fluids. The findings indicate that water-based nanofluid and water as a base fluid deliver higher profit (around 2.5 times higher) than therminol. This is due to the water's superior specific heat capacity (around 2.5 times higher) than therminol-VP1. However, the earned profit value for nanofluids is consistently lower than for their respective base fluids across all tested organic working fluids. This is attributed to the reduced specific heat capacity, higher thermal conductivity and increased heat transfer coefficient of nanofluids. Among the evaluated working fluids, R236fa and R236ea exhibited the highest performance and provided maximum profit, while R141b gives the lowest.

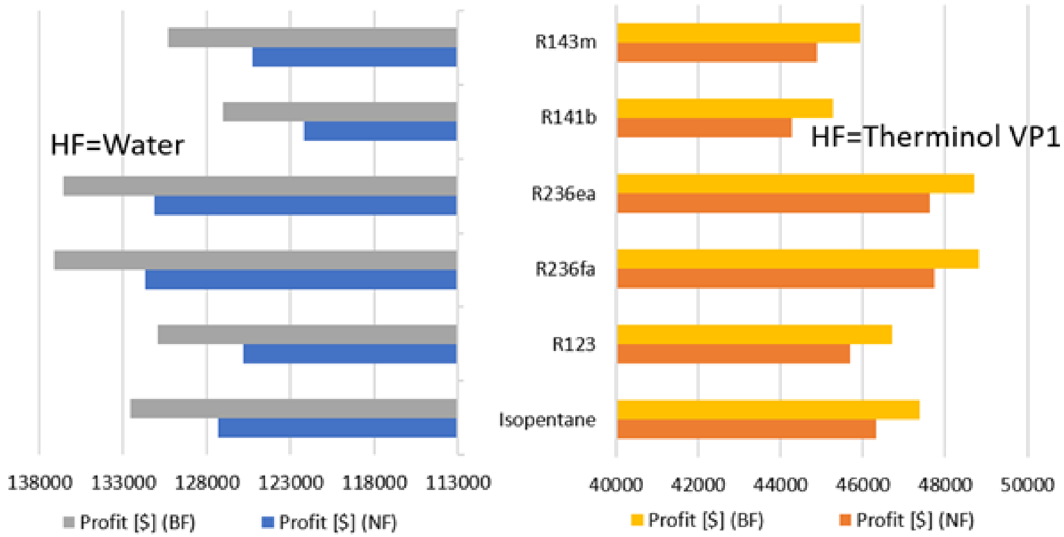

Figure 5.18. Earned profit comparison with different hot fluids and working fluids

5.4. Important Findings

It is important to find out the potential harnessing capacity of exhaust industrial heat to generate electricity with noticeable profit. In this regard, BRNS has provided the waste heat data of its nuclear power plant to generate electricity from its feasible location. The following outcomes are gathered from this study.

(i) Nine potential waste heat locations in nuclear power plants are identified and two feasible cases are proposed for bottoming ORC for waste heat recovery. Both cases are designed based on condenser temperature to optimize waste heat recovery.

(ii) Data from BRNS enabled the prediction of heat exchanger designs, component costs, overall power plant costs, net annual profit from surplus electricity, and environmental impact. This study proposed a capital cost correlation for alternators to accurately estimate system expenses.

(iii) Working fluid R245fa excelled in case-1, while R236ea was optimal for case-2, delivering higher yearly profits than R601a (Isopentane). Case 2, with a condenser temperature below 41°C, is recommended for NPP sites due to superior thermal and economic performance and faster capital returns. Both cases could generate 499.3 kW of electricity and an annual profit of 204.62 thousand USD, with a total capital investment of 764.96 thousand USD.

(iv) For a 40-year lifespan, the total NPV (capital and O&M investments) is 1.392 million USD, ensuring a minimum annual profit of 204.62 thousand USD.

(v) R236fa emerges as the most effective working fluid for ORC applications in terms of power output and profitability, followed by R236ea and isopentane (R601a). While R236fa offers the best thermodynamic performance, its high global warming potential (GWP: 9810) limits its usage in many countries, with R236ea (GWP: 1370) presenting a more environmentally viable option. However, both R236fa and R236ea require careful handling due to their low normal boiling points. So, if these drawbacks are considered, then isopentane is the best choice for the ORC application.

(vi) Experimental results showed significantly lower net power output and thermal efficiency compared to simulations due to constraints such as air-based cooling, evaporator under-sizing, mass flow rates and fixed hot fluid outlet temperatures but validated both cases to generate electricity.

(vii) Therminol-VP1-based nanofluids demonstrated efficiency improvements in waste heat recovery with required redesigned heat exchangers to fully utilize nanofluid advantages.

Chapter 6: Conclusions and Future Study

6.1. Conclusions

This study focusses the low-medium waste heat recovery through thermodynamic power cycle. Various thermodynamic power cycles are compared using thermo-techno-economic prospectives. Then, novel ejector-enhanced ORCs are comprehensively analyzed for efficient waste heat recovery. Lab-scale ORC system is developed and experimented using electrical heater input. Finally, a feasibility study is conducted to implement the ORC system to recover waste heat from nuclear power plant based on the data provided by BRNS, Mumbai. Key findings can be summarized as follows:

- ✓ The selection of an appropriate thermodynamic cycle for waste heat recovery depends significantly on the heat source and sink temperature ranges and the priorities regarding performance, cost, environmental impact, and operational feasibility.
- ✓ CO_2 Rankine cycle excels at low heat source temperatures and TFC outperforms at medium-grade heat source temperatures. ORCs (both dry and wet) emerge as versatile and reliable options, particularly for large-scale and distributed power generation, due to their balanced performance, economic viability, and technological maturity.
- ✓ EEORC-1 with R123 achieves the highest net work output (122.2 kW). The basic ORC with R123, however, delivers the highest thermal efficiency (3.8%), exergy efficiency (40%), and yearly profit ($73,143) at 70°C waste heat temperature (WHT). EEORC-1 excels in work output across 60–150°C (R123) and 155–180°C (R1233zd(E)). Thermal and exergy efficiencies improve with WHT, with the basic ORC consistently leading.
- ✓ Economically, the basic ORC (R123) excels under the M1 model, while M2 boosts EEORC-1 profits by 7.32% at 90°C WHT, especially with subsidies or reduced power costs. So, EEORC-1 delivers superior power output, while the M2 model ensures economic viability for advanced cycles, supporting wider adoption.
- ✓ Increasing heat input (5–11.5 kW) experimentally boosts net power (up to 0.939 kW) and cycle efficiency (2.34% to 8.08%) of ORC, with optimal efficiency at high heat input and moderate flow rates. Excessive flow rate reduces the cycle efficiency. The evaporator's effectiveness improves with heat input and flow rates (0.78–0.84), while the expander reaches peak efficiency at higher thermal loads and flow rates.

- ✓ Experimental findings highlight the importance of balancing input parameters to optimize ORC performance and demonstrate its potential for electricity generation from waste heat. Optimization and prediction using RSM-ANOVA were experimentally validated, confirming its suitability for future predictions.
- ✓ Nine potential waste heat sources in nuclear power plants (NPPs) were identified, and two feasible bottoming ORC cases were proposed for waste heat recovery based on condenser temperature, optimizing heat extraction and evaluating system costs, environmental, and economic benefits using BRNS data.
- ✓ R245fa is optimal for case-1, while R236ea delivers higher annual profits in case-2, which is recommended for condenser temperatures below 41°C. Case-2 offers the best thermal and economic performance, with faster capital returns. Both cases generate 499.3 kW and yield a 204.62 thousand USD annual profit from a 764.96 thousand USD investment. Over 40 years, the total investment of 1.392 million USD ensures consistent profitability, making the upgrade viable for NPPs.

The proposed EEORC-1 emerges as the optimal ORC, combining high power output and economic feasibility. Experimental validation reinforces the potential of ORCs in waste heat recovery, and their successful application in NPPs demonstrates their scalability and versatility. By adopting tailored ORC configurations and economic models, industries can achieve substantial energy recovery, cost savings, and environmental benefits, aligning with global sustainability goals.

6.2. Future Study

The following are the future recommendations that need to be incorporated to enhance the system's performance further.

1) More net power generation is possible at the same input parameter condition by using a mixture of working fluids. The azeotropic mixture offers better temperature glide between two sides of the heat exchanger fluid (i.e., hot side and cold side) so that higher turbine inlet temperature can be achieved to generate more power and thus cycle efficiency. Another benefit of using an azeotropic mixture is that power can be generated from lower evaporator outlet temperature conditions, making ORC available to harness power from ultra-low-grade waste energy sources.

2) Use of nanoparticles in base working fluid enhances the heat transfer coefficient of heat exchangers. By the use of nanofluid, the heat exchanger's size decreases for the same parameter condition and thus, production cost per unit of power decreases. Apart from nanofluid, other base working fluids should be explored that offer higher thermal stability, low environmental impact, and better adaptability to varying heat sources, such as ultra-low-grade waste heat or solar-thermal sources.
3) A trilateral flash cycle can also replace ORC for waste heat recovery, as it gives more power output, exergy efficiency and annual profit at medium-grade waste heat (Source). Two-phase flash expansion is the only challenge in complex turbine or expander design to incorporate the experimental setup of the trilateral flash cycle. However, this challenge was solved completely by the advanced coating technique on the turbine blade to avoid erosion and corrosion. Other turbine expansion alternatives are available, like screw turbines, radial-inflow turbines and modified impulse turbines.
4) Introducing an internal heat exchanger or a regenerator in the cycle can improve thermal efficiency by recovering heat from the working fluid before it enters the condenser. This reduces the amount of heat that needs to be extracted from the heat source, improving net power output.
5) Combining multiple ORC stages (Cascaded ORC) can increase overall system efficiency. The first stage utilizes high-temperature heat, while the second stage uses the waste heat from the first cycle.

References

[1] World electricity consumption 2021 | Statista n.d. https://www.statista.com/statistics/280704/world-power-consumption/ (accessed February 15, 2023).

[2] Dashboard - Central Electricity Authority n.d. https://cea.nic.in/dashboard/?lang=en (accessed August 28, 2023).

[3] Billewar SR, Londhe G, Mane PS. World Energy Demand. Integrated Green Energy Solutions 2023:275–316. https://doi.org/10.1002/9781394193738.CH36.

[4] Elwardany M, Nassib AM, Mohamed HA. Advancing sustainable thermal power generation: insights from recent energy and exergy studies. Process Safety and Environmental Protection 2024;183:617–44. https://doi.org/10.1016/J.PSEP.2024.01.039.

[5] Obobisa ES, Ahakwa I. Stimulating the adoption of green technology innovation, clean energy resources, green finance, and environmental taxes: The way to achieve net zero CO2 emissions in Europe? Technol Forecast Soc Change 2024;205:123489. https://doi.org/10.1016/J.TECHFORE.2024.123489.

[6] Kruger H, Meier H-J, Offermann D, Langnickel U. EFFICIENCY IN Efficiency in Electricity Generation 2003.

[7] Logan J, Marcy C, Mccall J, Flores-Espino F, Bloom A, Aabakken J, et al. Electricity Generation Baseline Report 2015.

[8] Application of hydrogen combustion for electrical and motive power generation. Science and Engineering of Hydrogen-Based Energy Technologies: Hydrogen Production and Practical Applications in Energy Generation 2018:259–78. https://doi.org/10.1016/B978-0-12-814251-6.00005-8.

[9] Patil VR, Biradar VI, Shreyas R, Garg P, Orosz MS, Thirumalai NC. Techno-economic comparison of solar organic Rankine cycle (ORC) and photovoltaic (PV) systems with energy storage. Renew Energy 2017;113:1250–60. https://doi.org/10.1016/J.RENENE.2017.06.107.

[10] Roy JP, Mishra MK, Misra A. Parametric optimization and performance analysis of a waste heat recovery system using Organic Rankine Cycle. Energy 2010;35:5049–62. https://doi.org/10.1016/J.ENERGY.2010.08.013.

[11] Dincer I, Bicer Y. Integration of conventional energy systems for multigeneration. Integrated Energy Systems for Multigeneration 2020:143–221. https://doi.org/10.1016/B978-0-12-809943-8.00004-2.

[12] Varma GVP, Srinivas T. Power generation from low temperature heat recovery. Renewable and Sustainable Energy Reviews 2017;75:402–14. https://doi.org/10.1016/J.RSER.2016.11.005.

[13] Ho T, Mao SS, Greif R. Comparison of the Organic Flash Cycle (OFC) to other advanced vapor cycles for intermediate and high temperature waste heat reclamation and solar thermal energy. Energy 2012;42:213–23. https://doi.org/10.1016/J.ENERGY.2012.03.067.

[14] Lee HY, Park SH, Kim KH. Comparative analysis of thermodynamic performance and optimization of organic flash cycle (OFC) and organic Rankine cycle (ORC). Appl Therm Eng 2016;100:680–90. https://doi.org/10.1016/J.APPLTHERMALENG.2016.01.158.

[15] Bronicki LY. History of Organic Rankine Cycle systems. Organic Rankine Cycle (ORC) Power Systems: Technologies and Applications 2017:25–66. https://doi.org/10.1016/B978-0-08-100510-1.00002-8.

[16] Lai KY, Lee YT, Chen MR, Liu YH. Comparison of the trilateral flash cycle and Rankine cycle with organic fluid using the pinch point temperature. Entropy 2019;21. https://doi.org/10.3390/e21121197.

[17] Fischer J. Comparison of trilateral cycles and organic Rankine cycles. Energy 2011;36:6208–19. https://doi.org/10.1016/J.ENERGY.2011.07.041.

[18] Iqbal MA, Rana S, Ahmadi M, Date A, Akbarzadeh A. Trilateral Flash Cycle (TFC): a promising thermodynamic cycle for low grade heat to power generation. Energy Procedia 2019;160:208–14. https://doi.org/10.1016/J.EGYPRO.2019.02.138.

[19] Chen Y, Lundqvist P. The Co2 transcritical power cycle for low grade heat recovery-discussion on temperature profiles in system heat exchangers. American Society of Mechanical Engineers, Power Division (Publication) POWER, vol. 1, 2011, p. 385–92. https://doi.org/10.1115/POWER2011-55075.

[20] Cayer E, Galanis N, Desilets M, Nesreddine H, Roy P. Analysis of a carbon dioxide transcritical power cycle using a low temperature source. Appl Energy 2009;86:1055–63. https://doi.org/10.1016/J.APENERGY.2008.09.018.

[21] Li S, Dai Y. Thermo-economic comparison of Kalina and CO2 transcritical power cycle for low temperature geothermal sources in China. Appl Therm Eng 2014;70:139–52. https://doi.org/10.1016/J.APPLTHERMALENG.2014.04.067.

[22] Ho T, Mao SS, Greif R. Increased power production through enhancements to the Organic Flash Cycle (OFC). Energy 2012;45:686–95. https://doi.org/10.1016/J.ENERGY.2012.07.023.

[23] Mondal S, De S. Power by waste heat recovery from low temperature industrial flue gas by Organic Flash Cycle (OFC) and transcritical-CO2 power cycle: A comparative study through combined thermodynamic and economic analysis. Energy 2017;121:832–40. https://doi.org/10.1016/J.ENERGY.2016.12.126.

[24] Meng F, Wang E, Zhang B, Zhang F, Zhao C. Thermo-economic analysis of transcritical CO2 power cycle and comparison with Kalina cycle and ORC for a low-temperature heat source. Energy Convers Manag 2019;195:1295–308. https://doi.org/10.1016/J.ENCONMAN.2019.05.091.

[25] Li Z, Lu Y, Huang Y, Qian G, Chen F, Yu X, et al. Comparison study of Trilateral Rankine Cycle, Organic Flash Cycle and basic Organic Rankine Cycle for low grade heat recovery. Energy Procedia 2017;142:1441–7. https://doi.org/10.1016/j.egypro.2017.12.532.

[26] Nair V. HFO refrigerants: A review of present status and future prospects. International Journal of Refrigeration 2021;122:156–70. https://doi.org/10.1016/J.IJREFRIG.2020.10.039.

[27] Li M, Wang J, He W, Wang B, Ma S, Dai Y. Experimental Evaluation of the Regenerative and Basic Organic Rankine Cycles for Low-Grade Heat Source Utilization. Journal of Energy Engineering 2013;139:190–7. https://doi.org/10.1061/(ASCE)EY.1943-7897.0000120/ASSET/43712150-3230-4FBF-A84F-1BAA09872C22/ASSETS/IMAGES/LARGE/FIGURE12.JPG.

[28] Chang JC, Chang CW, Hung TC, Lin JR, Huang KC. Experimental study and CFD approach for scroll type expander used in low-temperature organic Rankine cycle. Appl Therm Eng 2014;73:1444–52. https://doi.org/10.1016/J.APPLTHERMALENG.2014.08.050.

[29] Zhang YQ, Wu YT, Xia GD, Ma CF, Ji WN, Liu SW, et al. Development and experimental study on organic Rankine cycle system with single-screw expander for waste heat recovery from exhaust of diesel engine. Energy 2014;77:499–508. https://doi.org/10.1016/J.ENERGY.2014.09.034.

[30] Miao Z, Xu J, Yang X, Zou J. Operation and performance of a low temperature organic Rankine cycle. Appl Therm Eng 2015;75:1065–75. https://doi.org/10.1016/J.APPLTHERMALENG.2014.10.065.

[31] Shao L, Ma X, Wei X, Hou Z, Meng X. Design and experimental study of a small-sized organic Rankine cycle system under various cooling conditions. Energy 2017;130:236–45. https://doi.org/10.1016/J.ENERGY.2017.04.092.

[32] Pang KC, Chen SC, Hung TC, Feng YQ, Yang SC, Wong KW, et al. Experimental study on organic Rankine cycle utilizing R245fa, R123 and their mixtures to investigate the maximum power generation from low-grade heat. Energy 2017;133:636–51. https://doi.org/10.1016/J.ENERGY.2017.05.128.

[33] Ali Tarique M, Dincer I, Zamfirescu C. Experimental investigation of a scroll expander for an organic Rankine cycle. Int J Energy Res 2014;38:1825–34. https://doi.org/10.1002/ER.3189.

[34] Zheng N, Zhao L, Wang XD, Tan YT. Experimental verification of a rolling-piston expander that applied for low-temperature Organic Rankine Cycle. Appl Energy 2013;112:1265–74. https://doi.org/10.1016/J.APENERGY.2012.12.030.

[35] Yamada N, Watanabe M, Hoshi A. Experiment on pumpless Rankine-type cycle with scroll expander. Energy 2013;49:137–45. https://doi.org/10.1016/J.ENERGY.2012.10.027.

[36] Gao P, Jiang L, Wang LW, Wang RZ, Song FP. Simulation and experiments on an ORC system with different scroll expanders based on energy and exergy analysis. Appl Therm Eng 2015;75:880–8. https://doi.org/10.1016/J.APPLTHERMALENG.2014.10.044.

[37] Li L, Ge YT, Luo X, Tassou SA. Experimental investigations into power generation with low grade waste heat and R245fa Organic Rankine Cycles (ORCs). Appl Therm Eng 2017;115:815–24. https://doi.org/10.1016/J.APPLTHERMALENG.2017.01.024.

[38] Farrokhi M, Noie SH, Akbarzadeh AA. Preliminary experimental investigation of a natural gas-fired ORC-based micro-CHP system for residential buildings. Appl Therm Eng 2014;69:221–9. https://doi.org/10.1016/J.APPLTHERMALENG.2013.11.060.

[39] Zhao L, Bao J. Thermodynamic analysis of organic Rankine cycle using zeotropic mixtures. Appl Energy 2014;130:748–56. https://doi.org/10.1016/j.apenergy.2014.03.067.

[40] Wang Z, Zhao Y, Xia X, Pan H, Zhang S, Liu Z. Experimental evaluation of organic Rankine cycle using zeotropic mixture under different operation conditions. Energy 2023;264:126188. https://doi.org/10.1016/J.ENERGY.2022.126188.

[41] Zhu Y, Li W, Wang Y, Li H, Li S. Thermodynamic analysis and parametric optimization of ejector heat pump integrated with organic Rankine cycle combined cooling, heating and power system using zeotropic mixtures. Appl Therm Eng 2021;194. https://doi.org/10.1016/j.applthermaleng.2021.117097.
[42] Safarian S, Aramoun F. Energy and exergy assessments of modified Organic Rankine Cycles (ORCs). Energy Reports 2015;1:1–7. https://doi.org/10.1016/J.EGYR.2014.10.003.
[43] Zeynali A, Akbari A, Khalilian M. Investigation of the performance of modified organic Rankine cycles (ORCs) and modified trilateral flash cycles (TFCs) assisted by a solar pond. Solar Energy 2019;182:361–81. https://doi.org/10.1016/J.SOLENER.2019.03.001.
[44] Abam FI, Ekwe EB, Effiom SO, Ndukwu MC. A comparative performance analysis and thermo-sustainability indicators of modified low-heat organic Rankine cycles (ORCs): An exergy-based procedure. Energy Reports 2018;4:110–8. https://doi.org/10.1016/J.EGYR.2017.08.003.
[45] Kajurek J, Rusowicz A, Grzebielec A, Bujalski W, Futyma K, Rudowicz Z. Selection of refrigerants for a modified organic Rankine cycle. Energy 2019;168:1–8. https://doi.org/10.1016/J.ENERGY.2018.11.024.
[46] Kheiri R, Ghaebi H, Ebadollahi M, Rostamzadeh H. Thermodynamic modeling and performance analysis of four new integrated organic Rankine cycles (A comparative study). Appl Therm Eng 2017;122:103–17. https://doi.org/10.1016/J.APPLTHERMALENG.2017.04.150.
[47] Chen J, Huang Y, Niu Z, Chen Y, Luo X. Performance analysis of a novel organic Rankine cycle with a vapor-liquid ejector. Energy Convers Manag 2018;157:382–95. https://doi.org/10.1016/J.ENCONMAN.2017.11.038.
[48] Haghparast P, Sorin M V., Richard MA, Nesreddine H. Analysis and design optimization of an ejector integrated into an organic Rankine cycle. Appl Therm Eng 2019;159:113979. https://doi.org/10.1016/J.APPLTHERMALENG.2019.113979.
[49] Oyekale J, Petrollese M, Cau G. Modified auxiliary exergy costing in advanced exergoeconomic analysis applied to a hybrid solar-biomass organic Rankine cycle plant. Appl Energy 2020;268:114888. https://doi.org/10.1016/J.APENERGY.2020.114888.
[50] Tashtoush B, Algharbawi A ballah R. Parametric exergetic and energetic analysis of a novel modified organic rankine cycle with ejector. Thermal Science and Engineering Progress 2020;19. https://doi.org/10.1016/j.tsep.2020.100644.

[51] Zhang C, Lin J, Tan Y. Parametric study and working fluid selection of the parallel type organic Rankine cycle and ejector heat pump combined cycle. Solar Energy 2020;205:487–95. https://doi.org/10.1016/J.SOLENER.2020.05.099.

[52] Jafary S, Khalilarya S, Shawabkeh A, Wae-hayee M, Hashemian M. A complete energetic and exergetic analysis of a solar powered trigeneration system with two novel organic Rankine cycle (ORC) configurations. J Clean Prod 2021;281:124552. https://doi.org/10.1016/J.JCLEPRO.2020.124552.

[53] Saini P, Singh J, Sarkar J. Novel combined desalination, heating and power system: Energy, exergy, economic and environmental assessments. Renewable and Sustainable Energy Reviews 2021;151:111612. https://doi.org/10.1016/J.RSER.2021.111612.

[54] Yu G, Wang Q, Yu Z, Zhang N, Ming P. A Four-Hierarchy method for the design of organic Rankine cycle (ORC) power plants. Energy Convers Manag 2022;251:114996. https://doi.org/10.1016/J.ENCONMAN.2021.114996.

[55] Surendran A, Seshadri S. An ejector based Transcritical Regenerative Series Two-Stage Organic Rankine Cycle for dual/multi-source heat recovery applications. Thermal Science and Engineering Progress 2022;27. https://doi.org/10.1016/j.tsep.2021.101158.

[56] Li T, Gao H, Gao X, Meng N. Thermodynamic performance comparison of organic Rankine flash cycle with and without ejector for geothermal power output. Appl Therm Eng 2022;214:118846. https://doi.org/10.1016/J.APPLTHERMALENG.2022.118846.

[57] Li T, Gao H, Gao X. Synergetic mechanism of organic Rankine flash cycle with ejector for geothermal power generation enhancement. J Clean Prod 2022;375:134174. https://doi.org/10.1016/J.JCLEPRO.2022.134174.

[58] Varma GVP, Srinivas T. Power generation from low temperature heat recovery. Renewable and Sustainable Energy Reviews 2017;75:402–14. https://doi.org/10.1016/J.RSER.2016.11.005.

[59] Miao Z, Xu J, Zhang K. Experimental and modeling investigation of an organic Rankine cycle system based on the scroll expander. Energy 2017;134:35–49. https://doi.org/10.1016/J.ENERGY.2017.06.001.

[60] Lei B, Wang W, Wu YT, Ma CF, Wang JF, Zhang L, et al. Development and experimental study on a single screw expander integrated into an Organic Rankine Cycle. Energy 2016;116:43–52. https://doi.org/10.1016/J.ENERGY.2016.09.089.

[61] Feng J, Cheng X, Wang H, Zhao L, Wang H, Dong H. Performance analysis and multi-objective optimization of organic Rankine cycle for low-grade sinter waste heat

recovery. Case Studies in Thermal Engineering 2024;53:103915. https://doi.org/10.1016/J.CSITE.2023.103915.

[62] Yang WH, Hou PC, Shih WH, Hsu SW, Chen Y Bin. Realization and optimization of a binary cycle power generating system using a low-grade heat source. Journal of Mechanics 2022;38:166–75. https://doi.org/10.1093/JOM/UFAC014.

[63] Yan D, Yang F, Yang F, Zhang H, Guo Z, Li J, et al. Identifying the key system parameters of the organic Rankine cycle using the principal component analysis based on an experimental database. Energy Convers Manag 2021;240:114252. https://doi.org/10.1016/J.ENCONMAN.2021.114252.

[64] Fatigati F, Cipollone R. Experimental and theoretical assessment of the effects of electrical load variation on the operability of a small-scale Organic Rankine Cycle (ORC)-based unit equipped with a hermetic scroll expander. Energy 2024;311:133318. https://doi.org/10.1016/J.ENERGY.2024.133318.

[65] Gao Y, Song Q, Su W, Lin X, Sun Z, Huang Z, et al. Experimentally Identifying the Influences of Key Parameters for an Organic Rankine Cycle Using R123. Sustainability 2023, Vol 15, Page 814 2023;15:814. https://doi.org/10.3390/SU15010814.

[66] Shao L, Ma X, Wei X, Hou Z, Meng X. Design and experimental study of a small-sized organic Rankine cycle system under various cooling conditions. Energy 2017;130:236–45. https://doi.org/10.1016/J.ENERGY.2017.04.092.

[67] Zhang HH, Xi H, He YL, Zhang YW, Ning B. Experimental study of the organic rankine cycle under different heat and cooling conditions. Energy 2019;180:678–88. https://doi.org/10.1016/J.ENERGY.2019.05.072.

[68] Tsai YC, Feng YQ, Shuai Y, Lai JH, Leung MKH, Wei Y, et al. Experimental validation of a 0.3 kW ORC for the future purposes in the study of low-grade thermal to power conversion. Energy 2023;285:129422. https://doi.org/10.1016/J.ENERGY.2023.129422.

[69] Corigliano O, Algieri A, Fragiacomo P. Turning Data Center Waste Heat into Energy: A Guide to Organic Rankine Cycle System Design and Performance Evaluation. Applied Sciences 2024, Vol 14, Page 6046 2024;14:6046. https://doi.org/10.3390/APP14146046.

[70] Liu L, Zhu T, Wang T, Gao N. Experimental investigation on the effect of working fluid charge in a small-scale Organic Rankine Cycle under off-design conditions. Energy 2019;174:664–77. https://doi.org/10.1016/J.ENERGY.2019.03.013.

[71] Ayachi F, Ksayer EB, Neveu P, Zoughaib A. Experimental investigation and modeling of a hermetic scroll expander. Appl Energy 2016;181:256–67. https://doi.org/10.1016/J.APENERGY.2016.08.030.

[72] Badr O, O'Callaghan PW, Hussein M, Probert SD. Multi-vane expanders as prime movers for low-grade energy organic Rankine-cycle engines. Appl Energy 1984;16:129–46. https://doi.org/10.1016/0306-2619(84)90060-6.

[73] Giuffrida A. Improving the semi-empirical modelling of a single-screw expander for small organic Rankine cycles. Appl Energy 2017;193:356–68. https://doi.org/10.1016/J.APENERGY.2017.02.015.

[74] Zheng N, Zhao L, Wang XD, Tan YT. Experimental verification of a rolling-piston expander that applied for low-temperature Organic Rankine Cycle. Appl Energy 2013;112:1265–74. https://doi.org/10.1016/J.APENERGY.2012.12.030.

[75] Dumont O, Parthoens A, Dickes R, Lemort V. Experimental investigation and optimal performance assessment of four volumetric expanders (scroll, screw, piston and roots) tested in a small-scale organic Rankine cycle system. Energy 2018;165:1119–27. https://doi.org/10.1016/J.ENERGY.2018.06.182.

[76] Wang T, Liu L, Zhu T, Gao N. Experimental investigation of a small-scale Organic Rankine Cycle under off-design conditions: From the perspective of data fluctuation. Energy Convers Manag 2019;198:111826. https://doi.org/10.1016/J.ENCONMAN.2019.111826.

[77] Liang Y, Yu Z. Experimental investigation of an Organic Rankine cycle system using an oil-free scroll expander for low grade heat recovery. Int J Green Energy 2021;18:812–21. https://doi.org/10.1080/15435075.2021.1880915.

[78] Zou N, Zhang YP, Wang L, Ma S, Diop MA. Dimensional Variation and Parametrical Feasibility for Utilizing Aluminum Cast-House Flue Gases to Supplement Heat for the Organic Rankine Cycle (ORC). JOM 2024;76:1516–30. https://doi.org/10.1007/S11837-023-06357-6/FIGURES/6.

[79] Li YM, Hung TC, Wu CJ, Su TY, Xi H, Wang CC. Experimental investigation of 3-kW organic Rankine cycle (ORC) system subject to heat source conditions: A new appraisal for assessment. Energy 2021;217:119342. https://doi.org/10.1016/J.ENERGY.2020.119342.

[80] Zhou N, Wang X, Chen Z, Wang Z. Experimental study on Organic Rankine Cycle for waste heat recovery from low-temperature flue gas. Energy 2013;55:216–25. https://doi.org/10.1016/J.ENERGY.2013.03.047.

[81] Feng Y qiang, Xu K jing, Zhang Q, Hung TC, He Z xia, Xi H, et al. Experimental investigation and machine learning optimization of a small-scale organic Rankine cycle. Appl Therm Eng 2023;224:120120. https://doi.org/10.1016/J.APPLTHERMALENG.2023.120120.

[82] Wronski J, Imran M, Skovrup MJ, Haglind F. Experimental and numerical analysis of a reciprocating piston expander with variable valve timing for small-scale organic Rankine cycle power systems. Appl Energy 2019;247:403–16. https://doi.org/10.1016/J.APENERGY.2019.04.028.

[83] Bademlioglu AH, Canbolat AS, Yamankaradeniz N, Kaynakli O. Investigation of parameters affecting Organic Rankine Cycle efficiency by using Taguchi and ANOVA methods. Appl Therm Eng 2018;145:221–8. https://doi.org/10.1016/J.APPLTHERMALENG.2018.09.032.

[84] Tauveron N, Lhermet G, Payebien B, Caney N, Morin F. An Experimental Study of an Autonomous Heat Removal System Based on an Organic Rankine Cycle for an Advanced Nuclear Power Plant. Energies 2024, Vol 17, Page 5069 2024;17:5069. https://doi.org/10.3390/EN17205069.

[85] Kallis G, Roumpedakis TC, Pallis P, Koutantzi Z, Charalampidis A, Karellas S. Life cycle analysis of a waste heat recovery for marine engines Organic Rankine Cycle. Energy 2022;257:124698. https://doi.org/10.1016/J.ENERGY.2022.124698.

[86] Usman M, Imran M, Haglind F, Pesyridis A, Park BS. Experimental analysis of a micro-scale organic Rankine cycle system retrofitted to operate in grid-connected mode. Appl Therm Eng 2020;180:115889. https://doi.org/10.1016/J.APPLTHERMALENG.2020.115889.

[87] Hijriawan M, Pambudi NA, Wijayanto DS, Biddinika MK, Saw LH. Experimental analysis of R134a working fluid on Organic Rankine Cycle (ORC) systems with scroll-expander. Engineering Science and Technology, an International Journal 2022;29:101036. https://doi.org/10.1016/J.JESTCH.2021.06.016.

[88] Zhao YK, Lei B, Wu YT, Zhi RP, Wang W, Guo H, et al. Experimental study on the net efficiency of an Organic Rankine Cycle with single screw expander in different seasons. Energy 2018;165:769–75. https://doi.org/10.1016/J.ENERGY.2018.09.013.

[89] Wronski J, Imran M, Skovrup MJ, Haglind F. Experimental and numerical analysis of a reciprocating piston expander with variable valve timing for small-scale organic Rankine cycle power systems. Appl Energy 2019;247:403–16. https://doi.org/10.1016/J.APENERGY.2019.04.028.

[90] Li YM, Hung TC, Wu CJ, Su TY, Xi H, Wang CC. Experimental investigation of 3-kW organic Rankine cycle (ORC) system subject to heat source conditions: A new appraisal for assessment. Energy 2021;217:119342. https://doi.org/10.1016/J.ENERGY.2020.119342.

[91] Obara S, Tanaka R. Waste heat recovery system for nuclear power plants using the gas hydrate heat cycle. Appl Energy 2021;292:116667. https://doi.org/10.1016/J.APENERGY.2021.116667.

[92] Almomani B, Alkhalidi A, Olabi AG, Jouhara H. Expert opinions on strengths, weaknesses, opportunities, and threats of utilizing nuclear reactor waste heat for water desalination. Desalination 2023;564:116777. https://doi.org/10.1016/J.DESAL.2023.116777.

[93] Adak AK, Rao IS, Srivastava VK, Tewari PK. Nuclear desalination by waste heat utilisation in an advanced heavy water reactor. International Journal of Nuclear Desalination 2007;2:234–43. https://doi.org/10.1504/IJND.2007.013547.

[94] Adak AK, Tewari PK. Technical feasibility study for coupling a desalination plant to an Advanced Heavy Water Reactor. Desalination 2014;337:76–82. https://doi.org/10.1016/J.DESAL.2013.11.004.

[95] Landelle A, Tauveron N, Haberschill P, Revellin R, Colasson S. Organic Rankine cycle design and performance comparison based on experimental database. Appl Energy 2017;204:1172–87. https://doi.org/10.1016/J.APENERGY.2017.04.012.

[96] Nguyen VN, Pham NDK, Duong XQ, Tran VD, Pham MT, Rajamohan S, et al. Combination of solar with organic Rankine cycle as a potential solution for clean energy production. Sustainable Energy Technologies and Assessments 2023;57:103161. https://doi.org/10.1016/J.SETA.2023.103161.

[97] Escalante ESR, Balestieri JAP, de Carvalho JA. The organic Rankine cycle: A promising technology for electricity generation and thermal pollution mitigation. Energy 2022;247:123405. https://doi.org/10.1016/J.ENERGY.2022.123405.

[98] Olabi AG, Elsaid K, Sayed ET, Mahmoud MS, Wilberforce T, Hassiba RJ, et al. Application of nanofluids for enhanced waste heat recovery: A review. Nano Energy 2021;84:105871. https://doi.org/10.1016/J.NANOEN.2021.105871.

[99] Bhattad A, Sarkar J, Ghosh P. Energetic and Exergetic Performances of Plate Heat Exchanger Using Brine-Based Hybrid Nanofluid for Milk Chilling Application. Heat Transfer Engineering 2020;41:522–35. https://doi.org/10.1080/01457632.2018.1546770.

[100] Papapetrou M, Kosmadakis G. Resource, environmental, and economic aspects of SGHE. Salinity Gradient Heat Engines 2022:319–53. https://doi.org/10.1016/B978-0-08-102847-6.00006-1.

[101] Muley A, Manglik RM. Enhanced Heat Transfer Characteristics of Single-Phase Flows in a Plate Heat Exchanger with Mixed Chevron Plates. Journal of Enhanced Heat Transfer 1997;4:187–201. https://doi.org/10.1615/JEnhHeatTransf.v4.i3.30.

[102] García-Cascales JR, Vera-García F, Corberán-Salvador JM, Gonzálvez-Maciá J. Assessment of boiling and condensation heat transfer correlations in the modelling of plate heat exchangers. International Journal of Refrigeration 2007;30:1029–41. https://doi.org/10.1016/J.IJREFRIG.2007.01.004.

[103] Parikhani T, Azariyan H, Behrad R, Ghaebi H, Jannatkhah J. Thermodynamic and thermoeconomic analysis of a novel ammonia-water mixture combined cooling, heating, and power (CCHP) cycle. Renew Energy 2020;145:1158–75. https://doi.org/10.1016/J.RENENE.2019.06.100.

[104] Saini P, Singh J, Sarkar J. Thermodynamic, economic and environmental analyses of a novel solar energy driven small-scale combined cooling, heating and power system. Energy Convers Manag 2020;226:113542. https://doi.org/10.1016/J.ENCONMAN.2020.113542.

[105] DERC. Annexure-ELECTRICITY TARIFF SCHEDULE FOR FY 2021-22-BRPL, BYPL, TPDDL & NDMC Ensuring Quality, Accessibility and Availability (24X7) of Power at Affordable Price. BSES Delhi 2021. https://www.bsesdelhi.com/documents/55701/92678/Tariff_Schedule_for_FY_2021_22.pdf/e862f0b1-cbfe-2f63-84b1-e478c5021a0e?t=1633426006962 (accessed July 26, 2022).

[106] Times of India. Average power price on Indian Energy Exchange hits 13-year high in March - Times of India. The Times of India 2022. https://timesofindia.indiatimes.com/business/india-business/average-power-price-on-indian-energy-exchange-hits-13-year-high-in-march/articleshow/90692923.cms (accessed July 26, 2022).

[107] Hodge T, Fasching E. U.S. Energy Information Administration - EIA - Independent Statistics and Analysis. US Energy Information Administration 2022. https://www.eia.gov/todayinenergy/detail.php?id=51438 (accessed July 26, 2022).

[108] Roy J, Sarkar P, Biswas S, Choudhury A. Predictive equations for CO2 emission factors for coal combustion, their applicability in a thermal power plant and subsequent

assessment of uncertainty in CO2 estimation. Fuel 2009;88:792–8. https://doi.org/10.1016/J.FUEL.2008.11.023.

[109] Schlömer S, Bruckner T, Fulton L, Hertwich Austria E, McKinnon AU, Perczyk D, et al. III ANNEX Technology-specific Cost and Performance Parameters Editor: Lead Authors: Contributing Authors: to the Fifth Assessment Report of the Intergovernmental Panel on Climate Change [Edenhofer Technology-specific Cost and Performance Parameters Annex III AIII Contents 2014.

[110] Carbon Dioxide Emissions From Electricity - World Nuclear Association n.d. https://www.world-nuclear.org/information-library/energy-and-the-environment/carbon-dioxide-emissions-from-electricity.aspx (accessed July 15, 2023).

[111] Campos Rodríguez CE, Escobar Palacio JC, Venturini OJ, Silva Lora EE, Cobas VM, Marques Dos Santos D, et al. Exergetic and economic comparison of ORC and Kalina cycle for low temperature enhanced geothermal system in Brazil. Appl Therm Eng 2013;52:109–19. https://doi.org/10.1016/J.APPLTHERMALENG.2012.11.012.

[112] Hai T, Ashraf Ali M, Chaturvedi R, Fahad Almojil S, Ibrahim Almohana A, Fahmi Alali A, et al. A low-temperature driven organic Rankine cycle for waste heat recovery from a geothermal driven Kalina cycle: 4E analysis and optimization based on artificial intelligence. Sustainable Energy Technologies and Assessments 2023;55:102895. https://doi.org/10.1016/J.SETA.2022.102895.

[113] Chen LX, Hu P, Sheng CC, Zhang N, Xie MN, Wang FX. Thermodynamic analysis of three ejector based organic flash cycles for low grade waste heat recovery. Energy Convers Manag 2019;185:384–95. https://doi.org/10.1016/j.enconman.2019.02.016.

[114] Sarkar J. Generalized pinch point design method of subcritical-supercritical organic Rankine cycle for maximum heat recovery. Energy 2018;143:141–50. https://doi.org/10.1016/J.ENERGY.2017.10.057.

[115] Yari M. Performance analysis of the different organic Rankine cycles (ORCs) using dry fluids. International Journal of Exergy 2009;6:323–42. https://doi.org/10.1504/IJEX.2009.025324.

[116] Sim JB, Yook SJ, Kim YW. Performance Analysis of Organic Rankine Cycle with the Turbine Embedded in a Generator (TEG). Energies 2022, Vol 15, Page 309 2022;15:309. https://doi.org/10.3390/EN15010309.

[117] Renewable Industrial Process Heat | Renewable Heating and Cooling: The Thermal Energy Advantage | US EPA n.d.

https://19january2017snapshot.epa.gov/rhc/renewable-industrial-process-heat_.html (accessed July 8, 2024).
[118] Sonker VK, Chakraborty JP, Sarkar A. Development of a frugal solar still using phase change material and nanoparticles integrated with commercialization through a novel economic model. J Energy Storage 2022;51:104569. https://doi.org/10.1016/J.EST.2022.104569.
[119] Liu C, Wang S, Zhang C, Li Q, Xu X, Huo E. Experimental study of micro-scale organic Rankine cycle system based on scroll expander. Energy 2019;188:115930. https://doi.org/10.1016/J.ENERGY.2019.115930.
[120] Rayegan R, Tao YX. A procedure to select working fluids for Solar Organic Rankine Cycles (ORCs). Renew Energy 2011;36:659–70. https://doi.org/10.1016/J.RENENE.2010.07.010.
[121] Luo J, Chen G, Wang Q, Zhang S. Analysis on the optimal mixing pressure and efficiency limit of an ideal ejector. Energy Reports 2021;7:4335–47. https://doi.org/10.1016/J.EGYR.2021.07.024.
[122] Besagni G, Cristiani N, Croci L, Guédon GR, Inzoli F. Computational fluid-dynamics modelling of supersonic ejectors: Screening of modelling approaches, comprehensive validation and assessment of ejector component efficiencies. Appl Therm Eng 2021;186:116431. https://doi.org/10.1016/J.APPLTHERMALENG.2020.116431.
[123] Liu X, Zhang Y, Shen J. System performance optimization of ORC-based geo-plant with R245fa under different geothermal water inlet temperatures. Geothermics 2017;66:134–42. https://doi.org/10.1016/J.GEOTHERMICS.2016.12.004.
[124] Du Y, Pekris M, Tian G. Influence of sealing cavity geometries on flank clearance leakage and pressure imbalance of micro-scale transcritical CO2 scroll expander by CFD modelling. Energy 2023;282:128775. https://doi.org/10.1016/J.ENERGY.2023.128775.
[125] TRUING UP OF TARIFF FOR FY 2021-22, ANNUAL PERFORMANCE REVIEW (APR) FOR FY 2022-23 AND APPROVAL OF AGGREGATE REVENUE REQUIREMENT AND TARIFF FOR FY 2023-24 FOR Dakshinanchal Vidyut Vitran Nigam Ltd 2023.
[126] India electricity prices, June 2023 | GlobalPetrolPrices.com n.d. https://www.globalpetrolprices.com/India/electricity_prices/ (accessed February 19, 2024).
[127] EES: Engineering Equation Solver | F-Chart Software : Engineering Software n.d. https://fchartsoftware.com/ees/ (accessed July 15, 2023).

[128] Singh SK, Sarkar J. Energy, exergy and economic assessments of shell and tube condenser using hybrid nanofluid as coolant. International Communications in Heat and Mass Transfer 2018;98:41–8. https://doi.org/10.1016/J.ICHEATMASSTRANSFER.2018.08.005.

List of Publications

Research Journal Paper:

1) Srivastava M, Sarkar J, Sarkar A, Maheshwari NK, Antony A. 4E analysis and optimization of novel ejector-enhanced organic Rankine cycles by introducing new economic models. Thermal Science and Engineering Progress 2023;41:101855. https://doi.org/10.1016/J.TSEP.2023.101855.

2) M. Srivastava, J. Sarkar, A. Sarkar, N.K. Maheshwari, A. Antony, Techno-economic and 4E comparisons of various thermodynamic power cycles for low-medium grade heat recovery, Process Safety and Environmental Protection. 178 (2023) 528–539. https://doi.org/10.1016/J.PSEP.2023.08.041.

3) Srivastava M, Sarkar J, Sarkar A, Maheshwari NK, Antony A. Thermo-economic feasibility study to utilize ORC technology for waste heat recovery from Indian nuclear power plants. Energy 2024:131338. https://doi.org/10.1016/J.ENERGY.2024.131338.

4) Fabrication and experimental investigation of a laboratory-scale organic Rankine cycle and data-driven optimization. (Accepted in "Energy")

5) Experimental data-based optimisation and prediction of ORC technology by RSM method. (under preparation)

Conference paper:

1) Comparative energy-exergy analysis of ejector integration in ORC by optimization method for ultra-low to medium temperature heat sources. https://doi.org/10.1615/IHMTC-2023.2010.

2) Optimization and energy-exergy comparison of conventional modifications in ORC (organic Rankine cycle) technology for electricity generation. (FMFP Library)

3) Distributed renewable power generation using thermodynamic cycles: options and challenges. (ASTFE Library)

Book Chapter:

1) Thermodynamic cycle-based distributed renewable power generation: options and challenges. (ISEES Book Chapter)

2) Enhanced Waste Heat Recovery Using Nanofluid. (Elsevier Book Chapter)